Reconstituting the human COPII secretion system

Reconstituting the Human COPII Secretion System

Evgenia Alekova Markova
Thesis submitted for degree of Doctor of Philosophy
Birkbeck, University of London

March 2021

Declaration of Originality

The work presented in my thesis is my own. All sources of information referenced in this thesis are cited accordingly. Where this work has benefited from experimental work performed by others, this has been clearly cited in the *Materials and Methods*.

Copyright Declaration

Acknowledgements

It's been a very long journey, and I would like to thank the people who helped me get where I am today. I did not know there was so much compassion and kindness to go around.
Thank you to Giulia Zanetti, who has been so encouraging and supportive and kind when it was needed and pushed me when it was needed. I could not have hoped for a better PhD supervisor, or for a more inspiring one. I truly appreciate all your help throughout the years.
Thank you to all the lovely people in Birkbeck who made it feel like home: to Josh Hutchings for the insightful COPII and electron microscopy conversations and for showing me what a great scientist in the beginning of their career looks like, to Shomon Miah for teaching me how to purify proteins and how to navigate PhD life and life in general, to Alex Cook and Hugo Villanueva and Dina Molnar, for the acceptance and the lovely times at the George spent with what felt like family, to Carolyn Moores and Natalya Lukoyanova and Shu Chen and everyone else who makes Birkbeck into the unique and heart-warming environment that it is. To Steph Webb and Euan Pyle, who made the last year and a half bearable and who I'll miss dearly now that I'm starting the next stage.
Thank you to my colleagues at Heptares, in particular Ali Jazayeri and Dan Lamb, who inspired me to become a scientist and supported me at such an early stage of my career. Working at Heptares ignited my passion for structural biology, and it's safe to say I would not have started this PhD if it was not for that experience.

Thank you to my mother, who was by my side throughout this journey and throughout all journeys, the kindest person I've ever met who makes the world a warmer place just by being in it. Thank you to my father, who never stopped believing in me, for always showing up when it mattered the most, and for always having my best interest in mind.

Елена и Ради, без вас не знам какво щях да правя в тоя живот. С такива жени до мен ми порастват крила, добре, че ви има на тоя свят.

Leo, thank you for being my partner in every sense of the word, to celebrate the good times and get through the bad, and to enjoy being alive in the interim.

Abstract

The human coat protein II (COPII) secretion system is an essential membrane trafficking system that exports cargo from the endoplasmic reticulum. While significant insight into the COPII secretion system has been gained using yeast as a model organism, many questions about the COPII secretion system in higher eukaryotes remain unanswered: do human COPII proteins sculpt membranes like their yeast counterparts? Is cargo exported from the human endoplasmic reticulum via COPII carriers? What membrane morphologies do human COPII proteins generate, and how are those morphologies regulated to accommodate the wide range of cargoes exported from the endoplasmic reticulum? To assess whether human COPII proteins are capable of remodelling membranes, I established a minimal *in vitro* reconstitution system using purified proteins and model membranes. I purified human COPII proteins as expressed in *Escherichia coli* and insect cells and established that they were capable of membrane binding using liposome flotation assays. Furthermore, I used guanosine triphosphate (GTP) hydrolysis assays to characterize the enzymatic activity of the Sar1 GTPase, the initiating factor of COPII assembly. I observed that Sar1 has an intrinsic GTP hydrolysis activity, which is stimulated by other COPII components, indicating that the purified components have retained their biologically relevant functionality. Finally, I analysed human COPII assemblies on membranes using electron microscopy. This study established that human COPII components deform membranes, similarly to yeast COPII. Furthermore, they generate a range of diverse membrane morphologies. This suggests that the human COPII system can form a range of carriers to accommodate cargo exported from the human ER. Using cryo-electron microscopy, I observed that human COPII components form two discernible layers on membranes. The establishment of this *in vitro* reconstitution platform allows us to address outstanding questions about the functioning of this complex system, such as the importance of different COPII component paralogues in humans and the role of GTP hydrolysis in COPII-mediated membrane deformation. Furthermore, it is the first step to the structural analysis of human COPII assembled on membranes, which can provide insight into global COPII arrangement.

Table of Contents

Abbreviations

apoB	apolipoprotein B
ARF	adenosine diphosphate-ribosylation factor
ATP	adenosine triphosphate
CDP-DAG	cytidine diphosphate diacyl glycerol
Cer	ceramides
CLSD	cranio-lenticulo-sutural dysplasia
CMRD	chylomicron retention disease
COPI	coat protein I
COPII	coat protein II
CVs	column volumes
DNA	deoxyribonucleic acid
DOPA	dioleoyl phosphatidic acid
DOPS	dioleoyl phosphatidylserine
DTT	dithiothreitol
EDTA	ethylenediaminetetraacetic acid
EM	electron microscopy
ER	endoplasmic reticulum
ERES	endoplasmic reticulum exit sites
ERGIC	endoplasmic reticulum – Golgi intermediate compartment exit sites
GalCer	galactosylceramide
GAP	GTPase activating protein
GDP	guanine nucleoside diphosphate
GEF	guanine nucleotide exchange factor
GFP	green fluorescent protein
GST	glutathione S-transferase
GTP	guanosine triphosphate
GUVs	giant unilamellar vesicles
His	histidine
HRP	horseradish peroxidase
IPTG	Isopropyl β-D-1-thiogalactopyranoside
LB	lysogeny broth
LUVs	large unilamellar vesicles
MIA/cTAGE	melanoma inhibitory activity/cutaneous T-cell lymphoma-associated antigen
MW	molecular weight
PC	phosphatidylcholine
PDB ID	protein database identification code
PE	phosphatidylethanolamine
PI	phosphatidylinositol
PI(4)P	phosphatidylinositol 4-phosphate
PI(4,5)P2	phosphatidylinositol 4,5-diphosphate
PM	plasma membrane
PRD	proline-rich domain
RNA	ribonucleic acid

rpm	rotations per minute
SDS-PAGE	sodium dodecyl sulfate – polyacrylamide gel electrophoresis
SM	sphingomyelin
SOC	Super Optimal broth with Catabolite repression
TALI	Tango1-like
Tango1	Transport-and-Golgi Organisation 1
TEV	Tobacco Etch Virus
TFG	Trk-fused gene
TRAPPI	transport protein particle I
VSVG	vesicular stomatitis virus G protein
VTCs	vesicular tubular clusters
X-Gal	5-Bromo-4-chloro-3-indolyl β-D-galactopyranoside
YT	yeast triptone
YFP	yellow fluorescent protein

List of Figures

List of Tables

I. Introduction: COPII Trafficking in Mammals

I.1. Membrane Trafficking in Mammals

The intracellular organisation of proteins, lipids, and carbohydrates defines cell identity and lays the foundation for performing cellular functions. Intracellular trafficking is central to the proper distribution of biomolecules. In eukaryotic cells, where the intracellular environment is separated into membrane-bound compartments, a gentle balance is maintained between the preservation of organelle identities and efficient exchange between compartments. The secretory pathway traffics transmembrane and secreted proteins from the endoplasmic reticulum (ER) to the Golgi apparatus, their final intramembrane cellular location, or the cell surface (Zanetti *et al.*, 2012).

A range of different and complementary models have been established to encompass the diverse mechanisms of intracellular membrane trafficking. These include the fused compartments, kiss-and-run, and vesicular transport models, in which membranes bud from the originating compartment and fuse transiently or permanently with the acceptor membrane (Watson and Stephens, 2005).

In the vesicular transport model, cargo is transported between specific compartments in dedicated vesicles. Cargo in the donor compartment is recognised by the transport machinery either directly or through additional receptors. Cytoplasmic transport components are recruited to the nascent membrane, coating it and budding it into carriers (Bonifacino and Glick, 2004). The resulting cargo-loaded vesicles are then trafficked to the target compartment and fuse with the acceptor membrane to release their cargo (Watson and Stephens, 2005).

I.1.1. Mammalian Vesicular Trafficking

Although the basic foundations of the secretory pathway are conserved throughout the eukaryotic kingdom, the mammalian cell has more elaborate needs and more sophisticated responses to the environment than the simplest eukaryotic cells. This is reflected in the high

level of organisation of the mammalian secretory pathway and the plethora of components involved. Early secretion in mammals progresses through three membrane-bound compartments: the ER, the endoplasmic reticulum-Golgi intermediate compartment (ERGIC), and the Golgi apparatus. The ERGIC is absent in simpler eukaryotic organisms such as yeast, where vesicular trafficking progresses directly from the ER to the Golgi apparatus (Barlowe et al. 1994). In mammals, anterograde (i.e., forward) transport originates at the ER and proceeds in the direction of the ERGIC and the Golgi, while retrograde transport brings cargo back from the Golgi towards the ERGIC and the ER. The bi-directionality of traffic is essential for the recycling of the components of the transport machinery (Lippincott-Schwartz, 1993). Compared to yeast, the complexity of the mammalian cell and the large repertoire of trafficked cargo necessitate the involvement of a greater number of coat protein (COP), SNAP Receptor (SNARE), and Rab proteins (Bock *et al.*, 2001). The range of different subunits allows for cargo binding specificity and the accommodation of a fascinating range of molecules of different shapes, sizes, and surface charges (Wendeler, Paccaud and Hauri, 2007).

I.1.2. Coat complexes

Four major cytoplasmic coat protein complexes are known to mediate vesicular transport in eukaryotic cells: coat protein complexes I and II (COPI and COPII), clathrin, and retromer (Fig. 1.1) (Lee and Goldberg 2010). Their components are recruited to the membranes of specific intracellular compartments to mediate different steps of vesicle trafficking (Barlowe et al. 1994). COPI and COPII mediate trafficking events between the ER and the Golgi. In yeast, COPII is responsible for anterograde trafficking from the ER to the Golgi, while COPI mediates intra-Golgi transport and retrograde trafficking from the Golgi to the ER. In mammalian cells, COPII vesicles transport cargo to the additional compartment between the ER and the Golgi, the ERGIC. The mechanism of transport from the ERGIC to the Golgi is a matter of debate, as discussed in Section I.1.2.3. COPI is responsible for retrograde transport from the Golgi apparatus and the ERGIC, and between Golgi cisternae (Orci, Glick and Rothman, 1986; Ishii *et al.*, 2016). Clathrin, the first discovered and thoroughly characterised vesicle transport system, is responsible for endocytic transport from the plasma membrane and transport from the trans-Golgi to the endosomal network (Robinson, 1994). Retromer forms a coat that traffics cargo from the endosome to the trans-Golgi network and the plasma membrane (PM) (Seaman *et al.*, 1997; Temkin *et al.*, 2011; Kovtun *et al.*, 2018).

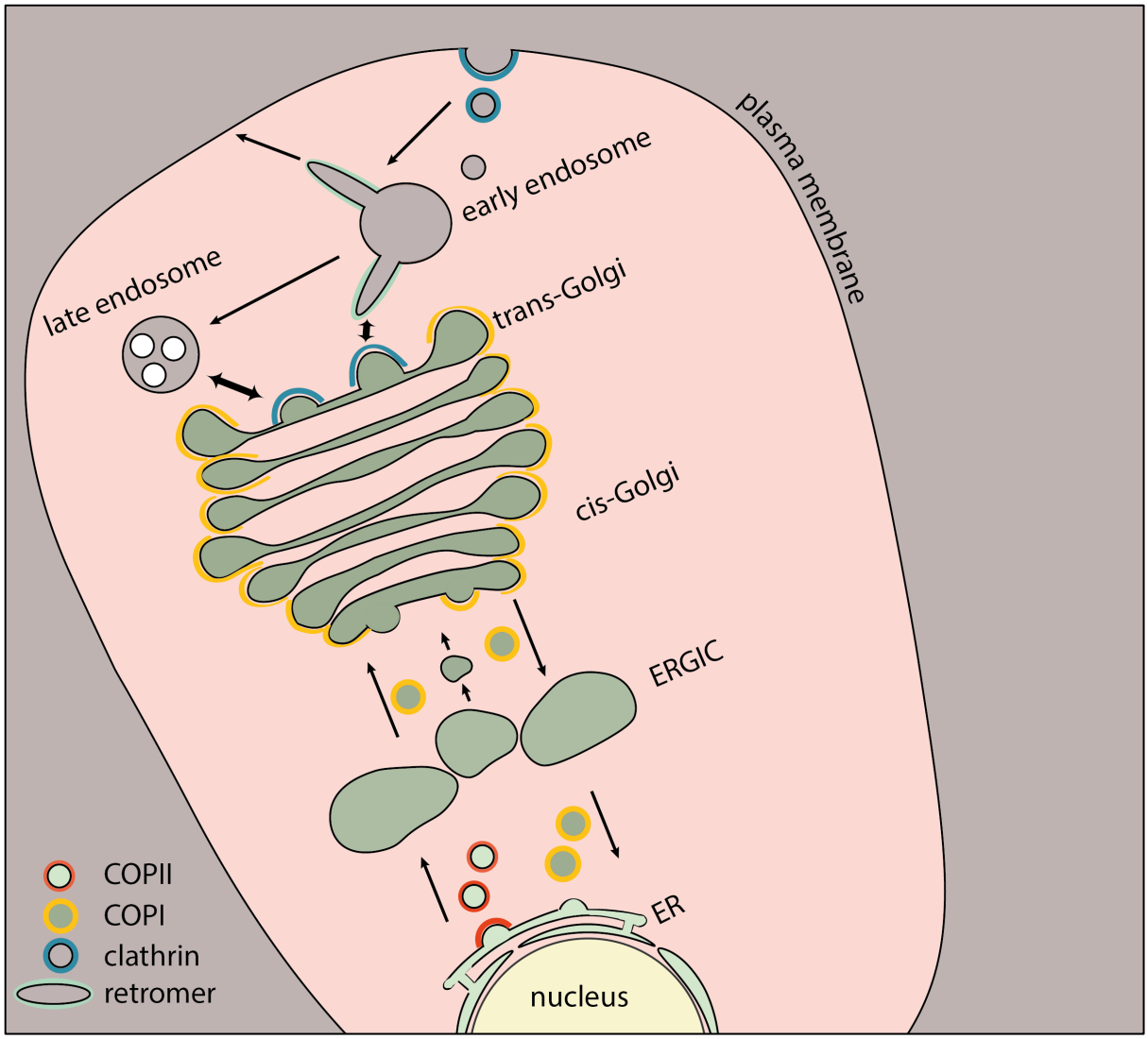

Figure 1.1: Coat complexes in the mammalian cell. In anterograde trafficking, COPII-coated vesicles transport cargo from the ER to the ERGIC. COPI carriers mediate retrograde trafficking from the cis-Golgi. The mechanism of cargo transport between the ERGIC and the cis-Golgi is unclear. Adapted from Markova and Zanetti, 2019.

I.1.3. The Early Secretory Pathway

I.1.3.1. ER and ER-exit sites

The endoplasmic reticulum is a complex and multifunctional intracellular compartment. A third of the proteome is translated by ribosomes associated with the ER membrane and translocated into the ER lumen. This includes both locally resident proteins and proteins that are destined for other cellular compartments, the cell membrane, or secretion. Correctly folded proteins destined for anterograde transport are recognised by the transport

machinery and its adaptors. They are packaged into coated membrane carriers and released in the direction of the Golgi apparatus (Alberts *et al.*, 2002).

In eukaryotic cells, vesicles are formed and secreted from well-defined and specialised ER and ER-proximal loci. Those ER exit sites (ERES) are organised in clusters and are characterised by membrane extensions 200-500nm in length and a high local curvature (Okamoto *et al.*, 2012). ERES have a high abundance of COPII proteins, recruited through interactions with ERES-resident proteins (Watson *et al.*, 2006). Furthermore, COPII proteins bind more strongly to curved membranes, hence ERES also concentrate COPII through their high curvature (Bannykh, Rowe and Balch, 1996; Fan, Roth and Zuber, 2003; Watson and Stephens, 2005). ERES serve as assembly platforms for COPII components and mark the budding-prone regions of the ER membrane, also expanding beyond it in the direction of the subsequent compartment, the ERGIC.

The abundance, distribution, and morphology of the ERES are organism and cell-line specific. There is an interesting link between the position of ERES and the compartment to which COPII vesicles are destined (Langhans *et al.*, 2012). In *Pichia pastoris*, ERES are positioned directly opposite the Golgi (Rossanese *et al.*, 1999). In mammalian cells, ERES are concentrated opposite the ERGIC, although they are also present in the peripheral ER (Langhans *et al.*, 2012). An example of structure reflecting function, this arrangement minimises secretory pathway cargo transport trajectory.

I.1.3.2. The ER-to-Golgi intermediate compartment

Opposite the ERES lies the ERGIC, also referred to as the vesicular tubular clusters (VTCs). The ERGIC had previously been classified as a sub-compartment of the ER or the cis-Golgi apparatus (Mellman and Simons, 1992; Sitia and Meldolesi, 1992). This was partially informed by the absence of ERGIC in yeast, where anterograde intracellular transport progresses directly from the ER to the Golgi apparatus. The ERGIC as a self-standing compartment was first identified and is still marked by the presence of the lectin ERGIC-53 (Schweizer *et al.*, 1988; Hauri and Schweizer, 1992; Bannykh, Rowe and Balch, 1996; Klumperman *et al.*, 1998). Subsequently, biochemical analysis established that the membrane composition of the ERGIC differs from those of both the ER and the Golgi (Appenzeller-Herzog, 2006). Two views of the ERGIC have been proposed to delineate its place in vesicular transport, which describe the ERGIC as either a dynamic, or a static entity.

The dynamic, or transport complex, model describes the ERGIC as a mobile compartment that plays an active role in transport to the Golgi apparatus. In this view, the ERGIC is a fusion of ER-derived COPII vesicles that migrates towards the Golgi via microtubules to fuse with or form part of the cis-Golgi apparatus. In contrast, in the stable compartment model the ERGIC is viewed as a static entity. According to this model, COPII vesicles reach the ERGIC and fuse with it to release their cargo, which is subsequently incorporated in COPI coated vesicles for ERGIC-Golgi transport via microtubules (Ben-Tekaya, 2005).

In support of the dynamic model, it was observed that when the transport of a model cargo, vesicular stomatitis virus G protein (VSVG), fused to green fluorescent protein (GFP), was tracked by fluorescence microscopy, large concentrated flexible structures travelled to the Golgi via microtubules (Presley *et al.*, 1997). While not rejecting the presence of a static ERGIC *per se*, the study raises questions about its size, structure, and complexity. Fluorescent microscopy visualisation of GFP-fused ERGIC-53 paints a more complicated picture: while the majority of ERGIC remains stable and shows an extremely wide distribution pattern, a small mobile population shows movement between individual stable ERGIC compartments (Ben-Tekaya, 2005). It has been observed that COPII vesicles can fuse to form a larger membrane compartment, which was suggested to bear resemblance to the ERGIC (Xu and Hay, 2004). The COPII coat dissociates prior to or simultaneously with carrier fusion with the ERGIC and is not observed on carriers between the ERGIC and the Golgi (Stephens, 2003). Further studies are needed to capture the nature of this complex and flexible membrane-bound compartment and to establish the role of COPII vesicles in its formation.

I.2. COPII Vesicle Formation

Important knowledge of the mechanism of COPII vesicle formation has been gained from genetic screens and reconstitutions of COPII vesicles *in vitro*. Historically, the majority of membrane trafficking studies have used *Saccharomyces cerevisiae* as a model organism, as the yeast genome was by far the best studied and most easily manipulated in the eukaryotic kingdom (Botstein and Fink 1988; Botstein and Fink 2011). Light was shed on this vesicular transport system through genetic screens in yeast, in which a plethora of genes involved in protein secretion and transport were discovered (Cooper GM, 2000). Further advances in the understanding of COPII trafficking were gained from biochemical reconstitutions of COPII budding using purified proteins and a membrane source (Barlowe *et al.*, 1994; Rowe *et al.*,

1996; Aridor *et al.*, 1998; Kim *et al.*, 2005; Boyadjiev *et al.*, 2006; Fromme *et al.*, 2007; Bacia *et al.*, 2011; Zanetti *et al.*, 2013; Gorur *et al.*, 2017; Hutchings *et al.*, 2018). In these studies, the proteins that were used were almost invariably from yeast. This foundational work has helped build a thorough understanding of the molecular mechanisms of COPII assembly, as described below. *In vitro* reconstitutions with mammalian COPII proteins are discussed in Section I.7.

In COPII vesicle formation, the cytoplasmic COPII proteins are sequentially assembled on the ER membrane. They induce and support membrane curvature, recognise cargo, and bud the membrane into cargo carriers (Fig.1.2). Briefly, Sar1 is recruited to specific ER sites and associates with the membrane exchanging guanine nucleoside diphosphate (GDP) for guanine nucleoside triphosphate (GTP). It then recruits Sec23/24, cytoplasmic heterodimers forming the COPII inner coat, which in turn recruit Sec13/31 heterotetramers that form the outer coat. This completes the COPII coat assembly, resulting in vesicle scission. Assemblies are short-lived due to an intrinsic propensity for disassembly. GTP hydrolysis by Sar1, stimulated by the specific GTPase activating protein (GAP) activity of Sec23/24, and in turn accelerated by Sec13/31, results in the shedding of Sar1 from the membrane and eventually in the dissociation of the COPII coat (Zanetti *et al.*, 2012) .

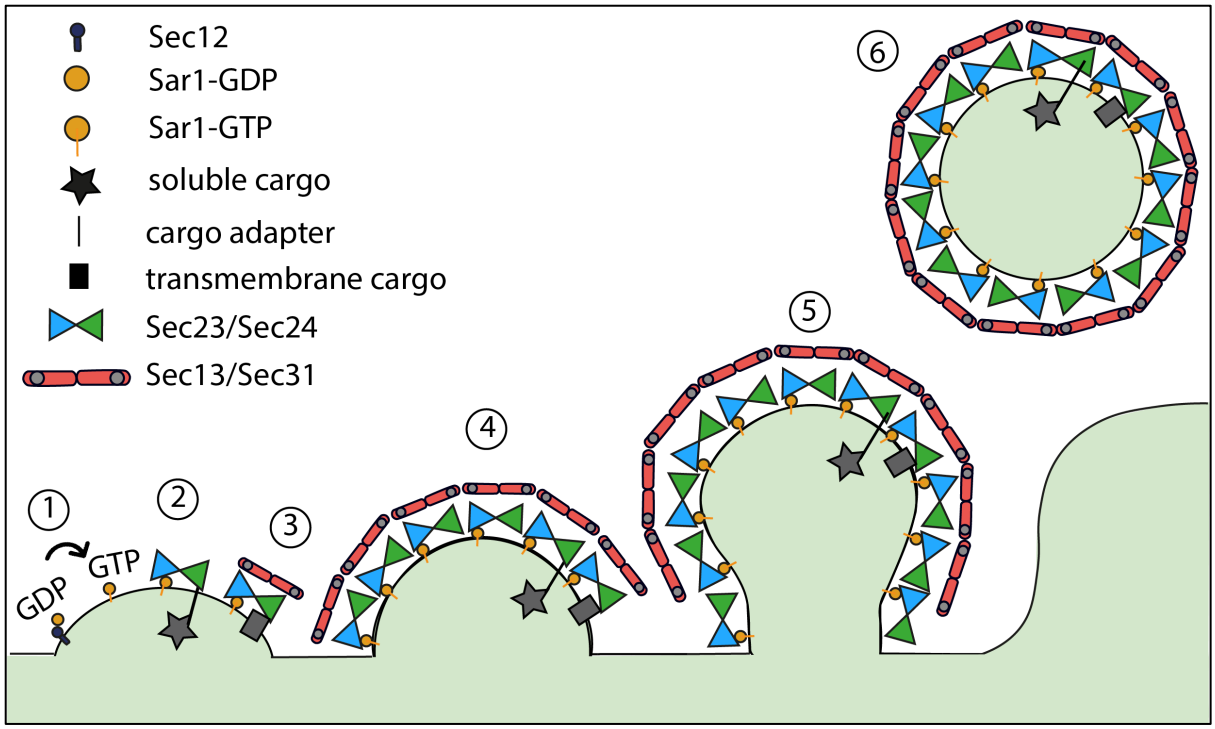

Figure 1.2: COPII assembly at ERES. (1) The Sar1 GTPase is activated by Sec12, which stimulates Sar1 to exchange GDP for GTP. Sar1 inserts an N-terminal helix into the membrane. (2) Inner coat components are recruited that bind Sar1 and cargo/cargo adapters. (3) The outer coat is recruited to Sar1-Sec23/24 complexes. (4) COPII components bend the ER membrane. (5) A membrane bud is formed. (6) A nascent COPII vesicle forms by scission from ERES.

I.2.1. Sar1 is activated

To promote membrane budding, the Sar1 GTPase requires GTP. Its exchange from GDP to GTP is facilitated by a Sar1-specific ER-localised guanine nucleotide exchange factor (GEF), Sec12 (Nakano, Brada and Schekman, 1988; Barlowe *et al.*, 1994; Weissman, Plutner and Balch, 2001; Bielli *et al.*, 2005). Sec12 is a transmembrane ER-resident protein with a prominent solenoid-fold cytoplasmic domain that binds Sar1 when stabilised by a potassium ion (McMahon *et al.*, 2012). Sar1 possesses an N-terminal helix that is essential for interaction with Sec12, as a 25-residue-amino-terminal truncation of Sar1 is incapable of Sec12 binding (Huang *et al.*, 2001). Sar1-GTP distribution and subsequent COPII vesicle formation is thereby spatially limited to the ER by Sec12 (Barlowe, 2003).

GTP binding introduces a conformational change in Sar1, which exposes its amphipathic N-terminal 25-residue helix that inserts into the outer leaflet of the ER membrane (Goldberg,

1998; Huang *et al.*, 2001; Bi, Corpina and Goldberg, 2002; Bielli *et al.*, 2005; Rao *et al.*, 2006; Hutchings *et al.*, 2018). Membrane curvature has been proposed to be a result of the asymmetric insertion of Sar1 into the outer, but not the inner membrane leaflet. This mechanism is termed 'bilayer coupling' and is based on the difference in composition between the two membrane leaflets. This asymmetry gives rise to membrane fluidity and an expansion of the outer membrane layer as compared to the inner layer, resulting in curvature induction (Sheetz and Singer, 1974; Huttner and Zimmerberg, 2001; Zimmerberg and McLaughlin, 2004). However, the insertion of amphipathic helices can generate curvature even on lipid monolayers (Kinuta *et al.*, 2002). An proposed alternative to the bilayer coupling mechanism is curvature generation through the restructuring of local lipid arrangement by the insertion of the amphipathic helix (McMahon and Gallop, 2005). The insertion of yeast Sar1 into the membrane has been directly visualised by cryo-electron tomography and subtomogram averaging, showing a 90° kink in the helix into the outer membrane leaflet (Hutchings *et al.*, 2018). The generated curvature could result from the asymmetric expansion of the outer leaflet or from local lipid rearrangement.

Sar1 can not only induce, but also sense membrane curvature, as it has been observed that purified Sar1 has a greater affinity for artificial membranes of high curvature *in vitro* (Hanna *et al.*, 2016). This is another factor, apart from the GDP-GTP exchange performed by Sec12, that limits Sar1 binding to ERES. The high local curvature of the ERES is proposed to be maintained by Sar1 and the essential ER-resident factor Sec16, which stabilises the GTP-bound state of Sar1 that binds the membrane (Supek *et al.*, 2002; Watson *et al.*, 2006). Regardless of the greater affinity of Sar1 for highly curved membranes, membrane models of varying curvatures, such as synthetic liposomes and giant unilamellar vesicles (GUVs), have supported yeast Sar1 binding and yeast COPII budding in *in vitro* studies (Lee *et al.*, 2004; Bacia *et al.*, 2011).

Sar1 plays multiple roles in COPII vesicle formation, including the sensing and induction of membrane curvature, and the recruitment of the rest of the COPII machinery. These two functions are seemingly independent, as a truncated form of yeast Sar1 that is deficient in inducing membrane curvature (lacking the N-terminal amphipathic helix), but binds to the membrane through an engineered tether, can still recruit COPII components (Lee *et al.*, 2004). Additionally, Sar1 is involved in the scission of the COPII vesicle from the ER membrane (Bielli

et al., 2005; Lee *et al.*, 2005; Hariri *et al.*, 2014). It has been proposed that Sar1 is concentrated at vesicle necks, due to its greater affinity for high curvature (Hariri *et al.*, 2014; Hanna *et al.*, 2016). The high local Sar1 concentration has been implicated in the disruption of local lipid packing, enabling vesicle scission (Bielli *et al.*, 2005; Lee *et al.*, 2005). Finally, GTP hydrolysis by Sar1 regulates the lifespan of COPII carriers, as Sar1 dissociates from the membrane upon GTP hydrolysis. This results in the eventual disassembly of COPII vesicles, as discussed in Section I.2.5. (Yoshihisa, Barlowe and Schekman, 1993; Antonny *et al.*, 2001).

I.2.2. Sec23/24 is recruited by Sar1

GTP-bound Sar1 recruits cytosolic Sec23/24 heterodimers by directly interacting with Sec23. Sec23/24 serves as a molecular adapter and binds cargo, increases membrane curvature, and recruits Sec13/31 (Matsuoka *et al.*, 1998; Russell and Stagg, 2010). The Sec23/24 dimer possesses a basic concave surface, which has been proposed to induce deformation of the ER membrane through electrostatic interactions with acidic membrane phospholipids (Bi, Corpina and Goldberg, 2002). Indeed, when the effects of different membrane lipid composition on interaction with the Sec23/24-Sar1 complex was tested using synthetic liposome models, a proportion of acidic phospholipids proved essential (Matsuoka *et al.*, 1998). In yeast, the curvature of the basic underside of Sec23/24 is compatible with the range of curvatures of COPII vesicles, which suggests that the shape of vesicles can be accommodated or moulded by the inner coat proteins (Bi, Corpina and Goldberg, 2002). Whether the inner coat is aided by the outer coat in inducing and maintaining COPII vesicle curvature is unclear (Barlowe *et al.*, 1994; Bi, Corpina and Goldberg, 2002).

The inner COPII coat is not only involved in establishing and supporting membrane curvature, but also in modulating the GTP cycle of Sar1. The GAP Sec23 specifically stimulates GTP hydrolysis by Sar1, and not by other related GTPases (Yoshihisa, Barlowe and Schekman, 1993). Under the GAP activity of yeast Sec23, yeast Sar1 hydrolyses GTP 10-15 times faster than its intrinsic rate (Yoshihisa, Barlowe and Schekman, 1993; Barlowe *et al.*, 1994; Oka and Nakano, 1994). As GTP hydrolysis by Sar1 leads to COPII disassembly, the recruitment of Sec23/24 is also the first step towards COPII disassembly (Section I.2.5) (Antonny *et al.*, 2001).

I.2.3. Sec23/24-Sar1 captures cargo

The Sar1-Sec23/24 ‘pre-budding complex’ recognises and recruits cargo destined for ER export. In yeast, Sec24 has been established as the main cargo adapter, although Sar1 and

Sec23 are also involved in the capture of some cargo and adapter proteins (Pagano *et al.*, 1999; Aridor *et al.*, 2001; Miller *et al.*, 2002, 2003; Mancias and Goldberg, 2007; Ma and Goldberg, 2016). The cytosolic portion of transmembrane cargo proteins is recognised either directly by Sec24 or by cargo adapters, while cargo in the ER lumen interacts with Sec24 through ER-resident transmembrane adapters (Barlowe, 2003). The cargo selectivity of Sec24 is determined by cytosolic ER exit signals (Mancias and Goldberg, 2008). In higher eukaryotes, analysis of the transport efficiency of the ERGIC-resident reporter protein ERGIC-53 fused to different exit signals showed that transport of cargoes with a particular signal is mediated by specific, albeit in part redundant, Sec24 paralogues (Wendeler, Paccaud and Hauri, 2007). The four different paralogues of Sec24 in mammalian cells have different affinities for specific cargo export sequences (Pagano *et al.*, 1999; Mancias and Goldberg, 2008). Different transport signal binding sites on Sec24 and one on the Sec23/24 interface have been mapped for a range of exit signals (Bonifacino and Glick, 2004). The full range of signals that can be differentially identified remains to be explored. Due to the diversity of cargo shapes, sizes, and surface charges, nascent carrier formation must be coupled to cargo recognition by the Sar1-Sec23/24 complex and further regulated by additional factors (Section I.5.2). However, how specific cargo recognition informs and modulates COPII vesicle formation is unclear.

In yeast, Sec23/24 binding to cargo assists the retainment of the complex on the membrane even after GTP hydrolysis by Sar1 (Sato and Nakano, 2005). Retaining the inner coat on vesicles after the dissociation of Sar1 can be of functional importance, both for the maintenance of vesicle curvature (Section I.2.2) and for fusion with the target membrane (Section I.2.5) (Cai *et al.*, 2007).

I.2.4. Sec13/31 is recruited

The Sec23/24-Sar1 complex recruits cytosolic Sec13/31 heterotetramers, which do not directly interact with the membrane. They assemble to form the outer COPII coat, overlaying the inner Sec23/24 coat (Matsuoka *et al.*, 2001). Sec31 interacts with the inner COPII coat through a disordered C-terminal proline-rich domain (PRD) (Bi, Mancias and Goldberg, 2007; Ma and Goldberg, 2016; Stancheva *et al.*, 2020). Sec13/31 can provide structure to the COPII vesicle (Barlowe *et al.*, 1994; Stagg *et al.*, 2006; Noble *et al.*, 2013), but also concentrate Sec23/24 heterodimers (Ma and Goldberg, 2016; Hutchings *et al.*, 2018). Furthermore, Sec13/31 affects Sar1 GTP hydrolysis by directly modulating Sec23 GAP activity. In yeast, the

GTP hydrolysis activity of Sar1 in the presence of Sec23/24 is enhanced ten-fold by Sec13/31. Hence, Sec13/31 promotes vesicle uncoating (Yoshihisa, Barlowe and Schekman, 1993; Antonny *et al.*, 2001). Therefore, while recruitment of the outer coat is the last step of COPII assembly, it also constitutes a major driver of coat disassembly.

I.2.5. COPII vesicles bud from the ER and fuse with the ERGIC

The mechanism of COPII vesicle scission from the ER is unclear, and the role of GTP hydrolysis in this process has been the subject of much debate. Some studies have suggested that GTP hydrolysis is not essential for vesicle formation. In these studies, semi-intact cells or liposome budding assays were used, and COPII vesicles were harvested by fast centrifugation (Oka and Nakano, 1994; Adolf *et al.*, 2013), which can potentially result in spontaneous vesicle fission, especially of membranes that are deformed and constricted by COPII. Contrasting observations show that GTP-locked Sar1 and Sar1 complexed with a non-hydrolysable GTP analogue are incapable of forming vesicles from semi-permeabilised cells (Schindler and Schekman, 2009).

GTP hydrolysis is central to the dissociation of the COPII coat following scission from the ER (Antonny *et al.*, 2001). When Sar1 hydrolyses GTP, as stimulated by the inner and outer COPII coats, it undergoes a conformational change and retracts its N-terminal helix from the membrane, resulting in its dissociation (Antonny et al. 2001). However, multiple lines of evidence suggest that Sec23/24 complexes remain associated with the membrane even in the absence of Sar1-GTP. In fact, the potential retainment of the inner COPII coat on vesicles has a functional significance, as Sec23 has been shown to mediate vesicle tethering in yeast (Cai *et al.*, 2007).

Sec23 directly interacts with Bet3, a sub-component of the transport protein particle I (TRAPPI) tethering complex. TRAPP complexes are required for Golgi fusion of COPII vesicles in yeast. Three forms of TRAPP (TRAPPI, II, and III) have been identified, with TRAPPI mostly implicated in vesicle tethering through Sec23 (Cai *et al.*, 2007). The interaction between Sec23 and the TRAPPI tethering complex mediates fusion of COPII vesicles with each other or with the acceptor Golgi compartment (Barlowe, 1997; Cai *et al.*, 2007; Lord *et al.*, 2011; Szul and Sztul, 2011). The TRAPP-Sec23 interaction suggests a need for outer coat disassembly for vesicle fusion with other vesicles or the acceptor membrane. The factor that is proposed to promote this disassembly in mammals is Trk-fused gene (TFG), a protein that assembles into

oligomers and colocalises with COPII carriers (Hanna *et al.*, 2017). Following vesicle scission from the ERES, TFG could outcompete the outer COPII coat through direct interaction with the inner coat. This could retain carriers at the ERGIC, restricting their diffusion, and allow for vesicle fusion with the ERGIC through exposing the inner coat to TRAPPI machinery (Hanna *et al.*, 2017).

Further evidence that suggests that COPII components could remain associated with vesicles after Sar1 disassociation is that Sec23/24 and Sec13/31 can self-assemble in the absence of Sar1-GTP, as established with purified human proteins (Stagg *et al.*, 2008). This underlines the strength of the interactions between COPII components in the absence of Sar1. Together with the observation that cargo stabilises Sec23/24 on the membrane (Section I.2.3), these findings suggest that Sar1 GTP hydrolysis and dissociation could precede the complete uncoating of the COPII vesicle.

GTP hydrolysis is essential for the completion of vesicle transport, as fusion with the Golgi apparatus is only efficient in vesicles generated with GTP, and not with non-hydrolysable GTP analogues (Barlowe, d'Enfert and Schekman, 1993; Oka and Nakano, 1994). Ultimately, after coat depolymerisation, COPII components diffuse back to the ER to form new carriers (Forster *et al.*, 2006).

I.3. COPII in the Export of Large Cargo

Canonical COPII vesicles are 60-80nm in diameter, as observed by thin section electron microscopy (EM) of *in vitro* reconstituted vesicles and *in situ* using immuno-electron tomography (Barlowe *et al.*, 1994; Zeuschner *et al.*, 2006). It has been proposed that their size is determined by the outer coat proteins, which self-assemble *in vitro* into cages of the same range of sizes (Antonny *et al.*, 2003; Stagg *et al.*, 2006). The size of canonical vesicles would not allow them to accommodate the large molecules that mammalian cells need to secrete, such as the elongated precursor of collagen, procollagen (300nm), prechylomicrons (75-450nm), laminin (120nm), and mucins (up to 300nm) (Saito *et al.*, 2009; Kesimer and Sheehan, 2012; Santos *et al.*, 2016). The export of these large cargoes is important for the functioning of mammalian organisms. Procollagens are trimeric helical assemblies, precursors of the fibrous collagen proteins, which are the main structural components of the extracellular matrix, forming 30% of human body protein dry weight (Bachinger *et al.*, 1982;

Junqueira and Carneiro, 2005). While procollagen molecules have traditionally been seen as inflexible rods, atomic force microscopy experiments have suggested that procollagen is best described as "semiflexible", with varying degrees of flexibility depending on pH and salt concentration (Rezaei, Lyons and Forde, 2018). Prechylomicrons are precursors of chylomicrons, lipoproteins found in the blood stream that are essential for efficient fat absorption (Hussain, 2000). Laminins are components of the extracellular matrix, regulating cell adhesion and differentiation (Petley-Ragan *et al.*, 2016). Mucins are the major constituent macromolecules of mucus, crucial for the protection of respiratory epithelia (Voynow and Fischer, 2006). COPII components are essential for large cargo export in *Caenorhabditis elegans*, *Drosophila melanogaster*, zebrafish, mice, and human immortalised cells (Roberts, Clucas and Johnstone, 2003; Lang *et al.*, 2006; Townley *et al.*, 2008; Pastor-Pareja and Xu, 2011; Zhu *et al.*, 2015). Certain mutations in specific paralogues of Sec23, Sec24, and Sar1 lead to dysfunctions in the secretion of large cargoes such as procollagens and prechylomicrons and are therefore implicated in genetic disease (Jones *et al.*, 2003; Boyadjiev *et al.*, 2006, 2011; Fromme *et al.*, 2007; Garbes *et al.*, 2015). This is probably due to an inability of COPII carriers formed with mutant variants of COPII components to accommodate size requirements (Jones *et al.*, 2003; Boyadjiev *et al.*, 2006). The proposed molecular mechanisms behind these diseases are discussed in further detail in Sections I.5.1.1 (Sar1) and I.5.1.2 (Sec23/24). While COPII proteins are essential for the export of large cargo, their precise role has been a matter of debate. COPII components have been proposed to form large carriers to accommodate large secretory cargo (discussed below), or to play an indirect role in large cargo export (see Section I.4) (Fromme and Schekman, 2005).

If COPII vesicles were to incorporate large cargo, a different, 'non-canonical' COPII packaging arrangement is necessary. Models for large COPII vesicles have been proposed from observations of *in vitro* reconstituted systems with purified yeast proteins and donor membranes. To delay coat dissociation, those studies suppress GTP hydrolysis by using non-hydrolysable GTP analogues, or the GTP hydrolysis-incompetent yeast Sar1-H77L mutant. Incubating membrane donors with purified COPII proteins in the absence of GTP hydrolysis results in long coated tubules emanating from the membrane donor (Bacia *et al.*, 2011; Zanetti *et al.*, 2013; Daum *et al.*, 2014; Hutchings *et al.*, 2018). COPII *in vitro* reconstitution studies have utilised cryo-electron tomography and subtomogram averaging to gain

structural insight into the assembled COPII tubules (Zanetti *et al.*, 2013; Hutchings *et al.*, 2018). In the absence of GTP hydrolysis by yeast Sar1, yeast Sec23/24-Sar1 heterotrimers form a lattice of helical arrays (Zanetti *et al.*, 2013; Hutchings *et al.*, 2018). This establishes the role of the inner coat not only as an adaptor/recruiter, but also as a structural determinant of membrane morphology. The inner coat lattice determines the orientation of Sar1 with respect to the membrane and templates an arrangement of Sar1 molecules that results in a parallel insertion of Sar1 helices. The helices are shallowly inserted into the outer leaflet of the membrane and then bend at approximately 90°, so that the bent regions align to the long axis of the tube. This enables the generation of membrane curvature (Hutchings *et al.*, 2018). The assembly of the inner coat lattice is promoted by its interaction with the outer coat components. Sec31 contains a proline rich domain (PRD) with multiple triple proline (PPP) motifs, and each PPP motif can bind the gelsolin-like domain of Sec23 (Ma and Goldberg, 2016). In this way, the PRD of Sec31 bridges adjacent Sec23/24 heterodimers, enabling their arrangement into an lattice (Hutchings *et al.*, 2018). It has been demonstrated that the outer coat can be flexible, as it can coat spherical or tubular membranes and form different polyhedral geometries when assembled *in vitro* depending on the presence or absence of an inner coat (Stagg *et al.*, 2006, 2008). The flexible properties of COPII lattices, both individually and in respect to each other, demonstrate potential for accommodating a large range of cargo (Stagg *et al.*, 2006, 2008; Zanetti *et al.*, 2013).

The regulation of the size of COPII carriers is linked to the regulation of the GTPase cycle of Sar1. As GTP hydrolysis by Sar1 results in coat dissociation, delaying this process can allow for the growth of a larger carrier (Antonny *et al.*, 2001). Several lines of evidence suggest that this proposed mechanism is relevant not only in *in vitro* reconstitutions, as discussed above, but also *in vivo*. In humans, the Sar1B paralogue is implicated in the export of large cargo (Shoulders, Stephens and Jones, 2004; Levic *et al.*, 2015; Sané *et al.*, 2019). Sar1B has a lower affinity for Sec31 when complexed with Sec23 compared to Sar1A, hence GTP hydrolysis by Sar1B could be stimulated less strongly by the COPII components (Section I.5.1.1.) (Fromme *et al.*, 2007). This paralogue could therefore allow for larger carrier growth by promoting slower coat dissociation.

Furthermore, the large cargo adapter Tango1, which enables procollagen export, is proposed to function by delaying GTP hydrolysis by Sar1 (Saito *et al.*, 2009; Malhotra and Erlmann,

2011). Tango1 interacts with Sec23 through its PPP motifs, similarly to, and perhaps in competition with, Sec31 (Ma and Goldberg, 2016). The GAP activity of Sec23 towards Sar1 would not be stimulated by Sec31 when Tango1 is bound, therefore coat dissociation would be delayed, allowing for the formation of a larger carrier (Saito *et al.*, 2009; Malhotra and Erlmann, 2011). Furthermore, the PPP motifs of Tango1, similarly to those of Sec31, can template inner coat assembly. Tango1 is discussed in-depth in Section I.5.2.3.

I.4. Mammalian COPII Vesicles *in vivo*

COPII components are essential for anterograde intracellular transport in mammals (Lang *et al.*, 2006; Yang *et al.*, 2013; Wang *et al.*, 2018). However, the existence of free mammalian COPII vesicles *in vivo* has been challenged, unlike that of COPII vesicles in yeast, which is universally accepted (Fromme and Schekman, 2005; Watson and Stephens, 2005). Mammalian COPII proteins have been suggested to organise the ERES and concentrate cargo, rather than coat transport carriers (Mironov *et al.*, 2003; Siddiqi, 2003). Scepticism is largely founded on concerns that COPII vesicles cannot accommodate the large cargoes exported from mammalian cells (Fromme and Schekman, 2005).

Staining studies of mammalian fibroblast cells, which secrete high amounts of collagen, have shown retainment of COPII at the ER and no association of COPII with secreted collagen cargo carriers (Mironov *et al.*, 2003). These observations were based on immunofluorescence and immunogold electron microscopy experiments which utilised a polyclonal antibody against a synthetic peptide from human collagen. However, a subsequent analysis using two separate monoclonal antibodies against collagen showed collagen colocalization with COPII (Gorur *et al.*, 2017). The authors of the latter study suggest that previous use of the polyclonal antibody raised against mature collagen might have prevented the detection of the procollagen species from the early secretory pathway (Gorur *et al.*, 2017). Correlative video/light electron microscopy and tomography have also been used to identify COPII-free procollagen carriers dissociated from the ER (Mironov *et al.*, 2003). Since it remains unclear how long the COPII coat is retained on vesicles after fission from the ER in live cells, it is possible that the vesicles were already uncoated at the time of observation.

Evidence in favour of a COPII vesicle model was derived from a combination of immuno-gold COPII labelling and electron cryo-electron tomography that showed COPII vesicles in fixed

HepG2 cells (Zeuschner *et al.*, 2006). The case was strengthened by a stochastic optical reconstruction microscopy study, where large COPII-coated procollagen carriers were observed in live cells (Gorur *et al.*, 2017). *In situ* microscopy studies at a high resolution can provide further insight into the precise role of COPII in mammalian anterograde vesicular transport.

I.5. Molecular Mechanisms of COPII

The COPII secretion system functions through the synergistic action of the COPII components, which polymerise to form higher order structures in the context of the intracellular environment. Hence, gaining an understanding of the complexities of COPII requires investigations on a spectrum of scales: from the structures of individual components and subcomplexes, to the structures of COPII assemblies, to the biochemical interactions of COPII components in the wider context of the cellular environment. Structures of individual COPII subunits and subcomplexes have been elucidated through X-ray crystallography and electron microscopy, providing valuable insight into the molecular foundations of COPII component function. COPII complexes have been studied by electron microscopy, shedding light on global mechanisms of assembly. The interactions of COPII components have been investigated in depth in biochemical and genetic studies. Finally, studies of the multiple paralogues of COPII components in mammals, some of which have diverged in function, have deepened our understanding of the fundamental mechanisms of paralogue-specific pathologies (Boyadjiev *et al.*, 2006; Fromme *et al.*, 2007; Kim *et al.*, 2012; Chen *et al.*, 2013; Garbes *et al.*, 2015). The insight gained into the COPII system at different scales is described below.

Sar1

Sec23/24

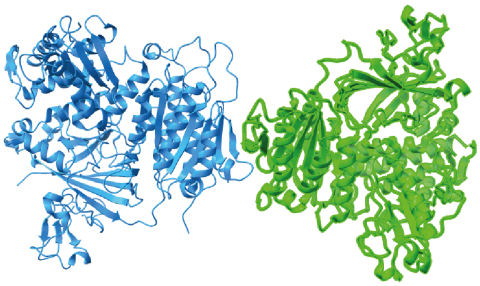

Sec13/31

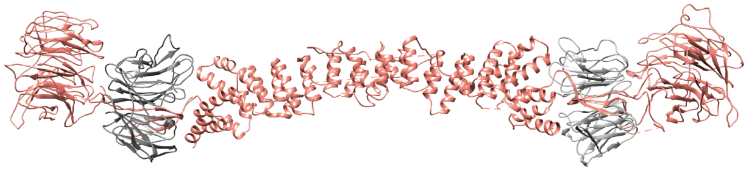

Figure 1.3: Available atomic models of the core COPII components. Crystal structure of human Sar1A-GDP (protein database identification code (PDB ID): 2gao). Crystal structure of the human Sec23A/24A heterodimer (PDB ID: 2nup). Atomic model of the yeast Sec13/31 heterotetramer, built from two crystal structures (PDB ID: 2pm6, 2pm9).

I.5.1. Core COPII components

I.5.1.1. The Sar1 GTPase

The agent that initiates vesicle formation and scission from the ER membrane is the small GTPase Sar1, which belongs to the adenosine diphosphate-ribosylation factor (ARF) family of the RAS superfamily (Nakano and Muramatsu, 1989; Yoshihisa, Barlowe and Schekman, 1993). The ARF family of GTPases are master regulators of the location of the budding process and the recruitment of COPII, COPI, and clathrin coats. They recruit the rest of the coat protein

complex in their GTP-bound form and are implicated in vesicle scission (Donaldson and Honda, 2005). Sar1 is a 22 kilodalton (kDa) magnesium-binding protein, composed of an N-terminal membrane-binding sequence, followed by a GTPase domain and C-terminal loop (Fig. 1.3, Fig.1.4) (Huang *et al.*, 2001).

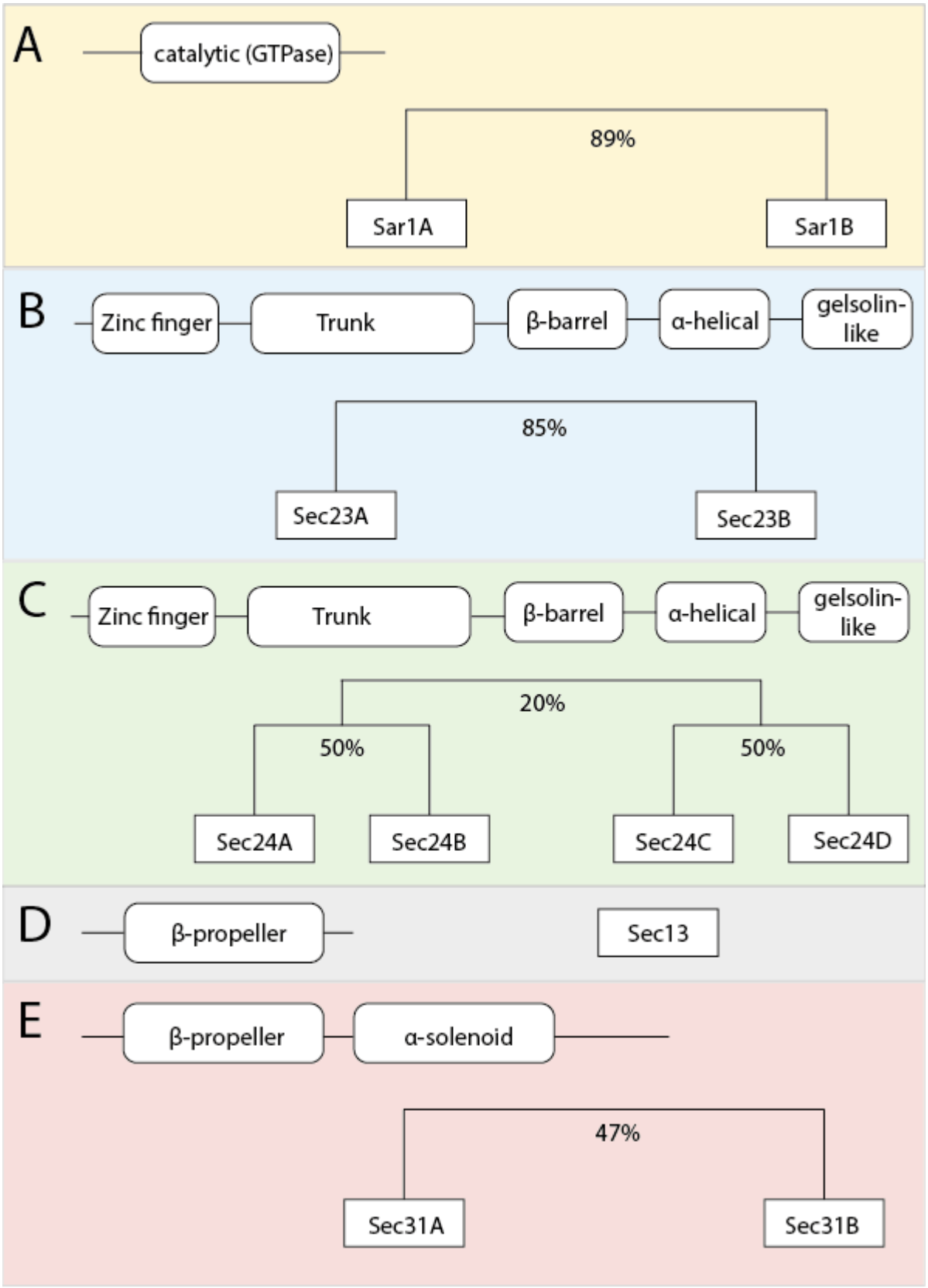

Figure 1.4: Domain structure and amino acid sequence similarity between paralogues of the human COPII secretion system subunits. Percentage similarities have been rounded up to the nearest whole number.

In vertebrates, there are two paralogues of Sar1, Sar1A and Sar1B, which are both competent in initiating COPII vesicle formation and differ in only 20 of 198 amino acids (Fig.1.4, Fig. 1.5) (Kuge *et al.*, 1994). However, the paralogues exhibit functional differences, as Sar1B, but not Sar1A, mutations are implicated in human disease (Jones *et al.*, 2003). Since Sar1A-Sec23/24 has a higher affinity for Sec13/31, Sec13/31 might stimulate the GAP activity of Sec23/24 on Sar1A more strongly, thereby resulting in faster GTP hydrolysis rates by Sar1A than by Sar1B (Fromme *et al.*, 2007). This could result in faster coat disassembly and the formation of smaller carriers with Sar1A. Sar1A is therefore proposed to participate in the formation canonical 60-90nm-sized COPIII vesicles for the transport of small cargo (Fromme, Orci and Schekman, 2008). Sar1B, on the other hand, is thought to specialise in the formation of larger carriers, as suggested by its implication in hereditary disorders caused by large cargo secretion deficits (Jones *et al.*, 2003). In these disorders, missense mutations of Sar1B result alter amino acid residues in its highly conserved GTP-binding pocket, rendering it incapable of GTP binding and therefore inactive (Jones *et al.*, 2003). Chylomicron retention disease (CMRD) is an early-onset autosomal recessive disease linked to Sar1B mutations, which cause a defect in the trafficking of chylomicrons (Jones *et al.*, 2003). The disease manifests in low cholesterol levels in the blood and an inability to absorb fats and fat-soluble vitamins D and E (Jones *et al.*, 2003). No mutations in Sar1A have been associated with the disease, underlining the specific role of Sar1B in the transport of the large chylomicron cargo.

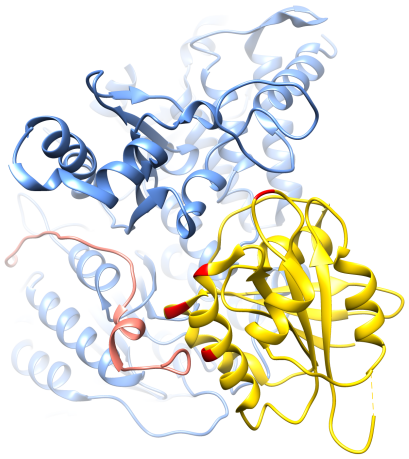

Figure 1.5: Differing residues (red) between Sar1A and Sar1B that lie on the interaction interface of Sar1 (yellow) with Sec23 (blue) and with Sec31 (pink). The crystal structure of yeast Sar1/Sec23/Sec31 was used (PDB ID: 2qtv). The sequences of yeast Sar1 and human Sar1A and Sar1B were aligned with Clustal Omega (Sievers *et al.*, 2011).

In vitro, Sar1 is capable of curving membranes in the absence of the other COPII components. Addition of Sar1 to artificial membranes yields two kinds of membrane deformation: soft tubular formations and rigid tubes, covered by protofilament-like organised lattices (Long *et al.*, 2010; Bacia *et al.*, 2011; Hariri *et al.*, 2014). When the structure of the tubes was analysed, dimers of Sar1 arranged in a lattice were observed (Hariri *et al.*, 2014). The role of Sar1 dimerisation *in vivo* remains uncharacterised. However, its potential importance is elucidated by the available hamster Sar1-GDP crystal structure, which also reveals a Sar1-GDP dimer (Huang *et al.*, 2001). It is unclear if the dimerisation observed in the crystal structure is physiologically relevant, or an artefact resulting from the high protein concentrations used for crystallisation. Whether Sar1 membrane deformation in the absence of the rest of the COPII machinery is relevant *in vivo* or is an *in vitro* artefact also remains to be established.

I.5.1.2. Sec23/24

Sec23/24 is a bow-shaped cytosolic dimer that contributes to deformation of the ER membrane upon recruitment by Sar1 (Yoshihisa, Barlowe and Schekman, 1993; Bi, Corpina and Goldberg, 2002).

Sec23 is a molecular hub that connects Sar1, Sec24, the outer COPII coat, and additional COPII adaptor proteins. Sec23 and Sec24 comprise of β-barrels, helical bunches, zinc-finger domains, and gelsolin-like repeats (Fig. 1.3, Fig. 1.4) (Bi, Corpina and Goldberg, 2002).

The interaction between Sar1 and the Sec23/24 heterodimer has been elucidated in two crystallographic studies – of Sar1-Sec23 and of Sar1-Sec23 complexed with a fragment of Sec31 - and a recent cryo-electron microscopy study (Bi, Corpina and Goldberg, 2002; Bi, Mancias and Goldberg, 2007; Hutchings *et al.*, 2018). Sar1 bound to the non-hydrolysable GTP analogue guanylyl imidodiphosphate, known as GMP-PNP, forms an extensive interface with Sec23, where an arginine side chain of Sec23 inserts into the Sar1 active site, promoting its GTPase activity (Bi, Corpina and Goldberg, 2002). Sec31 also converges with Sec23 at the Sar1 active site, stimulating the GAP activity of Sec23 (Bi, Mancias and Goldberg, 2007).

In vertebrates, there are two paralogues of Sec23, Sec23A and Sec23B, and four Sec24 paralogues, Sec24A-D. The two paralogues of Sec23, Sec23A and Sec23B, are 85% identical in sequence (Fig.1.4), but mutations in Sec23A and Sec23B have been implicated in distinct disease phenotypes. Mutations in Sec23A can cause cranio-lenticulo-sutural dysplasia (CLSD)

(Boyadjiev *et al.*, 2006). CLSD is an autosomal recessive bone formation disorder, resulting from defects in procollagen secretion that cause low bone density. Patient-derived fibroblasts have decreased collagen secretion efficiency and show an accumulation of biomolecules in the ER (Boyadjiev *et al.*, 2011; Kim *et al.*, 2012). Identified disease-causing mutations result in single amino acid substitutions in Sec23A, F382L and M702V, proximal to the binding site of the active fragment of Sec31 to Sec23. The binding of the active fragment accelerates the GAP activity of Sec23 towards Sar1 (Boyadjiev *et al.*, 2006; Fromme *et al.*, 2007; Kim *et al.*, 2012). When the efficiency of Sec23A-F382L to interact with the other COPII components was tested *in vitro*, Sec23A-F382L showed to be defective in the recruitment of Sec13/31 heterotetramers when Sar1B was used. This resulted in lack of vesicle formation. Sar1A could bind membranes and form vesicles with Sec23A-F382L, albeit with a lower efficiency, and Sec23A-F382L/Sec24 retained its GAP function towards Sar1A (Fromme *et al.*, 2007). These observations further underline the specific importance of Sar1B for large cargo export. The M702V mutation, on the other hand, did not affect Sec31 binding. Sec23-M702V was shown to stimulate the GTP hydrolysis rate of Sar1 further than wild-type Sec23. This resulted in premature dissociation of the COPII coat, blocking the export of procollagen (Kim *et al.*, 2012).

Mutations in Sec23B, and not Sec23A, are implicated in congenital dyserythropoietic anemias (Schwarz *et al.*, 2009). This heterogenous group of diseases results from the inefficient generation of red blood cells. The different phenotypes caused by Sec23A and Sec23B mutations *in vivo* could be the consequence of different expression patterns, as Sec23A can compensate for Sec23B deficiencies (Khoriaty *et al.*, 2017).

Sec23A is extensively regulated by post-translational modifications, including ubiquitylation and phosphorylation (Cohen *et al.*, 2003). Cysteine ubiquitylation sites on Sec23A are required for vesicle formation, and these modifications possibly affect the interaction of Sec23A with the membrane (Amodio *et al.*, 2017). ULK1, a kinase that is essential for multiple cell homeostasis pathways, such as autophagy and endocytosis, phosphorylates Sec23A at three different sites (Russell *et al.*, 2013; Gan *et al.*, 2017; Zhou *et al.*, 2017). This disrupts the interaction of Sec23A with Sec31 and inhibits ER to Golgi trafficking, probably due to lack of outer coat recruitment (Gan *et al.*, 2017). Furthermore, phosphorylation of Sec23 by a Golgi-resident kinase in yeast is implicated in vesicle fusion with the Golgi (Lord *et al.*, 2011).

The functional differences between the four Sec24 paralogues, Sec24A-D, have been studied using knock-out models in mice. Sec24A is non-essential, and its deletion results in normal mice with 40% plasma cholesterol reduction (Chen *et al.*, 2013). Sec24B knock-out mice only live up to birth and die due to craniorachischisis, a disorder in which both the brain and the neural tube remain open (Yang *et al.*, 2013). Sec24C and Sec24D deletions are embryonic lethal (Baines *et al.*, 2013; Adams *et al.*, 2014). Osteogenesis imperfecta, a bone formation disorder that is associated with defects in collagen secretion, can be caused by Sec24D mutations (Garbes *et al.*, 2015). When patient-derived fibroblasts were observed by electron microscopy, the deformation of ER domains compared to control fibroblasts from a healthy donor was visible (Garbes *et al.*, 2015). ER domains were distended, suggesting that the Sec24D mutation could affect general ER export. However, the efficiency of small cargo export was not measured. Hence, it remains unclear whether the decrease in procollagen export in osteogenesis imperfecta is due to a global decrease in export efficiency, or due to the specific importance of Sec24D for large cargo export. Experiments performed on cartilage cells isolated from zebrafish embryos provide further insight into the role of Sec24D in the export of large cargo (Sarmah *et al.*, 2010). Isolated cartilage cells with Sec24D mutations were observed using fluorescent labelling and microscopy. While type II collagen was not secreted from these cells, ER export of small membrane-bound cargoes was unaffected. This suggests that Sec24D is specifically involved in the export of large cargo (Sarmah *et al.*, 2010). Further evidence for this was obtained from studies of the expression patterns of different Sec24 paralogues in meduka fish using ribonucleic acid (RNA) *in situ* hybridisation (Ohisa *et al.*, 2010). Sec24D was preferentially expressed in the notochord and craniofacial cartilage, tissues rich in extracellular matrix components, such as collagen, while Sec24A-C isoforms were expressed ubiquitously.

Crystal structures of all four human Sec24 paralogues are available, complementing *in vivo* mutagenesis studies and providing insight into cargo recognition patterns (Mancias and Goldberg, 2008). Those exclude the highly variable N-terminal region of Sec24, which is disordered in crystal structures (Pagano *et al.*, 1999; Bi, Corpina and Goldberg, 2002).

In yeast, the regulation of Sec24 by glycosylation and phoshorylation has been demonstrated. Sec24 is unable to bind membranes in its deglycosylated and phosphorylated form, which has been proposed to regulate COPII trafficking during mitosis (Dudognon *et al.*, 2004).

I.5.1.3. Sec13/31

Sec13/31 are cytosolic heterotetramers, recruited to the pre-budding complex (Sar1-Sec23/24) through the unstructured C-terminal proline-rich region of Sec31 that interacts with Sec23 (Fath *et al.*, 2007). Sec13 and Sec31 form 150nm long elongated tetramers, or 'rods', which are the building blocks of outer coat polymers. Each tetramer consists of two Sec13/31 dimers that interact via the central α-solenoid domains of Sec31 (Stagg *et al.*, 2006, 2008). Each Sec13/31 dimer is formed by a strong interaction between Sec13 and Sec31: the two proteins fold together into a β-propeller, in which six blades, or WD40 repeats, are formed by the entire Sec13 molecule, and one blade is provided by a linker region of Sec31 (Fig. 1.6A) (Stagg *et al.*, 2006; Hsia *et al.*, 2007). The N-terminal domain of Sec31 forms another β-propeller domain, which constitutes the rod tips and mediates the interaction between rods, forming the 'vertices' of the assembly (Stagg *et al.*, 2006; Fath *et al.*, 2007; Zanetti *et al.*, 2013). At these vertices, the ends of two Sec13/31 rods interact directly with each other via their β-propeller domains (referred to as the 'plus ends' of the rods), while the ends of two other Sec13/31 rods (the 'minus' ends) contact them at the side (Fig. 1.6B) (Stagg *et al.*, 2008; Noble *et al.*, 2013; Zanetti *et al.*, 2013). The angles between the plus and minus ends of the rods at vertices can vary to allow for versatility of coat architecture. It has been proposed that the different conformations of Sec31 that enable the formation of 'plus' and 'minus' rod ends are dictated by a different extent of interaction between Sec13 and the α-solenoid domains of Sec31 (Noble *et al.*, 2013).

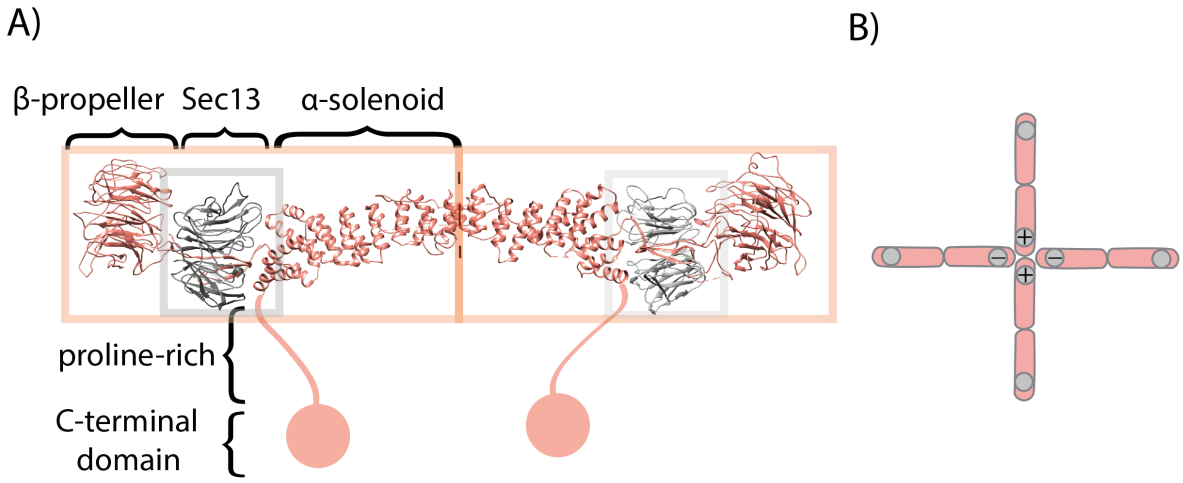

Figure 1.6: Domain organisation of Sec13/31 heterotetramers and their global arrangement in lattice formation. (A) Sec13/31 heterotetramers are formed by the interlocking of the α-

solenoid domains of Sec31 (atomic model from yeast, PDB ID: 2pm6). The structure of the C-terminal portion of Sec31, which includes the proline-rich region and the C-terminal domain, remains unresolved. (B) The arrangement of Sec13/31 heterotetramers at lattice vertices. 'Plus' ends contact each other directly, while 'minus' ends attach at the sides of vertices.

Significant structural insight was gained from studies of purified human Sec13/31, which can self-assemble *in vitro* in the absence of Sec23/24 and membrane (Stagg *et al.*, 2006; Noble *et al.*, 2013). The Sec13/31 assemblies, cages of 600Å diameter with cuboctahedral geometry, have been characterised by electron microscopy (Stagg *et al.*, 2006; Noble *et al.*, 2013). Sec13/31 assemblies have also been examined as assembled *in vitro* in the presence of Sec23/24, where they show a very similar packing arrangement to the Sec23/24-free cage (Stagg *et al.*, 2008). While, in this case, the majority of cages assemble as icosidodecahedrons, the underlying contacts described above - both the β-propeller vertex and the α-solenoid dimerisation interface - remain the same. This suggests that that the intrinsic flexibility of the outer cage is sufficient to tolerate different vesicle sizes (Stagg *et al.*, 2008). The extent of the flexibility of the outer coat was demonstrated in *in vitro* reconstitution assays using yeast proteins (Zanetti *et al.*, 2013). Purified Sec13/31 proteins were incubated with the inner coat components and Sar1 in the presence of membranes and a non-hydrolysable GTP analogue, added to retain the COPII components on the membrane. Using cryo-electron tomography, long tubules were observed protruding from the membrane donors, where the outer coat was organised in a rhomboidal lattice, coating the surface of the tubes. The contacts enabling the formation of the outer coat lattice were similar to those described for COPII cages. An essential difference in conformation that allowed the formation of tubular lattices was the 'hinge' angle in the middle of Sec13/31 rods. While in spherical cages, this angle was approximately 45˚, it was approximately 15˚ in the rhomboid lattice. Variations in this angle and the angles at which Sec13/31 rods contact each other at vertices can provide incredible versatility to the outer COPII coat, enabling it to create a wide range of shapes to accommodate cellular trafficking requirements.

In yeast, Sec13 is essential for cargo secretion, but this requirement can be circumvented by a genetic background that is proposed to have a decreased local cargo load, rendering the membrane easier to deform (Čopič *et al.*, 2012). This suggests that the membrane-remodeling

capabilities of Sec31 are increased by Sec13 *in vivo* and supports the insight gained from structural studies with human proteins: that Sec13 serves to provide rigidity to outer coat rods, here enabling the remodelling of cargo-loaded membranes (Čopič *et al.*, 2012; Noble *et al.*, 2013).

The domains forming the Sec13/31 coat are typical of vesicular carriers. Both clathrin adaptor proteins and COPI utilise connected β-propeller-α-solenoid domains. Also called 'protocoatomers', these domains reflect a common evolutionary origin, also shared by the ancient nuclear pore complex (Lee and Goldberg, 2010; Dodonova *et al.*, 2015).

Two paralogues of Sec31, Sec31A and Sec31B, and only one Sec13 are present in mammalian cells. Sec31A and Sec31B have 47% sequence similarity. Sec31A is 26% similar to the only yeast Sec31 paralogue, Sec31p, while Sec31B is 19% similar to Sec31p (Fig. 1.4). Sec31B relies on alternative splicing to produce a range of transcripts, which can be grouped in a short-form and a long-form family. The long form (Sec31B-F) is similar to Sec31A and Sec31p. Sec31B-T, the short form, remains uncharacterised, but is unlikely to participate in the formation of the COPII coat because it lacks the C-terminal proline-rich region necessary for the Sec23-Sec31 interaction (Stankewich, 2006).

I.5.2. Additional COPII-interacting partners

I.5.2.1. Sec12

In yeast, Sec12, the GEF of Sar1, is essential for COPII vesicle formation *in vivo* (Barlowe and Schekman, 1993). Sec12 was identified as a transmembrane glycoprotein with a prominent cytoplasmic domain (Nakano, Brada and Schekman, 1988; D'Enfert *et al.*, 1991). In *in vitro* biochemical studies of both yeast and mammalian systems, the requirement for Sec12 has been circumvented by using Sar1 pre-equilibrated with GMP-PNP (Matsuoka *et al.*, 1998; Hariri *et al.*, 2014). This suggests that the contribution of Sec12 to COPII vesicle formation *in vitro* is limited to its GEF function. Sec12 is not packaged into nascent COPII vesicles but is retained in the ER, ensuring the localisation of Sar1 GTP loading (Weissman, Plutner and Balch, 2001). In mammalian cells, Sec12 binds Sec16A, a peripheral membrane protein that associates with the ERES (Section I.5.2.2.). Sec16A has been hypothesised to contribute to Sec12 concentration in ERES (Montegna *et al.*, 2012). Sec12 could also be recruited to the ERES by cTAGE5, an interacting partner of Tango1, as discussed below.

I.5.2.2. Sec16

Sec16 is an essential protein that stably localises to the transitional ER in yeast and interacts with Sec23, Sec24, and Sec13 (Espenshade *et al.*, 1995; Gimeno, Espenshade and Kaiser, 1996). Sec16 has been proposed to act as a template for Sec13/31 assembly, as its interaction with Sec13 forms an interface reminiscing of that between Sec13 and Sec31 (Whittle and Schwartz, 2010). Homologues of Sec16 have been identified in mammalian cells – Sec16A, which has a short (Sec16S) and a long (Sec16L) isoform, and Sec16B. The short and the long Sec16A isoforms colocalise and form heteromeric assemblies that are essential to the formation of ERES (Bhattacharyya and Glick, 2007).

I.5.2.3. Tango1/cTAGE5

Transport-and-Golgi Organisation 1 (Tango1) is a transmembrane cargo adapter family from the melanoma inhibitory activity/cutaneous T-cell lymphoma-associated antigen (MIA/cTAGE) gene family (Bosserhoff, Moser and Buettner, 2004). Tango1 proteins localize at ERES and are conserved throughout metazoans but absent in yeast. They are proposed to enable the ER export of cargo that is too large to fit in canonical COPII vesicles, including collagen, laminin, and prechylomicrons (Saito *et al.*, 2009; Santos *et al.*, 2016). Tango1 can interact with procollagen and is proposed to form elaborate cellular machinery to regulate COPII assembly, enabling the formation of large carriers (Saito *et al.*, 2009; Wilson *et al.*, 2011; Ma and Goldberg, 2016; Maeda, Katada and Saito, 2017; Raote *et al.*, 2018).

The MIA/cTAGE family includes two Tango1 isoforms, Tango1 (Tango1-long) and Tango1-short, and nine other proteins that share similarities with the cytoplasmic portion of Tango1, including cTAGE5 and Tango1-like (TALI), which have been implicated in secretion (Feng, Yang and Pastor-Pareja, 2021). Tango1-long consists of three cytoplasmic domains, a transmembrane domain, and two ER-luminal domains. A cytoplasmic proline-rich domain (PRD) interacts with Sec23 and Sec16 (Saito *et al.*, 2009; Ma and Goldberg, 2016). Two cytoplasmic coiled-coil domains interact with cTAGE5 and Tango1-short and also recruit membranes from the ERGIC (Santos *et al.*, 2015). The ER-luminal domains include a third coiled-coil domain and a SH3-domain that interacts with a procollagen chaperone, Hsp47 (Saito *et al.*, 2009; Wilson *et al.*, 2011; Ma and Goldberg, 2016; Maeda, Katada and Saito, 2017). Tango1-short has the same structure as Tango1-long, but lacks ER-luminal domains, rendering it incapable of interacting with procollagen through Hsp47 (Raote *et al.*, 2018).

CTAGE5 has a conserved cytoplasmic domain organization similar to Tango1-long and interacts with Sec23, Sec22, and Sec12. Similarly to Tango1-short, it possesses no ER-luminal domains (Saito *et al.*, 2011, 2014; Wilson *et al.*, 2011; Raote *et al.*, 2017). TALI is a transmembrane protein that has a similar domain organisation to Tango1, consisting of a ER-lumenal SH3 domain, two cytoplasmic coiled-coil domains, and a cytoplasmic PRD (Santos *et al.*, 2016). TALI binds Tango1 and together with Tango1 is required for the export of apolipoprotein B (apoB), the main lipoprotein of chylomicrons (Santos *et al.*, 2016).

Tango1/cTAGE5 bind Sec23, and their interaction has been elucidated by a crystallographic study (Ma and Goldberg, 2016). Both Tango1 and cTAGE5 possess PRDs containing multiple triple proline (PPP) motifs that can bind Sec23, similarly to Sec31 (see Section I.3). This suggests a competition for inner coat binding between Tango1/cTAGE5 and Sec31 (Lee *et al.*, 2004; Stagg *et al.*, 2006; Ma and Goldberg, 2016). Since each PPP motif within the Tango1 and cTAGE5 PRDs can bind Sec23, the dimer can potentially bind multiple Sec23 molecules of the inner COPII coat (Ma and Goldberg, 2016). Binding Sec23 through PPP motifs can template the formation of a tubular inner coat lattice, which could allow the carrier to accommodate large cargo (Hutchings *et al.*, 2018). A hypothesis for the mechanism of action of Tango1 suggests that Tango1/cTAGE5 ensures cargo loading and then is gradually displaced by the forming Sec13/31 cage, thus remaining secluded to the ER-proximal parts of the forming carrier (Ma and Goldberg, 2016). Furthermore, as Sec13/31 increases Sar1 GTPase activity, delaying outer coat recruitment could allow for the formation of larger vesicles before vesicle fission or coat depolymerisation occurs. The structure of Tango1 has not been elucidated to date, and therefore the mechanism of its interaction with the rest of the COPII machinery remains unclear.

While Tango1 can delay GTP hydrolysis by Sar1, cTAGE5 can increase the local concentration of GTP-loaded Sar1 by recruiting Sec12. Sec12, which is responsible for the recruitment of Sar1 and its loading with GTP, is targeted to the ERES through its interaction with cTAGE5 (Maeda, Saito and Katada, 2016). While Sec12 is secluded from small COPII vesicles, it is enriched in large COPII vesicles (Yuan *et al.*, 2018)**.** Altogether, these observations suggest that a high local concentration of GTP-loaded Sar1 facilitates the formation of large carriers (Yuan *et al.*, 2018)**.** *In vivo*, the lack of Sec12 recruitment causes collagen export deficits, which are rescued by Sar1 overexpression (Tanabe *et al.*, 2016).

A well-studied client cargo of Tango1 is procollagen VII, a trimeric 350kDa assembly and the precursor of collagen, the main component of the extracellular matrix (Christiano *et al.*, 1994). Initially, it was proposed that the export of procollagen is enabled by two interactions: the indirect interaction of procollagen with the N-terminal SH3 domain of Tango1, and the dimerisation between Tango1 and cTAGE5 through their coiled-coil domains (Saito *et al.*, 2009, 2011). Surprisingly, a following study suggested that Tango1-short, which lacks the N-terminal SH3 domain, can substitute for Tango1-long in the export of procollagen (Maeda, Saito and Katada, 2016). The mechanism behind this requires further investigation. Large rings composed of the two isoforms of Tango1, short and long, and cTAGE5, were observed by super-resolution microscopy. The rings surrounded the COPII coat, suggesting the formation of a large assembly through lateral interactions at the base of the growing carrier (Liu *et al.*, 2017; Raote *et al.*, 2017; Reynolds *et al.*, 2019).

Tango1 recruits membranes from the ERGIC for collagen export, thereby directly satisfying the substantial membrane requirements of large carrier formation (Santos *et al.*, 2015). In this way, Tango1 can couple anterograde trafficking of cargo with the retrograde transport of the membrane components essential for carrier formation. A model of direct connectivity between the ER and ERGIC has been proposed, in which Tango1 tethers the two membrane compartments to each other (Raote *et al.*, 2018). However, the connections have not been directly observed and would raise questions about the mechanism of preservation of compartment identity. As the potential connections are likely to be short-lived and dependent on the presence of large cargo in the ER, their direct observation could remain challenging.

Whether Tango1 specifically functions to facilitate the export of large cargo is a matter of debate, as the secretion of horseradish peroxidase (HRP), a small soluble protein, is also partially impaired by Tango1 depletion (Bard *et al.*, 2006). There are two current hypotheses about why some small cargo is retained in the ER when Tango1 is depleted. Firstly, an accumulation and potential aggregation of large cargo in the ER can cause ER stress (Sano and Reed, 2013). Therefore, large cargo needs to be exported from the ER as soon as it is folded and, in the case of procollagen, assembled into its multimeric complex. Perhaps the timely formation of large carriers is prioritized, and small cytoplasmic proteins are non-specifically exported by these carriers in a mechanism similar to bulk flow. Alternatively, small cargo

could be retained in the ER in Tango1-depleted cells, congested by the accumulation of large cargo. Furthermore, emerging evidence suggests that Tango1 plays a double role in mammalian secretion: as a large cargo adaptor and as an organizing factor of ERES (Saito and Maeda, 2019). Both isoforms of Tango1 recruit Sec16, an ERES-organising protein, and a depletion of Tango1 results in fewer ERES and delayed secretion (Maeda, Katada and Saito, 2017). Further investigation is required to understand the role of Tango1 in establishing compartment morphology and in the secretion of large cargo versus general secretion.

CTAGE5 has been proposed to facilitate the export of procollagen in two ways: by building a molecular machine together with Tango1 to structure procollagen ER exit sites, and by enriching Sec12 in sites of procollagen secretion, enabling the formation of large carriers (Tanabe *et al.*, 2016; Raote *et al.*, 2017). CTAGE5 knockdown results in defects in procollagen export (Tanabe *et al.*, 2016). Expressing cTAGE5 mutants that are capable of binding Tango1, but not Sec12, in a cTAGE5 knockdown background, does not rescue procollagen secretion. However, expressing these mutants while overexpressing Sar1 capable of GTP hydrolysis rescues procollagen secretion (Tanabe *et al.*, 2016).

Importantly, Tango1/cTAGE5 deficiencies in mice and humans result in collagen export defects and bone formation issues. In mice, these phenotypes are characterised by an intracellular accumulation of collagen and an activation of the unfolded protein response (Wilson *et al.*, 2011). In humans, a truncation in Tango1 leads to a syndrome characterised by severe developmental abnormalities caused by collagen secretion defects. The genetic and medical analysis of the affected family suggests that the ratio of truncated to full-length Tango1 is key, and at higher ratios symptoms manifest (Lekszas *et al.*, 2020).

I.5.2.4. Additional factors

Multiple other factors are specifically implicated in the export of large cargo. Sedlin, a Tango1 interacting partner and TRAPP component, also affects the export of procollagen from mammalian cells. It acts by modulating the GTPase cycle of Sar1, possibly delaying vesicle fission (Venditti *et al.*, 2012).

The CUL3 ubiquitin ligase and its adaptor KLHL12 are involved in the export of large cargo (McCaughey and Stephens, 2018). CUL3-KLHL12 are essential for collagen secretion and are thought to facilitate the formation of large COPII carriers by monoubiquitinating Sec31.

Interestingly, the monoubiquitylation of Sec31 is not on a particular residue, as none of the lysine residues in Sec31 are essential for this modification (Jin *et al.*, 2012). Therefore, how this modification templates large carrier formation is unclear. The ubiquitination can be reversed by the ubiquitin-specific protease USP8 (Kawaguchi *et al.*, 2018). Ubiquitination of Sec31 could be physiologically regulated by calcium levels, through the regulation of components of the ligase machinery (McGourty *et al.*, 2016).

I.6. COPII cargo sorting and autophagy

Autophagy is an essential process in which cells degrade their cellular contents in response to environmental stress. During autophagy, organelles are engulfed in double-membrane structures named autophagosomes, which fuse with lysosomes and degrade their content to recycle nutrients (Glick, Barth and Macleod, 2010). COPII vesicles play an important role in satisfying the high membrane requirements of autophagy (Li, Huang and Wang, 2020). During starvation or stress, COPII vesicles contribute to autophagosome formation (Ge, Zhang and Schekman, 2014; Shima, Kirisako and Nakatogawa, 2019; Li, Huang and Wang, 2020). COPII proteins are not only involved in the general process of autophagy, but also more specifically in the autophagy of ER domains (Cui *et al.*, 2019). Misfolded protein domains within the ER are marked by ER-phagy receptors and recognised by Sec23/24, either directly or through adaptor proteins. Induction of ER-phagy in budding yeast results in an upregulation of ER-phagy receptors and of their interaction with Sec23 and Sec24 (Cui *et al.*, 2019). Hence, COPII components are involved not only in the secretion of correctly folded proteins, but also in the degradation of aggregates through ER-phagy. This underlines the important role of Sec23/24 in cargo control.

Aberrant expression of the inner coat COPII components has also been linked to ER stress and potentially human cancer (Jing, Wang and Liu, 2019). The involvement of COPII in clearing aggregated proteins from the ER strongly implicates it in many proteinopathies, including neurodegenerative disease.

I.7. *In vitro* reconstitutions of COPII

In vitro reconstitutions of the COPII secretion system utilise artificial membranes and purified proteins to provide valuable insight into COPII assembly. Minimal reconstitutions have proved indispensable for elucidating COPII mechanisms, even though they are incapable of fully

recreating the biochemical make-up of the membrane and the complexity of the protein machinery involved (Daum *et al.*, 2014).

A variety of lipid membrane models are used to investigate membrane dynamics in a defined minimal system with reproducible and known lipid and protein composition. Those include lipid bilayers, liposomes, microsomes, small, large, and giant unilamellar vesicles: models of different sizes and therefore different membrane curvatures. How the use of specific models impacts COPII recruitment and budding has not been thoroughly investigated. However, the choice of model is likely of consequence, as Sar1 membrane recruitment and GTPase activity increases with membrane curvature (Hanna *et al.*, 2016).

The chemical properties of membrane lipids can affect not only the recruitment of the COPII machinery, but also subsequent membrane remodeling (Daum *et al.*, 2014). The lipid requirements for COPII membrane binding *in vitro* have been investigated using flotation experiments (Matsuoka *et al.*, 1998). An optimal lipid composition for yeast COPII binding, termed 'major-minor mix', was discovered in experiments which estimate protein binding by co-fractionation with a floating lipid layer (Matsuoka *et al.*, 1998). The initial mixture that was tested in these experiments was similar in composition to microsomal membranes from yeast (Zinser and Daum, 1995). While yeast Sar1-GMP-PNP binds liposomes made from a mixture of the neutral DOPC-DOPE phospholipids, other COPII components fail to recruit. A negatively charged major mix, additionally containing the acidic phospholipids phosphatidylinositol (PI), dioleoyl phosphatidylserine (DOPS) and dioleoyl phosphatidic acid (DOPA), binds Sar1 and weakly recruits Sec23 and Sec13. A major-minor mix, containing additionally cholesterol, phosphatidylethanolamine (PE), and the acidic phospholipids phosphatidylinositol 4-phosphate (PI(4)P), phosphatidylinositol 4,5-diphosphate (PI(4,5)P2), and cytidine diphosphate diacyl glycerol (CDP-DAG), recruits COPII components more strongly than the major mix (Matsuoka *et al.*, 1998). Replacing a portion of the PI lipids with PI(4)P in particular dramatically increases recruitment of inner and outer coat components (Matsuoka *et al.*, 1998). Altogether, these results suggest that although initial Sar1-GMP-PNP binding to membranes is dependent on neutral phospholipids, acidic phospholipids interact more strongly with other COPII components (Matsuoka *et al.*, 1998; Matsuoka and Schekman, 2000). This could be due to the basic underside of the Sec23/24 heterodimer, which is proposed to electrostatically interact with the membrane (Bi, Corpina and Goldberg, 2002).

The mammalian ER, as measured from rat liver organelle samples, consists of 57% phosphatidylcholine (PC), 21% PE, 9% PI, 4% sphingomyelin (SM), 4% PS, and 5% other lipids (Vance, 2015). These include ceramides (Cer), galactosylceramide (GalCer), cholesterol, and triacylglycerol (Vance, 2015). This is similar, but not identical, to the optimal lipid composition that was established for yeast COPII binding, as discussed above. Investigating COPII binding to a lipid mixture identical to that of the native ER can help further unravel the lipid determinants of COPII membrane binding.

Apart from purified COPII proteins and a model membrane, a minimal reconstitution system would benefit from the incorporation of cargo. The long-standing need for *in vitro* budding reactions with large cargo was addressed by a cell-free budding assay, in which large spherical to ovoid COPII carriers loaded with procollagen I were reconstituted *in vitro* using purified proteins and microsomal membranes extracted from procollagen-expressing cells (Gorur *et al.*, 2017). This calls into question studies that suggest that COPII only functions to concentrate, but not encapsulate, large cargo (see Section I.4).

I.8. Project Aims

The importance of COPII for cargo trafficking in the mammalian cell is well-established, and so are the general mechanisms of COPII assembly. Structural information about individual core COPII components and subcomplexes is available; however, the human COPII coat assembled on membranes has not been observed and characterised. Outstanding questions remain: do human COPII components deform membranes for the export of cargo from the ER? Are human COPII proteins sufficient for membrane remodelling? What are the minimal requirements for reconstituting the functional human COPII secretion system? What is the role of GTP hydrolysis in COPII-mediated membrane deformation and scission? How do the two poorly characterised Sar1 paralogues, Sar1A and Sar1B, differ in their interaction with membranes and with other COPII components? Since Sar1B is specifically implicated in the export of large cargo, do the two Sar1 paralogues enable the generation of different membrane morphologies?

The first step to answering the questions above is a minimal reconstitution of the human COPII coat assembled on membranes. Human COPII membrane budding has never been reconstituted with defined minimal components, suggesting that the essential requirements

and conditions for human COPII assembly are still unestablished (Rowe *et al.*, 1996; Aridor *et al.*, 1998; Kim *et al.*, 2005; Boyadjiev *et al.*, 2006; Fromme *et al.*, 2007; Gorur *et al.*, 2017).

In addition to providing a platform for understanding the minimal requirements for budding, *in vitro* reconstitution experiments are a foundation for the structural analysis of the assembled COPII coat. The combination of cryo-electron tomography and subtomogram averaging has generated valuable insight into the molecular arrangements of the inner and outer coats of the yeast COPII secretion system (Zanetti *et al.*, 2013; Hutchings *et al.*, 2018). Structural analysis of the human COPII system reconstituted *in vitro* can elucidate the intermolecular interactions between COPII components as assembled on membranes and shed light onto global COPII arrangement. Furthermore, substituting with different COPII component paralogues in *in vitro* reconstitution reactions can help explain the role of multiple COPII component paralogues in humans in COPII assembly and membrane budding.

Finally, a minimal reconstitution of the human COPII secretion system can provide a platform for the investigation of COPII regulatory components. Understanding how COPII assembly is modulated by large cargo adaptors, such as Tango1/cTAGE5, can shed light on the mechanisms of formation of large carriers for the export of large cargo from human cells.

II. Materials and Methods

II.1. Human Sec23A/24C and Sec13/31A expression and purification from insect cells

II.1.1. Bacmid preparation

Deoxyribonucleic acid (DNA) constructs were visualised with SnapGene Viewer.

DNA constructs of human Sec23A, Sec24C, Sec13, and Sec31A were available in our laboratory. The sequences of the proteins of interest were in pFASTbacHTb plasmids, which are suitable for bacmid generation for insect cell expression. The pFASTBac-HTb vector contains a sequence encoding a 6x Histidine (His) affinity tag, followed by a Tobacco Etch Virus (TEV) cleavage site directly upstream from the insertion site for the construct of interest. Upon expression, this results in an N-terminal His-TEV polypeptide sequence appended to proteins of interest (Fig. 2.1). Sec24C and Sec31A had been directly inserted into the pFASBacHTb vector. For Sec23A and Sec13, the 6x His – TEV sequence had been removed.

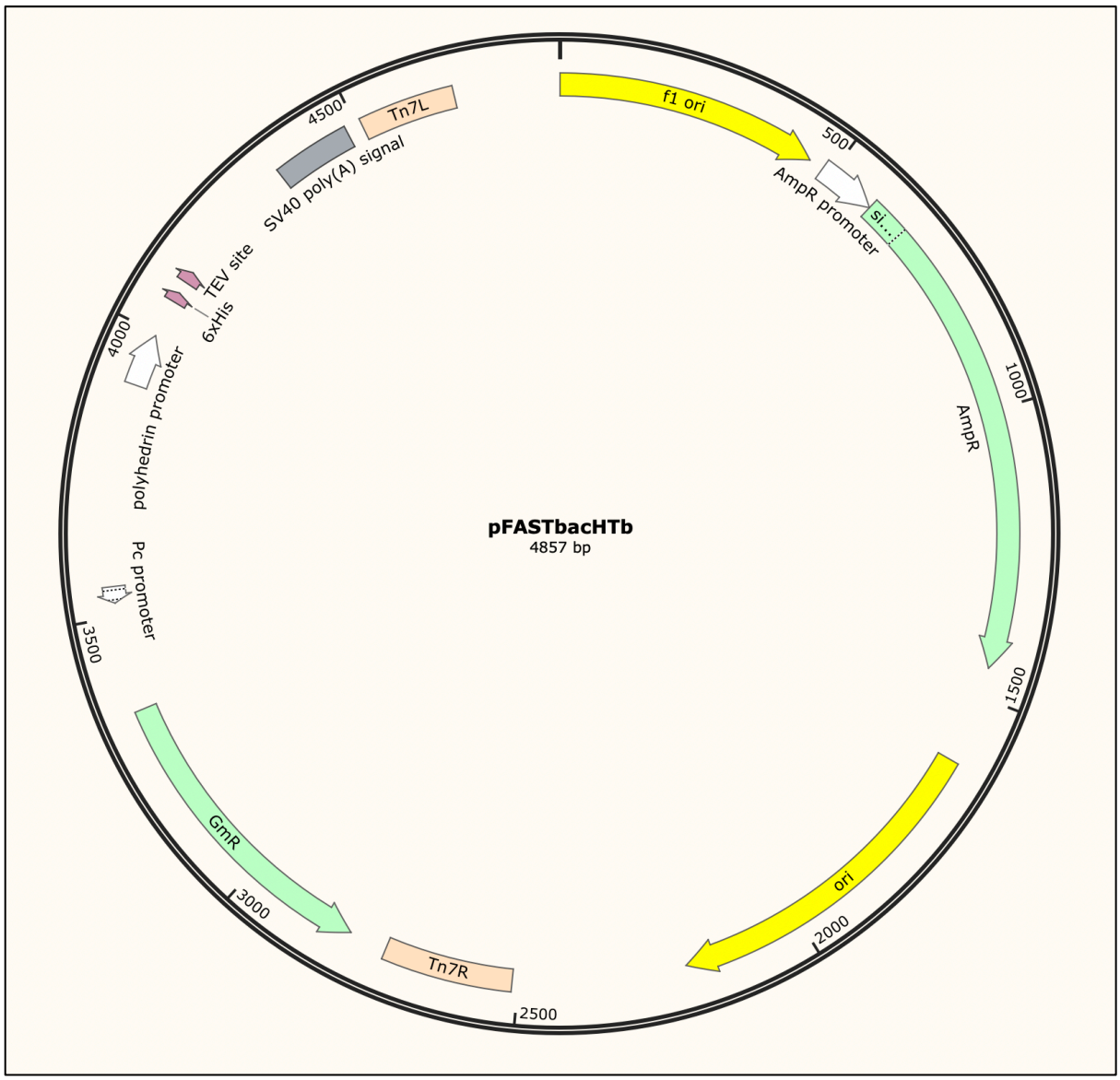

Figure 2.1: Map of pFASTbacHTb, as generated by SnapGene Viewer. The sequence encoding the protein of interest is under the control of a polyhedrin promoter. Upstream of the insertion site is a sequence encoding a 6xHis-tag, followed by a sequence encoding a TEV protease recognition sequence. This plasmid contains genes encoding ampicillin resistance (AmpR) and gentamycin resistance (GmR).

I transformed the relevant pFASTBac constructs into bacmid-containing DH10EMBacY cells, resulting in the insertion of the constructs into the bacmid. For each transformation, 1µl of plasmid DNA was added to 100µl of electrocompetent DH10EMBacY cells, containing the bacmid, pre-thawed on ice for 10 min. The mixture was transferred to a pre-chilled 1mm electroporation cuvette, and cells were electroporated by electric pulse (1800V, 200Ω). 900µl

of Super Optimal broth with Catabolite repression (SOC) medium (ThermoFisher Scientific) was added immediately, and the mixture was transferred to a round-bottom tube and incubated in a shaking incubator for 6h at 37 °C at 250 rotations per minute (rpm). 150µl and 50µl of transformation culture were plated onto selective lysogeny broth (LB) Agar plates containing 50µg/ml kanamycin, 10µg/ml tetracyclin, 7µg/ml gentamycin, 20µg/ml 5-bromo-4-chloro-3-indolyl β-D-galactoside (X-gal), and 120µg/ml isopropyl β-D-1 thiogalactopyranoside (IPTG) (Sigma-Aldrich). The plates were incubated at 37 °C for two days, and white colonies (those contaning pFASTbac-HTb correctly inserted in the bacmid) were selected and re-streaked onto selective LB Agar plates, as described above. White colonies were selected again and expanded overnight by incubation in 5ml LB Broth with kanamycin, tetracyclin, and gentamycin at concentrations as described above, in a shaking incubator at 37 °C, 220 rpm.

Bacmid minipreps were performed following a protocol adapted from the Department of Molecular Biology and Biological Physics, University of Virginia. The overnight cultures described above were centrifuged for 5 min at 3668 x g using a JS-5.3 swinging rotor (Beckman Coulter). The supernatant was removed using a vacuum aspirator, and the pellet was resuspended in 300µl of P1 Buffer (Qiagen). 300µl of P2 buffer (Qiagen) was added, and the samples were mixed by inversion and incubated for 5 min at room temperature. 300µl of cold N3 buffer (Qiagen) were added, and samples were gently mixed by inversion and placed on ice for 10 min. During this step, a precipitate of protein/genomic DNA forms. To separate the precipitate, samples were centrifuged for 10 min at 21,130 x g using the 5424R benchtop centrifuge (Eppendorf). The supernatant was transferred to a tube containing 800µl of room-temperature isopropanol. The reaction was mixed by inversion and placed at -20°C for 60 min. The sample was then centrifuged for 15 min at 21,130 x g using a benchtop microcentrifuge (5424R, Eppendorf). The supernatant was removed, and 500µl of 70% ethanol were added. After mixing by inversion, the tube was centrifuged for 10 min at 21,130 x g using the 5424R benchtop centrifuge (Eppendorf). The ethanol wash step was repeated. All the supernatant was carefully removed, and the pellet was air-dried in sterile conditions. The pellet was resuspended in 40µl of sterile water. Bacmid concentration was measured using Nanodrop (Thermofisher Scientific), and bacmids were used for transfection of Sf9 insect cells.

II.1.2. Transfection of Sf9 insect cells

Sf9 insect cells were grown in sterile conditions in Insect Xpress media with L-glutamine (Lonza) at 27°C in a shaking incubator at 100 rpm. For all experiments, healthy cells were used i.e. uninfected cells that double approximately every 24h, monitored in the 5 days prior to use. Prior to transfection, 2ml of healthy Sf9 cells at a density of $0.5x10^6$ counts/ml were plated onto Nunclon Delta Surface 6-well plates (Thermofisher) and allowed to adhere for 30min. Transfection mixture was prepared, containing 200µl medium, 750ng bacmid, and 4µl transfectant (FuGENE HD Transfection reagent, Promega). The transfection mixture was mixed by gentle flicking and incubated for 30min at room temperature. The mixture was added slowly and drop-wise to the plated cells, and the cells were incubated for 5 days. Cells were assessed for fluorescence after 5 days, as EMBacY produces yellow fluorescent protein (YFP) as a marker; if more than 40% of cells were fluorescent, media was collected, which contained the P0 virus. The 2ml of virus-containing media were added to 50ml of Sf9 cells at a density of $1x10^6$ counts/ml. After 5 days, cells were centrifuged at 873 x g for 20 min using a JS-5.3 swinging rotor (Beckman Coulter), and the supernatant, containing the P1 virus, was collected and stored in a light-proof container at 4°C.

II.1.3. Expression with Bac-to-Bac expression system

For protein expression, Sf9 cells at $1x10^6$ counts/ml were co-infected with 3ml/L of virus for expression of His-tagged proteins (Sec24C, Sec31A) and with 9ml/L for proteins to be co-purified (Sec23A, Sec13). The virus was directly added to the Sf9 cells, and the cultures were returned to the shaking incubator (Lonza) at 27°C for 72h. After this time, cells were checked for YFP fluorescence as described above and harvested by centrifugation at 998 x g for 20min using a fixed-angle JLA-8.1000 rotor (Beckman Coulter). The supernatant was discarded, and the pellet was utilised fresh or stored at -80°C.

II.1.4. Purification from insect cell culture

For protein purifications from insect cell culture, I utilised 5ml HisTRAP columns (Sigma-Aldrich) connected to an ÄKTA Prime system (GE Healthcare Lifesciences), a 1ml MonoQ column (Sigma-Aldrich) connected to an ÄKTA Pure system (GE Healthcare Lifesciences), and a 2.4ml Superdex 200 column (GE LifeSciences) connected to an ÄKTA Micro system (GE Healthcare Lifesciences). Chemical compounds were purchased from Sigma-Aldrich. Where His-tag cleavage was performed, TEV protease, purified in-house (by Hutchings, J., Brown, N.),

was used at 1:10 protein of interest:TEV protease molar ratio. All purification steps were performed at 4°C. Final protein concentrations were measured using a QuickStart Bradford assay (BioRad), where absorbance was measured by Nanodrop (Thermofisher Scientific).

Sec31A forms a stable complex and co-purifies with Sec13. Sec13/31A was purified using a three-step purification protocol. Cell pellets were resuspended in 50ml HisTRAP buffer A (20mM HEPES pH 7.5, 10% glycerol, 250mM sorbitol, 300mM KOAc, 1mM dithiothreitol (DTT), 10mM imidazole) plus 2 protease inhibitor tablets (Sigma) per liter of cell culture. Cells were lysed using a pre-chilled 50ml glass dounce homogenizer, and cell lysis was assessed by staining with Trypan Blue (Thermofisher Scientific). Lysate was filtered using 0.45µm filters (Sartorius) and centrifuged at 136,660 x g for 1 hour at 4°C using a Ti45 fixed-angle rotor (Beckman Coulter). A 5ml HisTRAP column was equilibrated with HisTRAP buffer A for a minimum of 10 column volumes (CVs), and the centrifugation supernatant was loaded at 1ml/min. The column was washed with 25mM imidazole for 15 CVs, with 60mM imidazole for 20 CVs, and then eluted using a gradient from 60 to 500mM imidazole for 4 CVs. Samples were analysed using sodium dodecyl sulfate – polyacrylamide gel electrophoresis (SDS-PAGE, see Section II. 3.).

Selected samples were pooled, and TEV protease was added. The reaction was transferred to a pocket of Spectra/Por dialysis tubing (Spectrum Labs), which was placed in a beaker containing 2L of HisTRAP A buffer. The dialysis beaker was stirred with a magnetic stirrer overnight at 4°C.

The overnight cleavage product was recovered from the dialysis pocket and loaded onto a 5ml HisTRAP column at 1ml/min. This step was performed to allow His-TEV, His-tag fragments, and Sec13/31A complexes with an uncleaved His-tag to attach to the HisTRAP column and be removed from the solution. The above ÄKTA programme was run again.

The flow-through was collected and diluted 1:4 in MonoQ buffer A (20mM Tris-HCl pH 7.5, 1mM MgOAc, 1mM DTT, 10% glycerol) to lower salt concentration. A 1ml MonoQ column was pre-washed with MonoQ buffer B (20mM Tris-HCl pH 7.5, 1mM MgOAc, 1mM DTT, 10% glycerol, 1M NaCl) and equilibrated in MonoQ buffer A. The diluted post-dialysis HisTRAP flow-through was loaded at 1ml/min. The column was washed with 50mM NaCl for 10CVs, and a step elution was performed at 500mM NaCl for 10CV. Samples were analysed by SDS-

PAGE. Selected fractions were pooled, aliquoted, flash-frozen using liquid nitrogen, and stored at -80°C. Sec13/31A aliquots were gel-filtrated using Superdex 200 equilibrated in HKM buffer (20mM HEPES, 125mM KOAc, 1mM MgOAc, pH 7.5) prior to use in COPII reactions that were analysed by electron microscopy.

Sec24C forms a stable complex and co-purifies with Sec23A. Sec23A/24C was purified using a two-step purification protocol, using a HisTRAP column, followed by salt dilution and a MonoQ column. The His-tag on Sec24 was retained. Buffers and the general purification protocol were the same as described above for Sec13/31A, apart from the specifications below. The HisTRAP purification programme consisted of a first column wash with 20mM imidazole for 15 CVs, a second column wash with 50mM imidazole for 20 CVs, and a gradient elution using from 50 to 500mM imidazole for 4 CVs. Eluted fractions were analysed by SDS-PAGE, and salt dilution was performed by diluting the identified fractions 1:6 with MonoQ buffer A. The monoQ column was washed with 50mM NaCl. Serial step elution from the monoQ column was performed using 200mM, 300mM, 400mM, 500mM, 600mM, and 1M NaCl. Sec23A/24C eluted at 300mM NaCl. Samples were analysed by SDS-PAGE, aliquoted, flash-frozen using liquid nitrogen, and stored at -80°C.

II.2. Human Sar1A and Sar1B expression and purification from *Escherichia coli*

II.2.1. Expression in *E. coli*

A DNA construct of Sar1A in the pETM-11 vector (Fig. 2.2) was available In our lab, in which the Sar1A sequence was preceded by an N-terminal 6xHis-tag sequence, followed by a TEV protease cleavage site sequence.

I generated a construct of Sar1A with a C-terminal 6xHis-tag in the pETM-11 vector. Oligonucleotide primers were designed manually, and their melting temperatures were assessed with Tm calculator (ThermoFisher Scientific). They were ordered lyophilised from Eurofins Genomics. The Sar1A-pETM-11 construct containing an N-terminal 6xHis-TEV was used as a template. Oligonucleotides used are shown in Table 2.1, and their annealing positions are illustrated in Fig. 2.2 and 2.3.

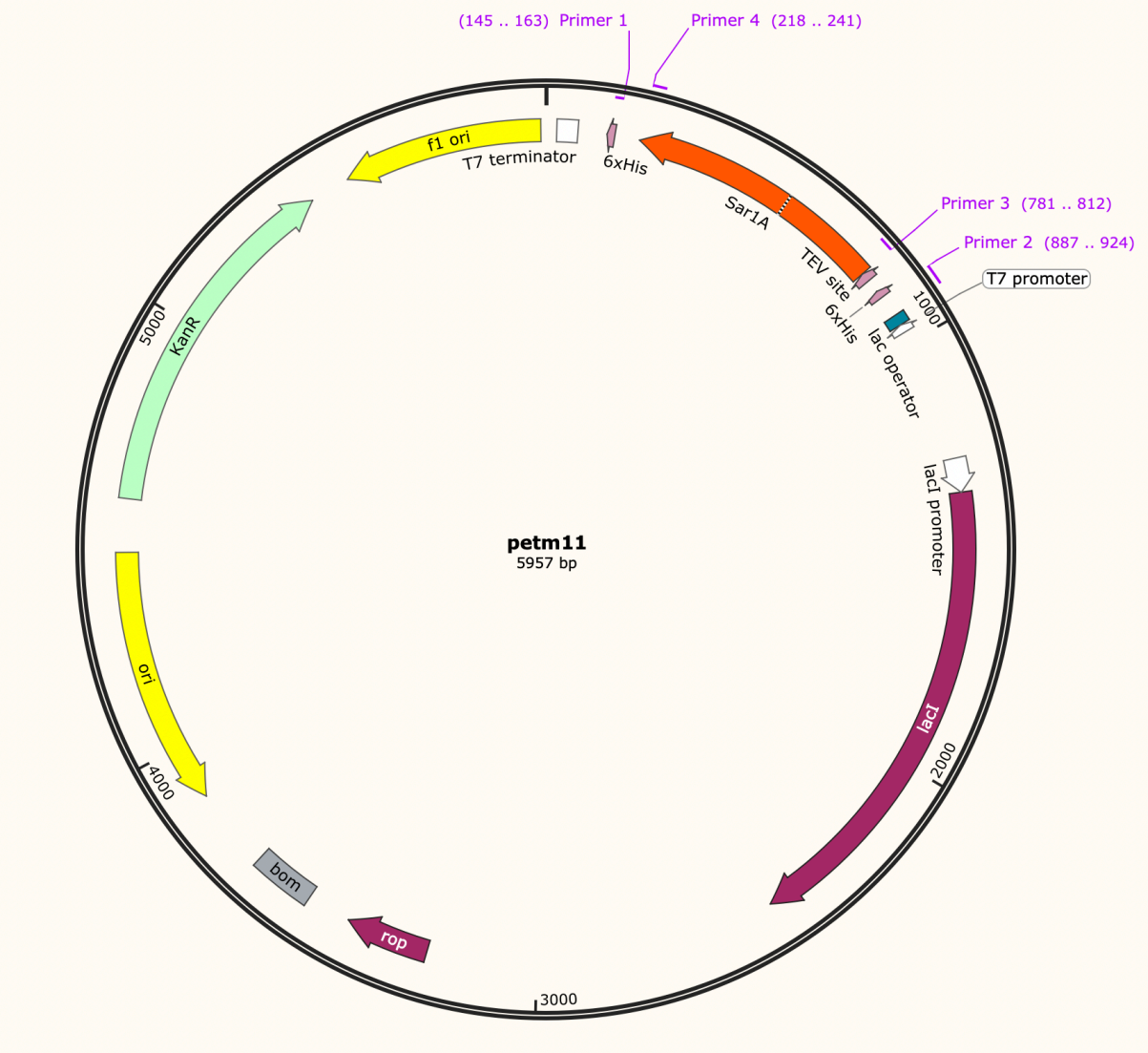

Figure 2.2: Map of pETM-11 containing the Sar1A sequence, as generated by SnapGene Viewer. The sequence of interest is inserted downstream of a T7 promoter. Directly downstream of the promoter, upstream of the sequence of interest, a sequence encoding a 6xHis-tag, followed by a TEV protease cleavage site, is positioned. The plasmid contains a gene encoding for kanamycin resistance (KanR). The annealing positions of the nucleotides for the generation of C-terminally His-tagged Sar1A are shown.

The pETM-11 vector was amplified using primer 1, which anneals to the vector at the 6xHis sequence downstream of the Sar1A sequence, and primer 2, which anneals to the vector upstream of the 6xHis-TEV site and downstream of the T7 promoter and lac operator. The Sar1A sequence was amplified using primer 3, which anneals to the start of the Sar1A sequence, with an overhang sequence complementary to primer 1, and primer 4, which

anneals to the end of the Sar1A sequence and diverges in sequence at the stop codon, with an overhang sequence complementary to primer 2.

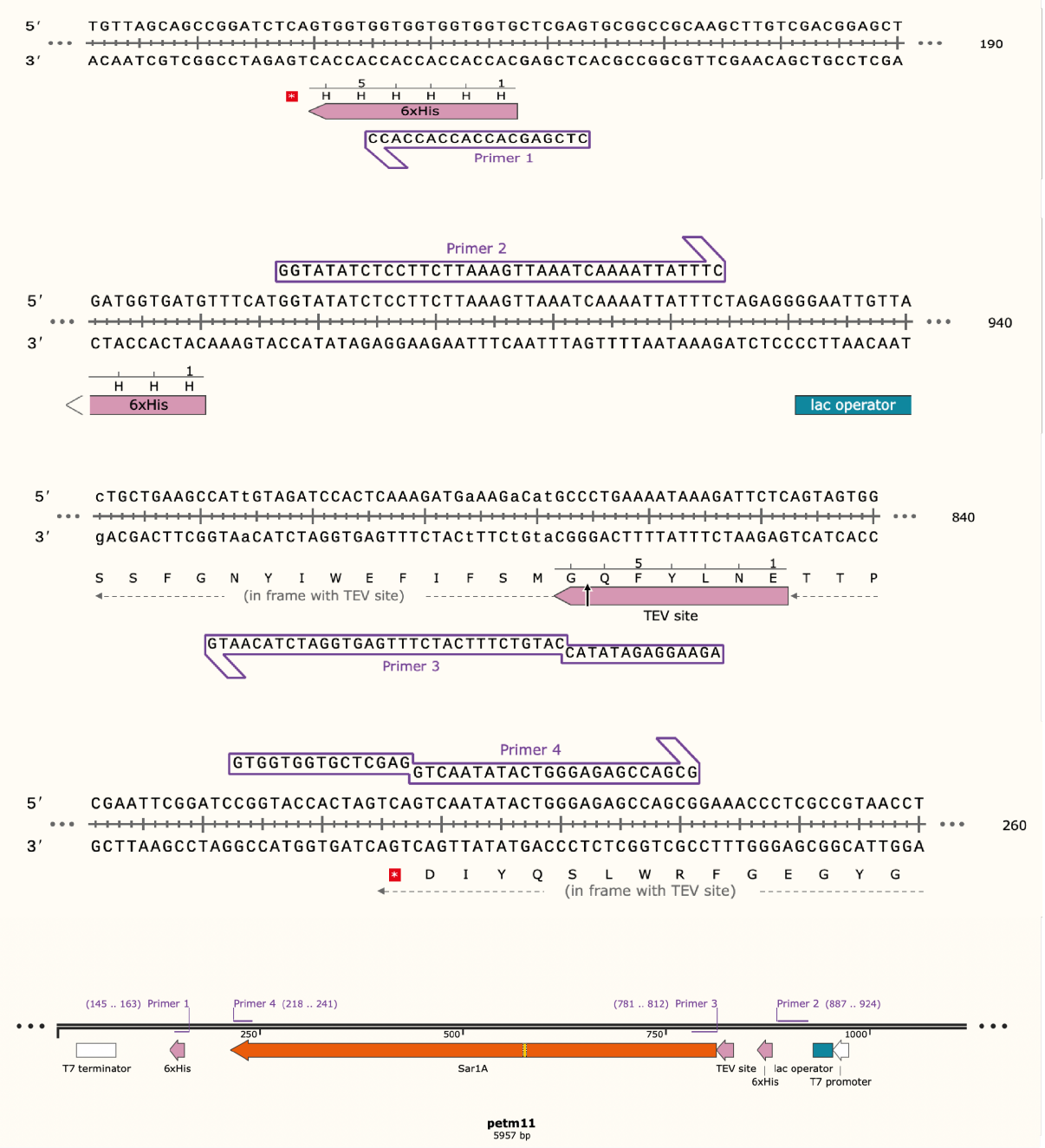

Figure 2.3: Annealing positions for the oligonucleotides used for the generation of a construct encoding a C-terminally His-tagged Sar1A protein.

Primer	Direction	Sequence
1	forward	CTCGAGCACCACCACCACC
2	reverse	GGTATATCTCCTTCTTAAAGTTAAATCAAAATTATTTC
3	forward	AGAAGGAGATATACCATGTCTTTCATCTTTGAGTGGATCTACAATG
4	reverse	GTGGTGGTGCTCGAGGTCAATATACTGGGAGAGCCAGCG

Table 2.1: Sequences of the oligonucleotides used for the generation of a Sar1A construct with a C-terminal His-tag in the pETM-11 vector.

Sequences were amplified using Q5 High-Fidelity DNA polymerase (NEB). The vector and the insert were purified by running the reaction products on an agarose gel and excising the appropriate bands. The vector and the insert were ligated using T4 DNA ligase (NEB) at a 1:3 ratio of vector to insert. Per 20µl of ligation reaction, 2µl of T4 ligase buffer (NEB) and 1µl of T4 DNA ligase (NEB) were added. Nuclease-free water (NEB) was added to a total volume of 20µl. The reaction was mixed and incubated at room temperature for 10 min. Following incubation, the enzyme was inactivated using a 10 min 65°C incubation step.

5ng of ligation product was added into 50µl of DH5α competent cells (Thermo Fisher Scientific). The mixture was incubated on ice for 30 min, and cells were permeabilised by heat shock at 42°C for 30 sec. 950µl pre-warmed SOC media was immediately added, and the cells were transferred to a shaking incubator at 37°C, 250rpm. After 1h, 50ul of the cell mixture was spread onto pre-warmed LB Agar plates with 50µg/ml kanamycin.

DNA constructs of Sar1A and Sar1B in the pGEX-2T vector were available in our lab (Fig. 2.4). Their expression produces Sar1 with an N-terminal glutathione S-transferase (GST) affinity tag, followed by a thrombin cleavage site.

All generated plasmids were transformed into BL21 *E. coli* cells. For each transformation, 100ng of the plasmid were added to 50µl of pre-thawed cells, and the mixture was flicked gently and incubated on ice for 30 min. Cell membranes were made permeable by exposing

the mixture to heat shock at 42°C for 10 sec. The mixture was then incubated on ice for 5 min. 950µl of pre-warmed SOC media were added, and the cells were placed in a shaking incubator at 37°C, 250rpm. After 1h, 50ul of the cell mixture was spread onto pre-warmed selective LB Agar plates with 50µg/ml ampicillin (for cultures transformed with pGEX-2T) or 50µg/ml kanamycin (for pETM-11). Colonies were picked and grown in 5ml of LB Broth with 50µg/ml kanamycin (for pETM-11) or 50µg/ml ampicillin (for pGEX-2T) at 37°C overnight, in a shaking incubator at 250rpm. The 5ml cultures were diluted in 1L of 2 Yeast Triptone (YT) media (16g Bacto Tryptone, 10g Bacto Yeast Extract, 5g NaCl per litre), and the appropriate antibiotic was added at 50µg/ml. Cells were grown at 37°C in a shaking incubator at 250rpm to an A600 of 0.3, transferred to 25 °C, and further grown to an A600 of 0.8. Sar1 expression was induced by adding 0.1mM IPTG to the cultures. The protein was expressed for 2h at 25 °C in a shaking incubator at 250rpm. Cells were harvested by centrifugation for 20 minutes at 5053 x g using a JLA-8.1000 fixed-angle rotor (Beckman Coulter). Cell pellets were frozen at -80°C.

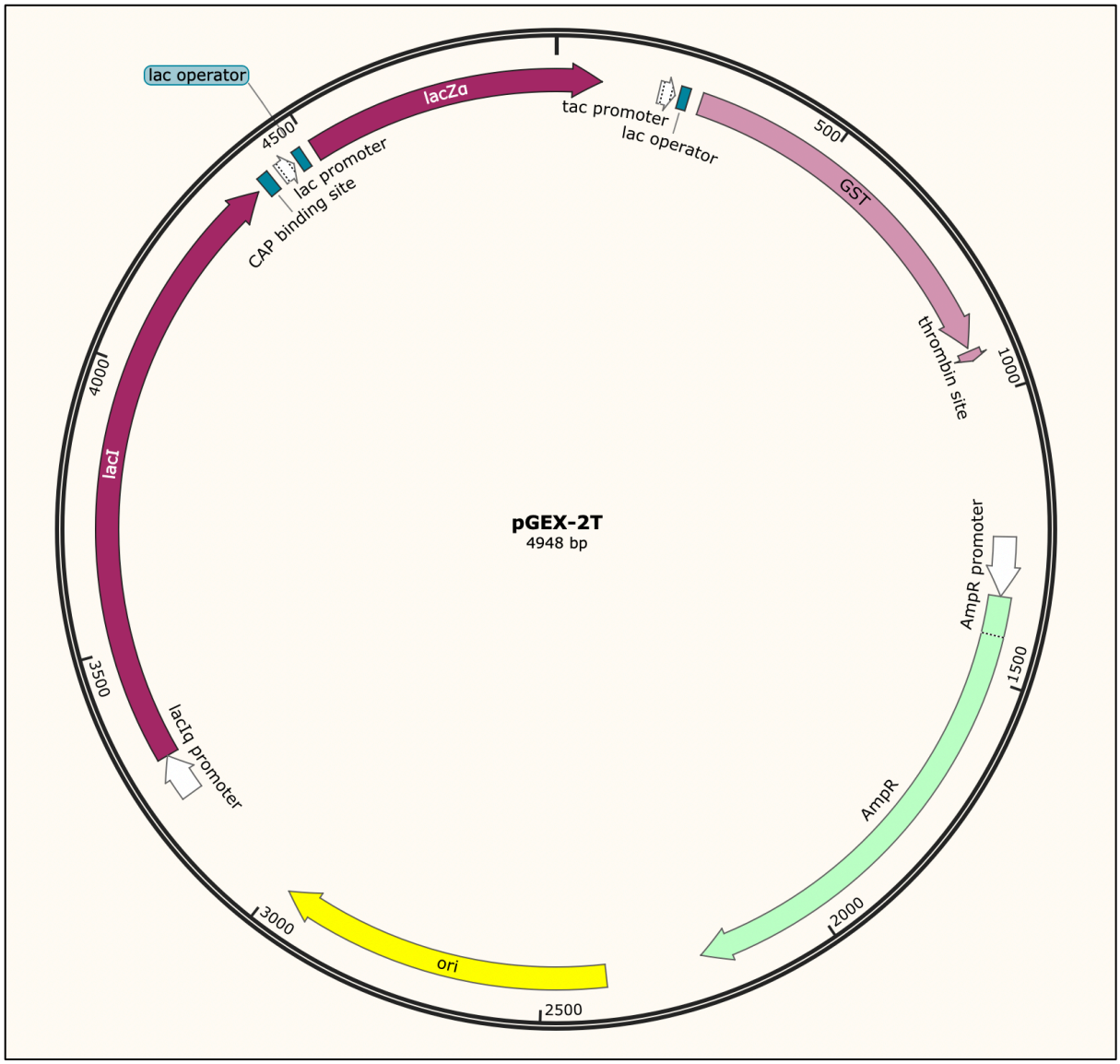

Figure 2.4: Map of pGEX-2T, as generated by SnapGene Viewer. The sequence encoding the protein of interest is inserted into the vector under a tac promoter. Downstream of the tac promoter, prior to the insertion site of the sequence of interest, is a sequence encoding a GST-tag, followed by a sequence encoding a thrombin protease cleavage site. The plasmid contains an ampicillin resistance gene (AmpR).

II.2.2. Sar1 purification from E. coli

II.2.2.1. Sar1 N-terminal and C-terminal His-tag purification

Cells were resuspended in 50ml HisTRAP buffer A (20mM HEPES pH 7.5, 10% glycerol, 250mM sorbitol, 300mM KOAc, 1mM DTT, 10mM imidazole) per litre of cell culture. They were treated with 20mg lysozyme for 20 minutes, and further lysed using three sonication steps of

30s at 40% intensity, with pulses of 1s and pauses of 2s, using a high-intensity ultrasonic processor (Vibra cell, Sonics). Lysate was centrifuged at 164,685 x g for 1 hour at 4°C using a Ti70 fixed-angle rotor (Beckman Coulter). A 5ml HisTRAP column was equilibrated with HisTRAP buffer A for a minimum of 10 CVs, and the centrifugation supernatant was loaded at 1ml/min. The column was washed with 25mM imidazole for 15 CVs, with 60mM imidazole for 20 CVs, and then eluted using a gradient from 60 to 500mM imidazole for 4 CVs. Samples were analysed on an SDS-PAGE, and selected samples were pooled. For C-terminally His-tagged Sar1, the pooled sample was concentrated using a 10kDa cut-off concentrator (Amicon), aliquoted and frozen at -80°C. For N-terminally His-tagged Sar1, the sample was cleaved with TEV protease overnight and dialysed against 2L HisTRAP A buffer, as described above in the Sec13/31A purification protocol. The overnight cleavage product was loaded onto a 5ml HisTRAP column pre-equilibrated in HisTRAP Buffer A at 1ml/min. This step functioned to retain His-TEV, His-tag fragments, and Sar1 with an uncleaved His-tag on the HisTRAP column. The above programme was run again. The flow-through, containing Sar1 with a cleaved N-terminal His-tag, was collected and analysed by SDS-PAGE. It was then concentrated using a 10kDa cut-off concentrator (Amicon), aliquoted, flash-frozen using liquid nitrogen, and stored at -80°C.

II.2.2.2. Sar1 N-terminal GST-tag purification

Pellets were resuspended in 25ml TBST (50 mM Tris, 150 mM NaCl, 0.1% Tween-20, pH 7.4) and treated with 20mg lysozyme for 20 minutes. After incubation, Triton X-100 was added to a final concentration of 1%, and the sample was mixed by inversion. Cells were lysed using three sonication steps of 30s, with pulses of 1s and pauses of 2s, at 40% intensity, using a high-intensity Vibra cell sonicator (Sonics). The cell lysate was cleared by centrifugation at 164,685 x g at 4°C for 1h using a Ti70 fixed-angle rotor (Beckman Coulter) . 4ml of Glutathione Sepharose High Performance resin (Merck) were washed and pre-equilibrated with 10 CVs of TBST. All centrifugation steps were performed at 500 x g for 5 min at 4°C. The equilibrated glutathione beads were incubated with the lysate supernatant for 2h at 4°C on a rolling bench-top mixer. After incubation, the beads were washed with 40 CV TBST (50mM Tris, 150mM NaCl, pH 7.4, 0.1% Tween), 15 CV TBS (50mM Tris, 150mM NaCl, pH 7.4), and 15 CV TCB (50 mM Tris, 250 mM KoAc, 5 mM $CaCl_2$, pH 8.0). The beads were incubated with 4U thrombin protease (GE Healthcare) and 10µM GDP overnight at 4°C on a rolling bench-top mixer. Beads

were transferred to an empty gravity flow column. The eluted fraction was collected, and another 10 CVs of buffer were added to the beads and collected. Peak fractions were pooled and concentrated using a 10kDa cut-off concentrator (Amicon), and aliquots were frozen and stored at -80°C.

II.3. SDS-PAGE analysis

For SDS-PAGE analysis, unless otherwise specified, 12µl of protein sample were added to 4µl of gel-loading dye containing DTT. The mixed sample was incubated at 94°C for 5 minutes and centrifuged at maximum speed for 1 minute. Samples were loaded onto NuPAGE 4-12% Bis-Tris pre-cast gels (Thermofisher Scientific) with 5µl of Precision Plus unstained protein ladder (Biorad). Gels were run for 45 min at 210 V in MOPS buffer (Sigma-Aldrich). Gels were stained with InstaBlue (Expedeon) for 30min or more and de-stained with deionized water. They were imaged on a CanoScan scanner (Canon) or ChemiDoc MP imaging system (BioRad).

II.4. Preparation of donor membranes

II.4.1. Preparation of major-minor lipid mixture with cholesterol

The following lipids were ordered from Avanti Polar Lipids: DOPC, DOPE, DOPA, PI (liver), PI (4) P, PI (4,5) P2, CDP-DAG. Texas Red-DHPE was ordered from ThermoFisher Scientific. Lipids were dissolved in the appropriate volume of chloroform and mixed to the following molar percentages: 51% DOPC, 22% DOPE, 8% DOPS, 5% DOPA, 8% PI (liver), 2.2% PI(4)P, 0.8% PI (4,5) P2, 2% CDP-DAG, 1% TX-DHPE to a final lipid concentration of 2mg/ml. Cholesterol was added to 20% of the total weight of the mixture. The mixture was aliquoted into 250µl aliquots in glass vials with chloroform-resistant caps (ThermoFisher Scientific), dried with argon gas, and stored at -20°C.

II.4.2. Electroformation of giant unilamellar vesicles

Lipid stock aliquots were dissolved in 50µl of a 2:1 chloroform: methanol solvent, resulting in a total lipid concentration of 10mg/ml. 20µl of solution were taken up with a glass syringe and applied to the electroconductive sides of two indium tin oxide-coated glass slides, as identified by an electroconductivity measurement. The solution was spread to a thin layer on the glass slides using a coverslip. Glass slides were dried on a 60°C heat block for 5 min, and the electroconductive surfaces were turned towards each other and separated by a silicone ring to form a chamber. The chamber was filled with 500ml of 300mM filtered sucrose

solution. Metal tape was attached to the electroconductive sides of the chamber, to which clipper electrodes were attached. A 10Hz sinusoidal current at 3 Volts effective voltage was applied for 6 hours, resulting in the swelling of the lipids and the formation of giant unilamellar vesicles. Those were harvested and added to 500ml of 300mM filtered glucose solution and left overnight at 4°C. Pellets were formed as the sucrose-filled vesicles sank to the bottom of the tube. The sucrose-glucose mixture that overlaid the pellets was removed, and the pellet was retained up to 24h at 4°C prior to use. For quality analysis, vesicles were pipetted onto glass slides and analysed by fluorescence microscopy.

II.4.3. Liposome preparation

Liposomes were prepared from lipid stock aliquots. Aliquots were resuspended in 500µl of HKM buffer, pH 6.8. This resulted in a cloudy mixture. Three cycles of the following were repeated: vortexing for 1 min, sonication in an ultra-sonic bath (Bransonic 5510, Branson) for 10 min, flash-freezing, and thawing under a warm water stream. Following this procedure, the cloudiness of the lipid mixture was visibly reduced significantly. Liposomes were generated using the Avanti Mini Extruder, using a membrane filter with a pore size of 400nm (Whatman, GE Healthcare), using 21 passes through the membrane. Liposome preparations were assessed by negative-stain EM before use in liposome flotation assays.

II.5. COPII reconstitution reactions

To reconstitute mammalian COPII budding reactions *in vitro* for analysis by electron microscopy, giant unilamellar vesicles (GUVs) were combined with Sec23A/24C and Sec13/31A purified from insect cells, and Sar1A and Sar1B purified from *E. coli* (Fig.2.5). For yeast COPII controls, Sar1, Sec23/24, and Sec13/31 were used as purified by Joshua Hutchings in-house. Reactions contained 1mM GMP-PNP or a GDP (Sigma-Aldrich), 2.5mM ethylenediaminetetraacetic acid (EDTA), and 10% GUVs. The volume was made up to 30µl with HKM buffer, pH 6.8. Reactions were incubated at room temperature for one hour and prepared for electron microscopy analysis.

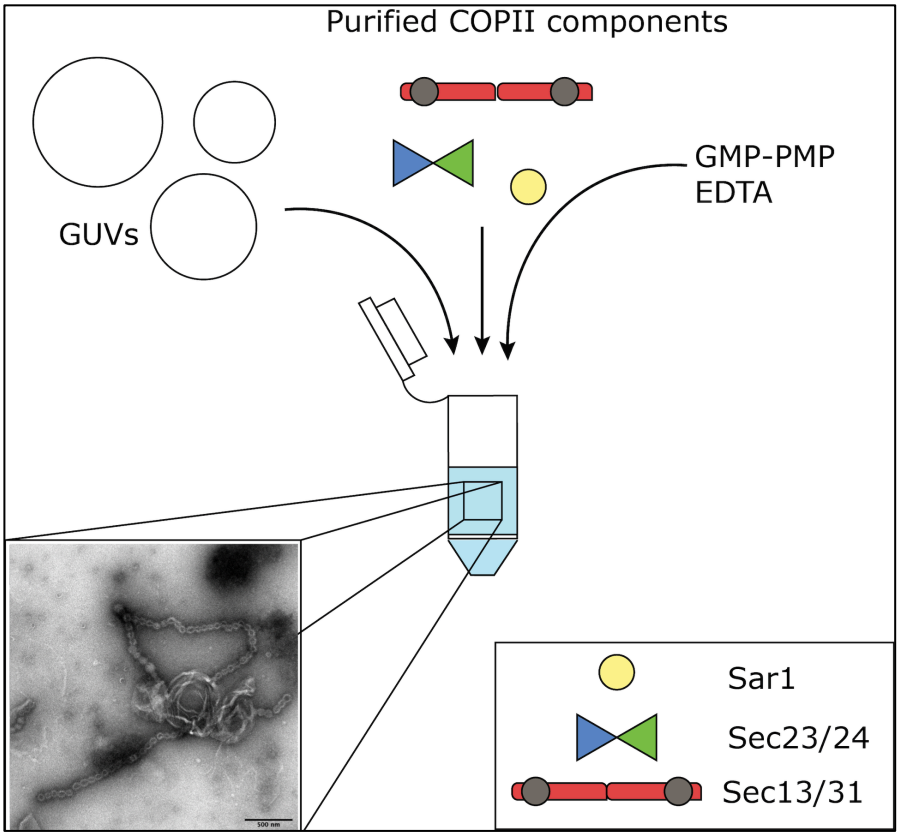

Figure 2.5: Reconstitution of COPII budding, adapted from Markova and Zanetti, 2019 (Markova and Zanetti, 2019). Purified COPII components are incubated with GUVs in the presence of GMP-PNP and EDTA. Membrane budding is analysed by electron microscopy (EM).

II.6. Electron Microscopy

II.6.1. Preparation of negative stain electron microscopy grids

For negative staining, Carbon Support Film Square Grids, 300 mesh, 5-6 nm (Electron Microscopy Sciences) were glow-discharged using a PELCO easiGlow Glow Discharge Cleaning System (Ted Pella, Inc). 4µl of reaction volume were pipetted onto the grid and incubated for 1 minute. The grid was picked up using sharp-ended tweezers, inverted, and stained sequentially in three drops of filtered 2% uranyl acetate. After 1 min incubation, the stain was blotted with filter paper.

II.6.2. Preparation of cryo-electron microscopy grids

Samples for cryo-electron microscopy were prepared using a Vitrobot (ThermoFisher Scientific). Lacey carbon film on 300 mesh copper support grids (Agar Scientific) were glow-discharged using a PELCO easiGlow Glow Discharge Cleaning System (Ted Pella, Inc). 4µl of reaction volume were pipetted onto the grid. The reaction was left to absorb into the grid for 1 min, blotted away, and frozen in liquid ethane. Grids were stored in liquid nitrogen.

II.6.3. Electron microscopy analysis

Samples were analysed on T10 or T12 electron microscope (Tecnai), which was aligned using common procedures. Data was collected on a Gatan CCD camera, typically with an exposure time of 1s per micrograph, using Serial EM software (Mastronarde, 2003). Micrographs were analysed using ImageJ software (Schneider, Rasband and Eliceiri, 2012).

II.7. GTP hydrolysis assays

To characterise GTPase activity of human Sar1A and Sar1B in the presence or absence of Sec23A/24C and Sec13/31A, the commercial GTPase/GAP/GEF-Glo assay was used (Promega). The assay was performed using manufacturer's instructions and adapted as applied previously to the study of *C. elegans* COPII (Hanna *et al.*, 2016). Sar1 was serially diluted in GEF buffer. Unless otherwise specified, the total reaction (25µl) consisted of Sar1 at the respective concentration, 320nM Sec23A/24C or GEF buffer, 320nM Sec13/31A or GEF buffer, 1mM DTT, and 5µM GTP in GEF buffer. Reactions were incubated in a solid white 96-well plate for 30 min, and 25µl of GTPase-Glo reagent were added and incubated for 30 min. The GTPase-Glo reagent converts any GTP remaining in the reaction to adenosine triphosphate (ATP). 25µl of detection reagent were added, which detects ATP in the reaction using a thermostable luciferase, producing a luminescent signal. The reaction was incubated with detection reagent for 10 min. Luminescent signal was measured on a FLUOstar Omega plate reader.

II.8. Liposome flotation assays

Liposome flotation assays were performed using a protocol adapted from Elizabeth Miller, MRC LMB (Fig. 2.6) (Miller *et al.*, 2002). In a 75µl reaction, 50µg liposomes were mixed with 1µM human Sar1, 320nM Sec23A/24C, and 520nM Sec13/31A, in HKM buffer, pH 6.8, with 1mM GMP-PNP or GDP and incubated for 1h at 30°C. For yeast COPII controls, we used Sar1,

Sec23/24, and Sec13/31 purified by Joshua Hutchings in-house. The reaction was adjusted to 1M sucrose, using sucrose-HKM, and a final volume of 350µl. The adjusted reaction was transferred to a centrifuge tube and overlaid with 350ul 0.75M sucrose-HKM and with 20ul HKM buffer. Reactions were centrifuged for 5h at 4°C at 279,982 x g using a Sw55Ti swinging rotor (Beckman Coulter). A flotation fraction of 20ul was collected from the top of the tube, followed by consecutive 100ul fractions. Liposome recovery was measured by diluting 2µl of recovered lipid (i.e., the floating fraction) in 50µl HKM with 0.1% Triton X-100 and comparison to a liposome dilution series. Fractions were analysed by SDS-PAGE.

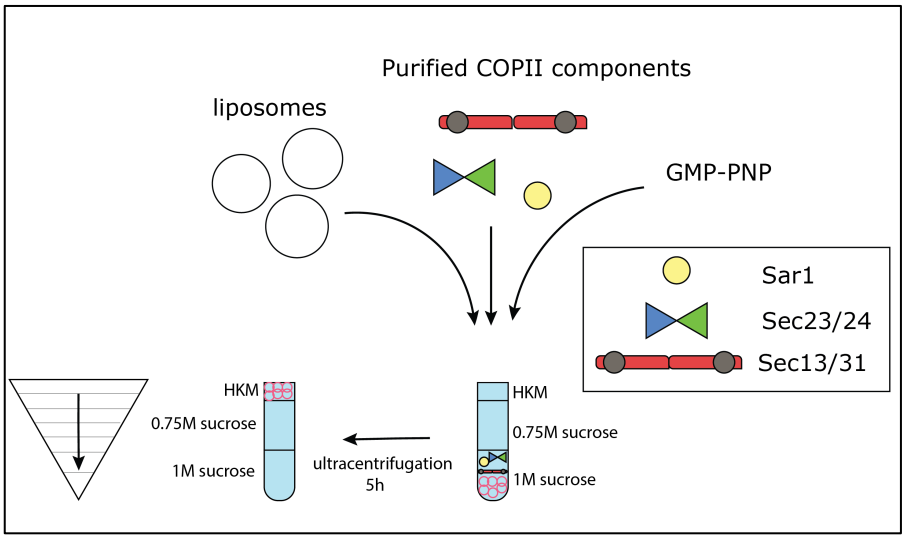

Figure 2.6: Liposome flotation assay diagram. COPII reconstitution reactions are incubated with liposomes in the presence of GMP-PNP. Reactions are adjusted to 1M sucrose and overlayed with 0.75M sucrose, followed by HKM buffer. Following centrifugation, liposomes are recovered from the floating fraction.

III. Biochemical Analysis of Human COPII Assembly on Membranes

In this chapter, I describe the establishment of a system for the reconstitution and characterisation of human COPII assemblies *in vitro*. To this end, I purified the human COPII components Sec23A/24C and Sec13/31A from insect cells and human Sar1A and Sar1B from *E. coli*. I assessed and optimised the membrane binding activity of purified COPII components and show recruitment of COPII proteins to artificial membranes using liposome flotation assays. Furthermore, I characterised the enzymatic activity of the purified proteins, confirming that the human Sar1 paralogues I purified have an intrinsic GTPase activity. In *in vitro* GTP hydrolysis assays, the GTPase activity of Sar1 was stimulated by the addition of Sec23A/24C and further accelerated by the addition of Sec13/31A. I further compare the GTPase activities of the two Sar1 paralogues using purified protein obtained from multiple protein purifications. Altogether, I have reconstituted the functional human COPII secretion system *in vitro*.

III.1. Previous Work

Studies of the human COPII secretion system have been impeded by the absence of a minimal *in vitro* reconstitution system containing a defined set of purified proteins and membrane models. The minimal requirements for human COPII vesicle formation are unestablished, as COPII vesicle budding from model membranes has never been achieved with purified human proteins in the absence of cytosol.

Kim et al. established a cell-free reconstitution of mammalian COPII membrane binding (Kim *et al.*, 2005). The authors used purified hamster Sar1, mouse 23A/human 24C, and human 13/31A, and successfully reconstituted COPII binding to synthetic liposomes. They further assessed whether COPII components were capable of remodelling cell-derived ER membranes and generating transport carriers in *in vitro* reconstitution reactions. They concluded that

purified mammalian COPII proteins were insufficient for membrane remodelling, and that the addition of rat liver cytosol was required for membrane budding. They hypothesise that an additional factor, providing an essential unknown function, was present in the cytosol. The authors conclude that the core mammalian COPII proteins are insufficient for the generation of cargo carriers in mammals. Alternatively, they reason that another Sec24 isoform apart from Sec24C could be needed for the packaging of the two particular cargo molecules that they monitored.

The membrane binding assay for mammalian COPII components that was used by Kim et al. as described above has since been applied to the study of membrane recruitment of mutant forms of human Sec23, which are implicated in craniofacial disease (Boyadjiev *et al.*, 2006; Fromme *et al.*, 2007). Both studies replicate membrane binding of purified COPII components to synthetic liposomes and utilise cytosol for membrane budding reactions. A cell-free reconstitution of human COPII carriers has shown packaging of procollagen cargo into carriers formed by purified human COPII proteins and cytosol (Gorur *et al.*, 2017). This is a promising development for the *in vitro* study of COPII carriers loaded with large cargo. In this chapter, I describe the establishment of a minimal human COPII reconstitution system using defined components - purified proteins and model membranes - in the absence of additional cytosolic factors.

III.2. Purification of COPII Proteins

To reconstitute the human COPII system, I optimised the expression and purification of the two human Sar1 paralogues, Sar1A and Sar1B, the inner coat heterodimers Sec23A/24C, and the outer coat heterotetramers Sec13/31A.

III.2.1. Purification of Sec13/31A

The human Sec13 and Sec31A genes were cloned into separate vectors for insect cell virus generation. A hexa-histidine tag, followed by a TEV cleavage site, was introduced on the N-terminus of Sec31A to allow for metal ion affinity purification. Sec13 contained no tag, and Sec31A and Sec13 were simultaneously expressed by co-infecting insect cells for co-purification. Insect cells were infected with a three-fold excess of Sec13 virus with respect to Sec31A to ensure they were purified in stoichiometric amounts for complex formation.

The purification of Sec13/31A was designed based on the purification protocol for the yeast Sec13/31 complex that was previously established in our laboratory. Briefly, the complex was immobilised to a metal affinity resin via the N-terminal His-tag of Sec31 and further purified by ion affinity chromatography (Fig. 3.1).

In the original purification protocol, the His-tag on Sec31 was retained. However, it was since established that the N-terminus of yeast Sec31 is essential for outer coat interactions, and that a His-tag positioned on the N-terminus disrupts the formation of an outer coat lattice (Hutchings *et al.*, 2018). Therefore, I optimised the purification protocol for Sec13/31A to include a TEV cleavage step, removing the His-tag after metal affinity chromatography. To remove uncleaved Sec31A, the cleaved His-tag, and the His-tagged TEV protease, I introduced a reverse affinity chromatography step. To allow for these contaminants to bind to the metal ion column during the reverse affinity step, I lowered the high imidazole concentration of the sample after metal affinity chromatography using a dialysis step. Lowering the imidazole concentration also allows more efficient His-tag cleavage, as high imidazole concentrations can result in lower TEV cleavage efficiency (Yeliseev, Zoubak and Gawrisch, 2007). Hence, I performed dialysis into a low imidazole buffer simultaneously with TEV cleavage overnight.

I aimed to produce sufficiently concentrated protein to allow for the screening of a wide range of concentrations in *in vitro* reconstitution experiments. Initially, I eluted Sec13/31A from ion exchange columns using gradient elution, and then attempted to concentrate the protein using commercial protein concentrators. I observed that the concentration of Sec13/31A did not increase proportionally to the volume reduction during concentration, suggesting its association with the protein concentrator membrane. Having established that Sec13/31A elutes between 50 and 600mM NaCl during gradient elution from the ion exchange column, I instead concentrated Sec13/31A by substituting the gradient elution during ion affinity with a step-elution with 600mM NaCl. This resulted in the elution of protein at concentrations of above 1 mg/ml. The purification of Sec13/31A is shown in Figures 3.1, 3.2, and 3.3.

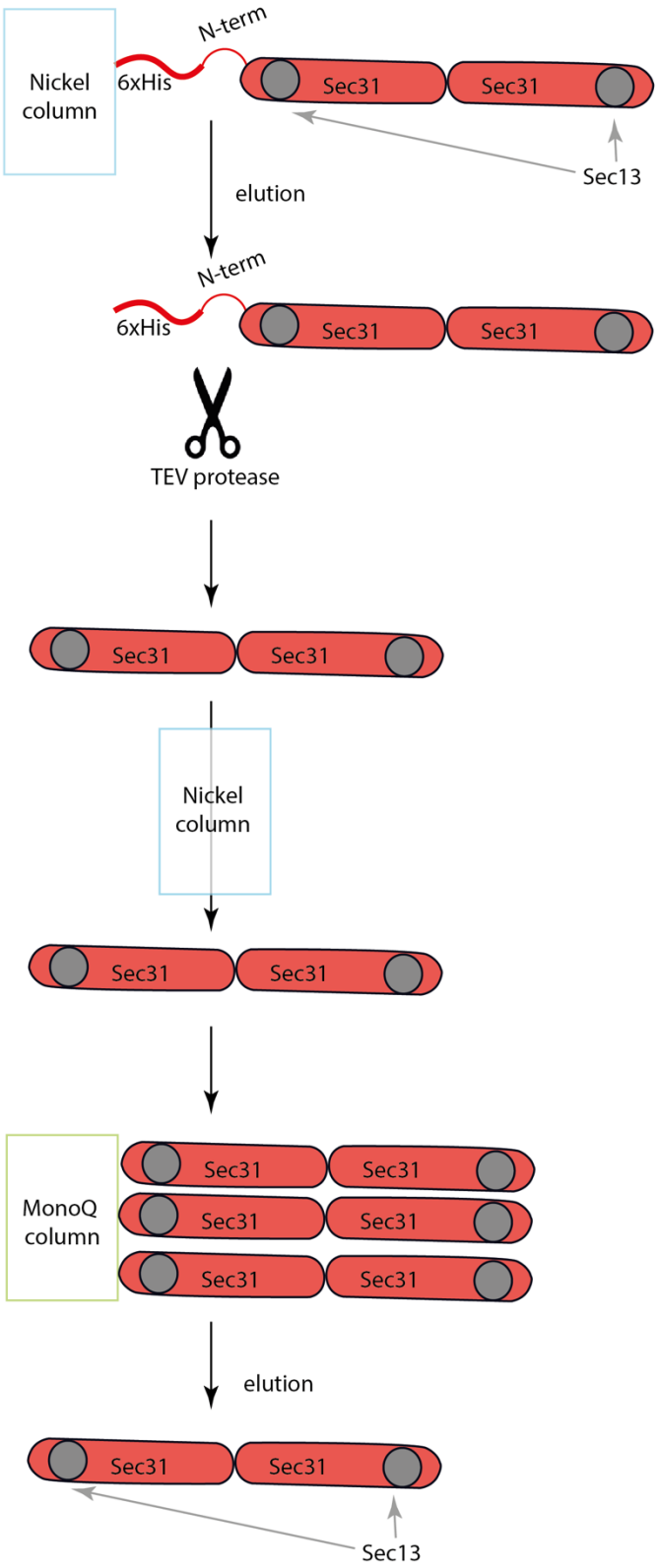

Figure 3.1: Diagram of the purification process of the Sec13/31A heterotetrameric complex. Sec13/31A was purified using metal ion (nickel) affinity purification, followed by a reverse metal affinity step and ion exchange purification using a MonoQ anion exchange column.

Sec13/31A formed a stable complex, as shown by the presence of Sec13 throughout the purification. The formation of a Sec13/31A complex suggests that both proteins are correctly folded. While in SDS-PAGE analysis (Fig. 3.3B), the band corresponding to the molecular weight (MW) of Sec31A is sharp, the band corresponding to the MW of Sec13 is smeared, suggesting the presence of multiple species. Human Sec13 is proposed to be phosphorylated at two positions, S184 and S309 (Olsen *et al.*, 2010; Zhou *et al.*, 2013). The presence of multiple phosphorylation states of Sec13 in the sample could explain the appearance of the band.

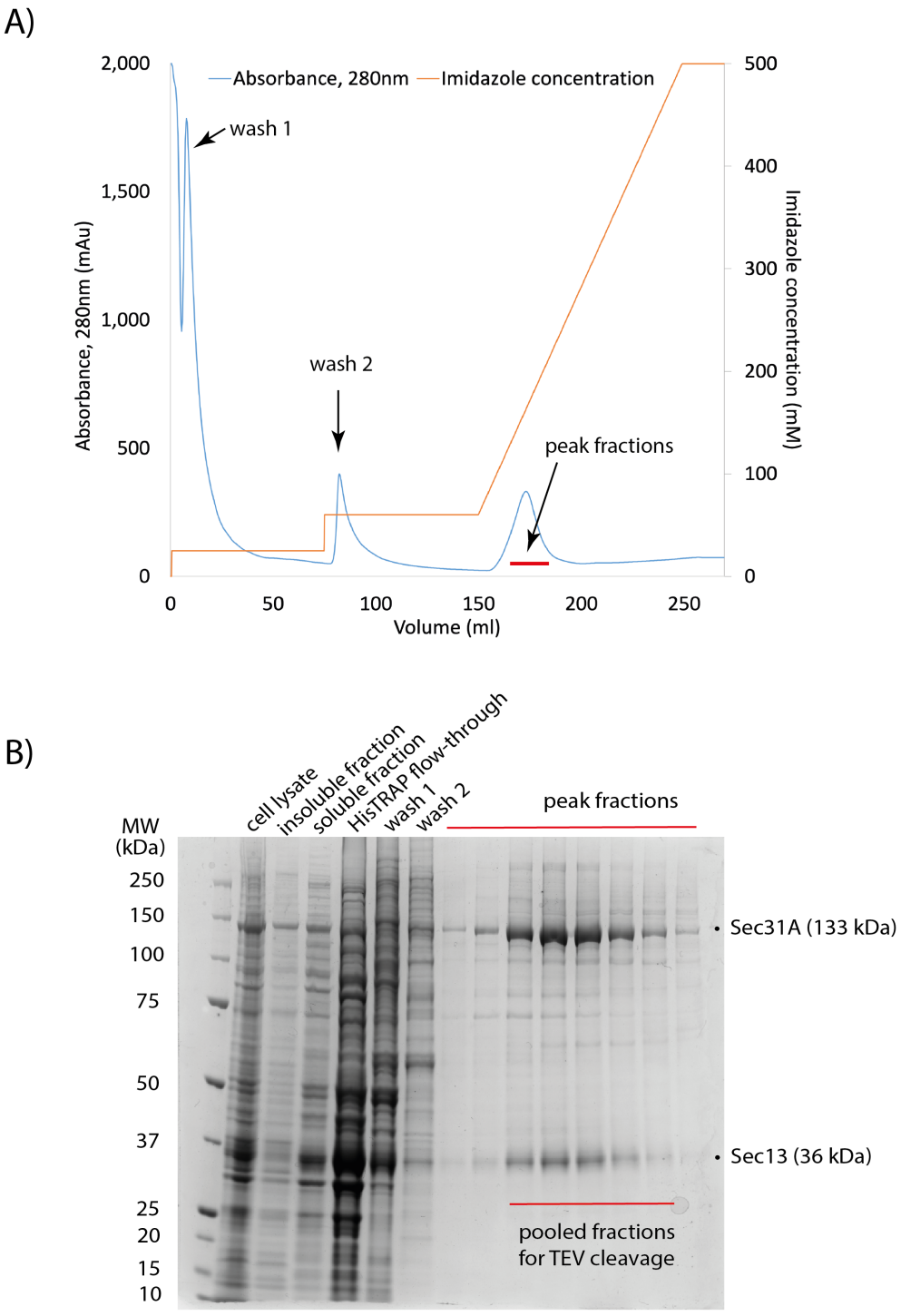

Figure 3.2: Metal ion affinity purification of Sec13/31A using a hexa-histidine tag on Sec31A. A representative purification is shown. Sec13/31A bind and co-purify. (A) Sec13/31A elutes as a monodisperse peak from a HisTRAP column at an average concentration of 200mM imidazole. (B) SDS-PAGE analysis of HisTRAP fractions.

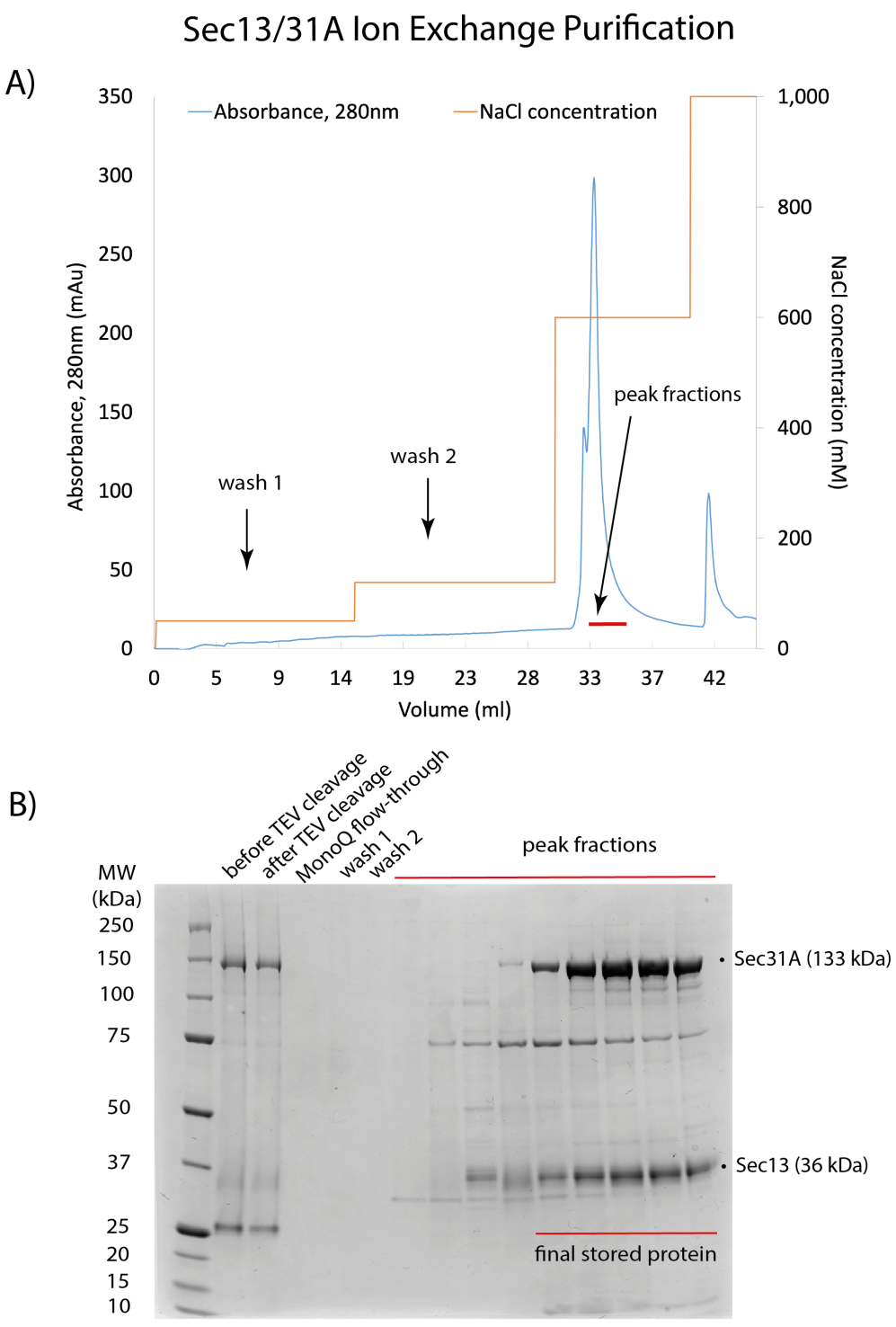

Figure 3.3: Anion exchange purification of Sec13/31A. A representative purification is shown. (A) Sec13/31A elutes as a monodisperse peak from a MonoQ column at 600mM NaCl. (B) SDS-PAGE analysis of MonoQ fractions.

Throughout optimisation, all Sec13/31A purifications yielded protein samples that, when analysed by SDS-PAGE, showed multiple faint bands under the band corresponding to the molecular weight of Sec31. This suggests that Sec31 is undergoing degradation during the purification process.

To assess whether the purified Sec13/31A is functional despite the degradation, I analysed its ability to self-assemble. Self-assemblies of human Sec13/31, or cages, have been observed in previous reports (Stagg *et al.*, 2006; Noble *et al.*, 2013). When I analysed purified Sec13/31A by negative stain EM, I observed Sec13/31A cages (Fig. 3.4). This suggests that the purified outer coat components can form functional assemblies.

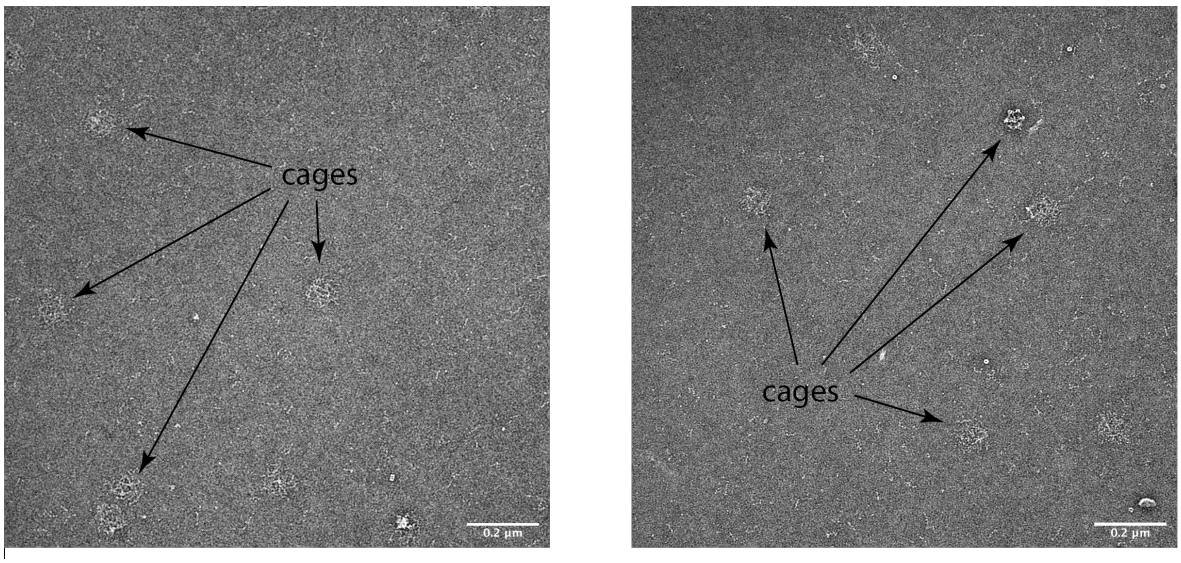

Figure 3.4: Cages of Sec13/31A observed by negative stain EM. Sec13/31A was added to the grids at a concentration of 30μg/ml in HKM buffer.

The buffer conditions under which I observe cage assembly are comparable to those of previous studies. Studies of human COPII cages used protein dialysis into high salt buffer to allow for cage assembly (Stagg *et al.*, 2006; Noble *et al.*, 2013). For cryo-EM analysis, samples were dialysed into a low-salt buffer. Lowering the salt concentration before cryo-EM sample preparation is beneficial, as higher salt concentrations decrease contrast during electron microscopy imaging (Drulyte *et al.*, 2018). In the final Sec13/31A purification step, I used a high salt buffer (20mM Tris-HCl pH 7.5, 600mM NaCl, 1mM MgOAc, 1mM DTT, 10% glycerol)

step-elution from a anion exchange column. For imaging, I diluted the sample 16-fold into low salt HKM buffer (20mM HEPES pH 6.8, 160mM KOAc, 1mM $MgCl_2$).

The cages that I observed using negative stain EM were of a range of diameters between 680Å and 920Å (Fig. 3.5). This range of diameters is similar to the one previously observed for yeast and human Sec13/31 cages (Antonny *et al.*, 2003; Stagg *et al.*, 2006, 2008; Bhattacharya, O'Donnell and Stagg, 2012).

Previous studies have suggested that sample preparation methods are important for the homogeneity of Sec13/31 cages and must therefore be considered for high-resolution structure determination (Noble *et al.*, 2013). Analysis of Sec13/31A cryo-EM grids using cryo-electron tomography suggested that significant amounts of unassembled Sec13/31A were present in the sample, which were contributing to sample heterogeneity and were an impediment to imaging. To separate Sec13/31A that was incorporated into cages from unassembled proteins, the authors centrifuged the sample through a sucrose-glutaraldehyde gradient. While I observe little background signal in negative stain EM, this procedure could be beneficial for the preparation of grids of Sec13/31 cages.

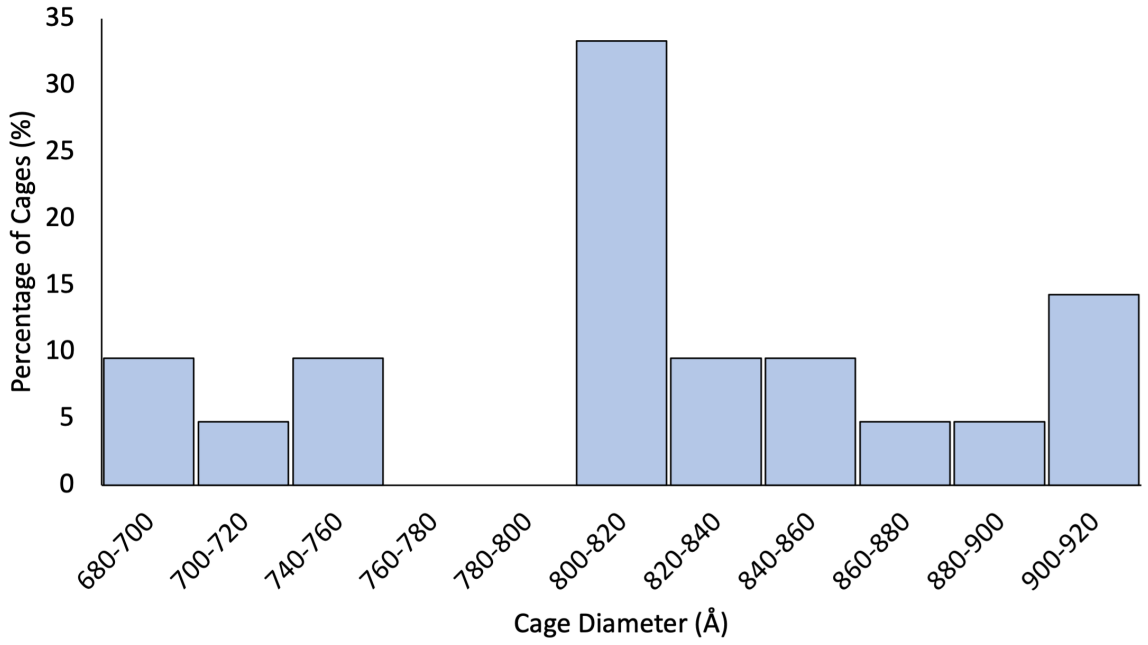

Figure 3.5: Size distribution of purified human Sec13/31A cages assembled *in vitro*.

III.2.2. Purification of Sec23A/24C

Human Sec23A and Sec24C genes were cloned into separate vectors for insect cell virus generation. A N-terminal hexa-histidine tag was introduced on Sec24C to allow for metal ion affinity chromatography. The proteins were co-expressed in Sf9 cells. As Sec23A was purified using co-purification with the tagged Sec24C, a three-fold excess of Sec23A virus was added to insect cells, compared to the Sec24C virus. The purification of Sec23A/24C is shown in Figures 3.6, 3.7, and 3.8.

Initially, the purification of human Sec23A/24C was based on the human Sec13/31A purification protocol, which was optimised as discussed above. However, during the overnight cleavage and dialysis step, Sec23A/24C non-specifically associated with the dialysis tubing, which I determined by measuring the concentration of the sample before and after dialysis. The dialysis step therefore resulted in purifications with consistently low protein yield and concentration. To increase protein yield, the overnight dialysis and cleavage step was eliminated, and the His-tag on the Sec24C was retained. The N-terminus of Sec24C is highly variable and has not been shown to be involved in the interactions between core COPII components (Pagano *et al.*, 1999; Bi, Corpina and Goldberg, 2002). In yeast reconstitutions, the inner coat can assemble with or without the His-tag on Sec24C (Hutchings, J., Pyle, E., personal communication). Hence, I hypothesised that the retainment of the His-tag would not disrupt COPII assembly in reconstitution reactions. (Indeed, the purified Sec23A/24C was capable of forming an inner coat, see *COPII Budding Reactions by Electron Microscopy*, Section IV.3.2). The optimisation allowed for the purification of Sec23A/24C to 0.3mg/ml, which is sufficient for its use in COPII budding reactions. Attempts to concentrate Sec23A/24C to a concentration above 0.35mg/ml resulted in its aggregation (data not shown), which is consistent with previous observations of the aggregation-prone nature of the yeast inner coat proteins (Antonny *et al.*, 2003).

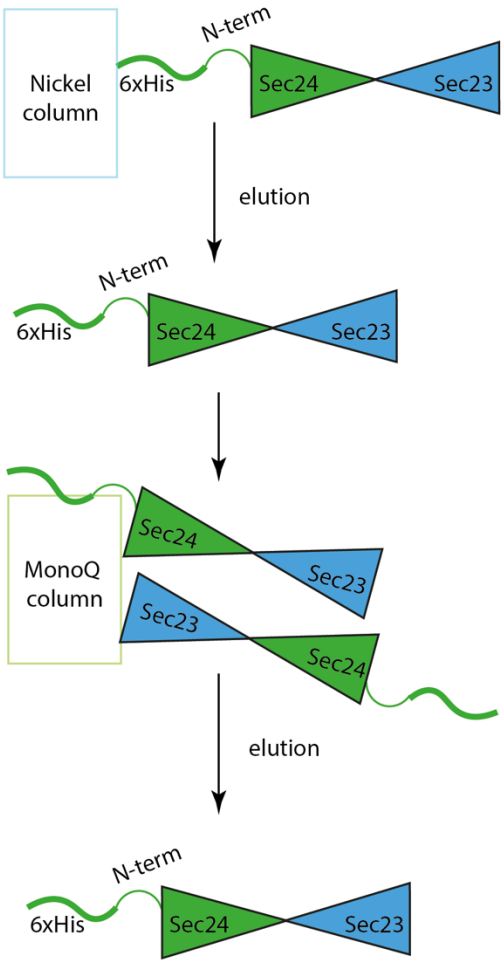

Figure 3.6: Diagram of the purification process of the Sec23A/24C heterodimeric complex. Sec23A/24C was purified using metal ion (nickel) affinity purification, followed by ion exchange purification using a MonoQ anion exchange column.

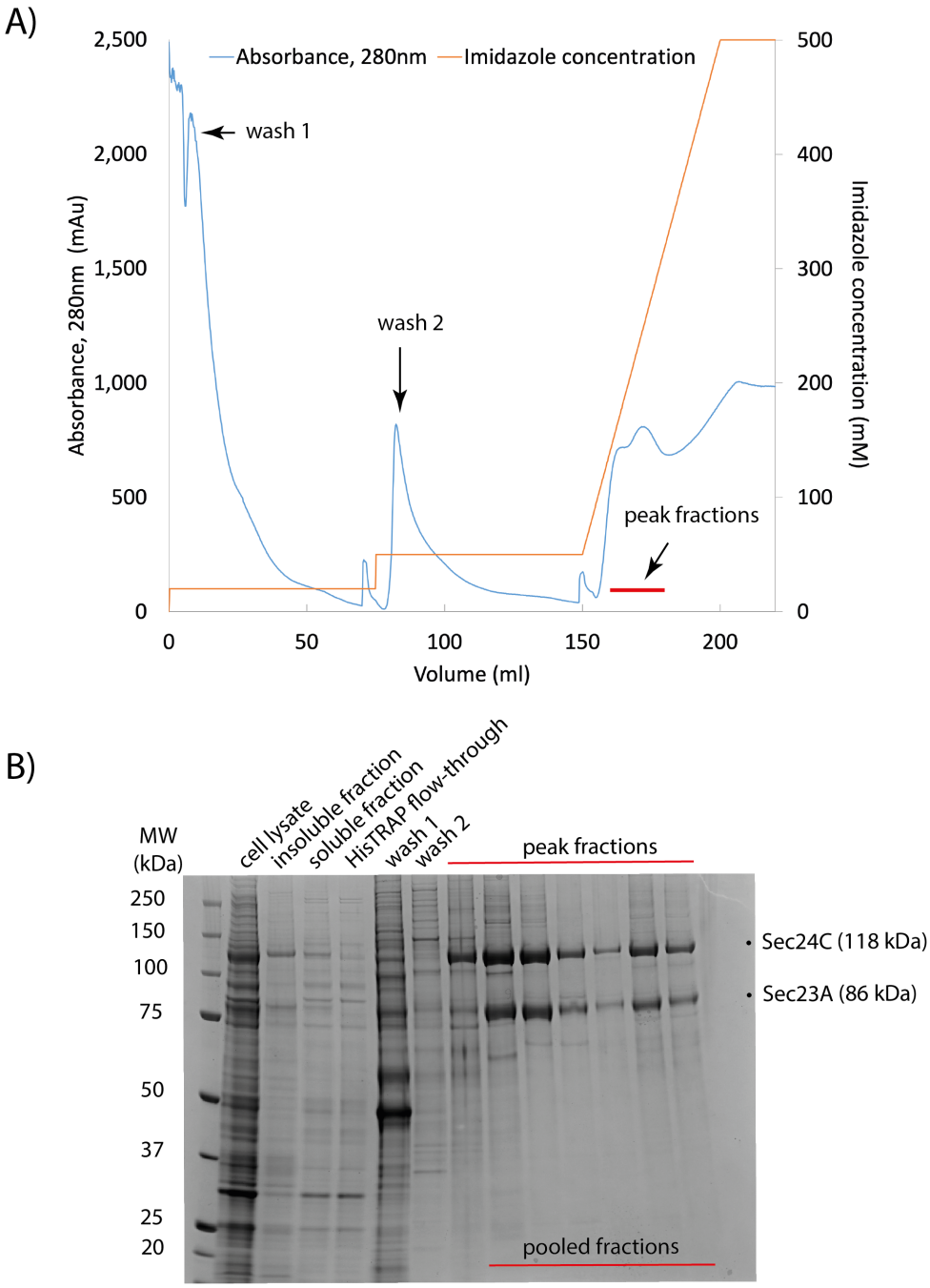

Figure 3.7: Metal ion affinity purification of Sec23A/24C using a hexa-histidine tag on Sec24C. A representative purification is shown. Sec23A/24C bind and co-purify. (A) Sec23A/24C elutes from a HisTRAP column at an average concentration of 200mM imidazole. (B) SDS-PAGE analysis of HisTRAP fractions.

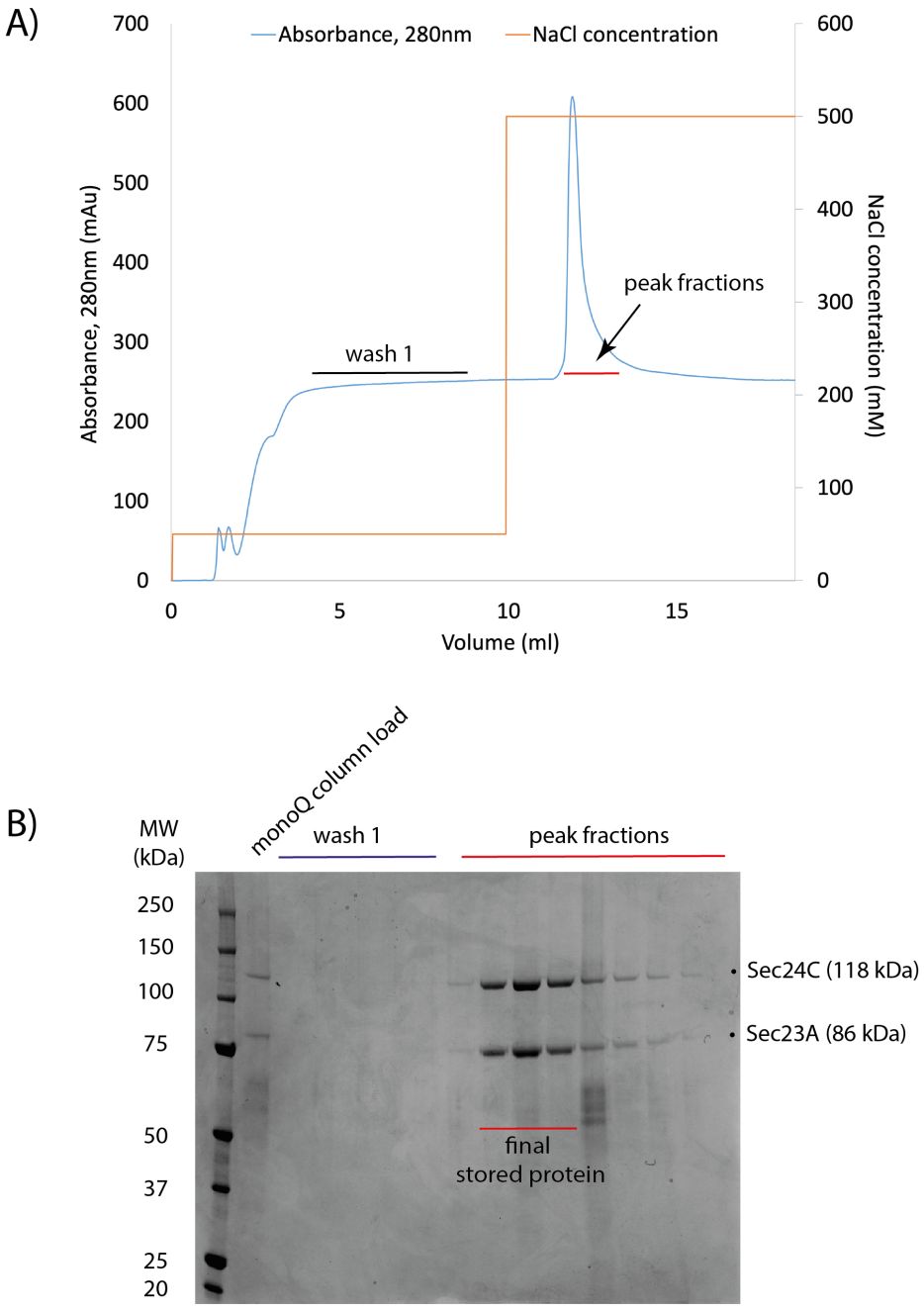

Figure 3.8: Anion exchange purification of Sec23A/24C. A representative purification is shown. (A) Sec23A/24C elutes from a MonoQ column as a monodisperse peak at 500mM NaCl. (B) SDS-PAGE analysis of MonoQ fractions.

III.2.3. Purification of Sar1

Initially, Sar1A was cloned into an *E. coli* expression vector with a N-terminal hexa-histidine tag, followed by a TEV protease cleavage site. The protein was purified using a metal ion

affinity purification protocol. The N-terminus of Sar1 is essential for membrane binding (Goldberg, 1998; Huang *et al.*, 2001; Bi, Corpina and Goldberg, 2002; Bielli *et al.*, 2005; Hutchings *et al.*, 2018). Therefore, to expose the N-terminus, the N-terminal His-tag was cleaved overnight using TEV protease. The cleavage step was performed simultaneously with dialysis into a low-imidazole buffer to allow for reverse metal ion affinity chromatography. In the reverse affinity step, the cleaved His-tag, the uncleaved protein fraction, and the His-tagged TEV protease were removed. The purification method is illustrated in Figure 3.9B, and the final purified protein is shown in Figure 3.9C, lane 2.

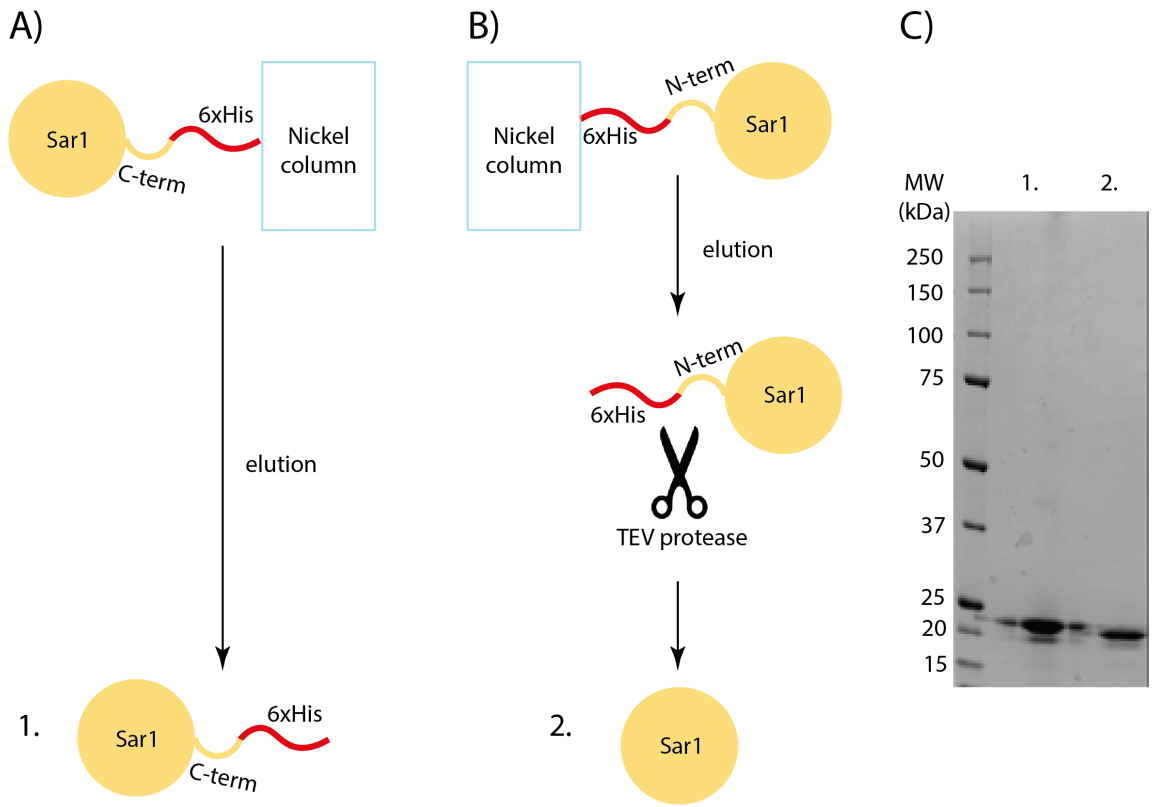

Figure 3.9: Metal ion affinity purification of Sar1A with a hexa-histidine tag. (A) Schematic of the purification of Sar1 with a C-terminal His-tag, which was retained. (B) Schematic of the purification of Sar1 with an N-terminal His-tag, cleaved with TEV protease after the nickel affinity binding step. (C) SDS-PAGE analysis of the final purified proteins: 1. Sar1A with a retained C-terminal tag, purified as shown in (A). 2. Sar1A with a cleaved N-terminal tag, purified as shown in (B).

While Sar1 appears pure and is of the expected molecular weight, liposome flotation assays showed that the protein was unable to bind membranes (see Section III.3.). To assess whether degradation or loss of the N-terminal helix of Sar1 could be the reason for lack of membrane binding, the purified Sar1A protein was commercially analysed by mass spectrometry and proved intact. I hypothesised that the initial presence of the N-terminal tag or the process of its cleavage could have disrupted the native conformation of Sar1. To assess whether this could be the reason behind the lack of membrane binding, I generated a construct encoding for Sar1 with a C-terminal hexa-histidine tag, instead of the N-terminal tag. The C-terminal His-tag was retained. The purification process is illustrated in Figure 3.9A, and the final purified protein is shown in Figure 3.9C, gel lane 1. This protein also proved unable to bind membranes when assessed using liposome flotation assays.

Finally, I turned to purifying Sar1 using a glutathione affinity purification protocol that has previously been used for hamster Sar1 purification in the literature and shown to yield functional protein (Kim *et al.*, 2005). I generated a DNA construct encoding for Sar1A with an N-terminal GST-tag, followed by a thrombin cleavage site, expressed the protein and purified it using glutathione affinity purification. The tag was cleaved overnight after the affinity step to expose the N-terminus of Sar1 and to allow for Sar1 membrane binding (Goldberg, 1998; Huang *et al.*, 2001; Bi, Corpina and Goldberg, 2002; Bielli *et al.*, 2005; Rao *et al.*, 2006; Hutchings *et al.*, 2018). GDP was added to a 10µM concentration during the cleavage step to stabilise the inactive (GDP-bound) conformation of Sar1 after the cleavage of the bulky N-terminal GST-tag. Nucleotide addition can enhance protein stability (Waldron and Murphy, 2003) and ensure that the protein population is in a single conformational state. Using this purification protocol (Fig. 3.10A), I observed a prominent band corresponding to the molecular weight of Sar1A, 22kDa (Fig. 3.10B).

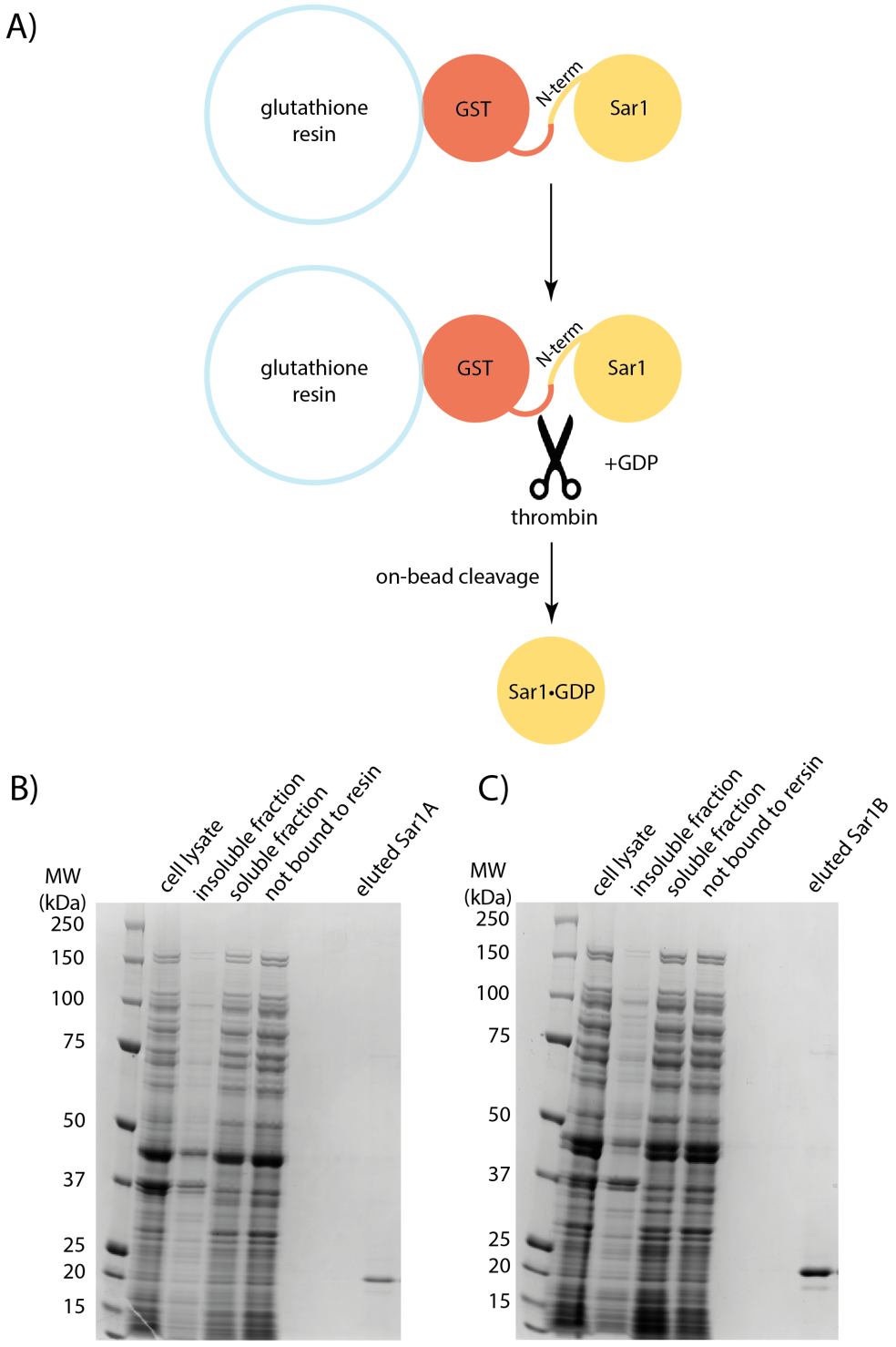

Figure 3.10: Glutathione affinity purification of Sar1A and Sar1B. (A) Purification procedure schematic. The GST-tag on Sar1 is used in the initial affinity step and is subsequently cleaved with thrombin protease in the presence of GDP. (B) SDS-PAGE analysis of selected fractions from the purification of Sar1A with a cleaved N-terminal GST-tag (Mw 22kDa). (C) SDS-PAGE analysis of fractions throughout the purification of Sar1B with a cleaved N-terminal GST-tag (Mw 22kDa).

When tested in liposome flotation assays, the protein obtained with the latter method showed to be functional and bound membranes (see Section III.3.).

The amino acid sequences of the cleaved N-terminally His-tagged Sar1A and the cleaved N-terminally GST-tagged Sar1A are the same, and it is difficult to reason why the latter is active in membrane binding while the former is not. The differences in membrane binding between the two could be due to differences in conformation. This could be caused by the different construct design and purification procedures and is addressed in further detail in the *Discussion*.

Building up on the optimisation performed for Sar1A, I cloned Sar1B with an N-terminal GST-tag, followed by a thrombin cleavage site, and purified it using glutathione affinity purification (Fig. 3.10B). The purification produced protein that corresponded to the molecular weight of Sar1B, 22kDa (Fig. 3.10C) The ability of this protein to bind membranes was confirmed using liposome flotation assays (see Section III.3.).

III.3. COPII Membrane Binding

Initially, I attempted to characterise the binding of purified human COPII proteins to donor membranes using negative stain EM analysis of *in vitro* reconstitution experiments. I observed that the COPII components I initially purified were not efficient in deforming membranes and that they did not form a stable coat (see *COPII Budding Reactions by Electron Microscopy*, Section IV.2). I hypothesised that this was due to poor Sar1 binding to membranes, which could result in insufficient COPII component recruitment for coat formation. Observing assemblies by EM does not allow for quantitative assessment of membrane binding. Therefore, to assess and improve membrane binding of purified COPII components, I used a membrane recruitment assay.

I set out to assess the binding of COPII components to liposomes in the presence of GMP-PNP or GDP. Upon GDP to GTP exchange, Sar1 is proposed to undergo a conformational change and project an N-terminal helix which inserts into membranes (Goldberg, 1998; Huang *et al.*, 2001; Bi, Corpina and Goldberg, 2002; Bielli *et al.*, 2005; Rao *et al.*, 2006; Hutchings *et al.*, 2018). Upon GTP hydrolysis, Sar1 undergoes an opposing conformational change, retracting its N-terminal helix (Antonny *et al.*, 2001). Hence, I expected that Sar1 would be recruited to liposomes in the presence of a GTP analogue, and less so in the presence of GDP.

I used yeast COPII components previously purified in our laboratory as a positive control during my initial optimisation of liposome flotation reactions. The binding of yeast COPII proteins to liposomes in liposome flotation assays has been well-established in the literature (Matsuoka *et al.*, 1998, 2001; Matsuoka and Schekman, 2000; Bigay and Antonny, 2006). The binding of this particular set of purified yeast proteins has been shown previously by our collaborators (Hutchings *et al.*, 2018). I observed that using this assay, I can detect membrane recruitment of yeast COPII components in the presence of GMP-PNP (Fig. 3.11, see *Methods*, Fig. 2.6). To optimise the amount of liposomes to use in liposome flotation assays, I tested the recovery of yeast COPII proteins in the floating fraction when using 10 µg and 50 µg of liposomes. Faint bands corresponding to yeast COPII proteins can be observed in the floating fraction with 10µg of liposomes per reaction (Fig. 3.11A, Gel lane 2). More intense bands corresponding to COPII can be observed in the floating fraction when the amount of liposomes used in the reaction is increased to 50µg (Fig. 3.11B, Gel lane 1). As increasing the amount of liposomes from 10µg to 50µg increases the recovery of yeast COPII proteins, 50µg of liposomes were used in further liposome flotation reactions.

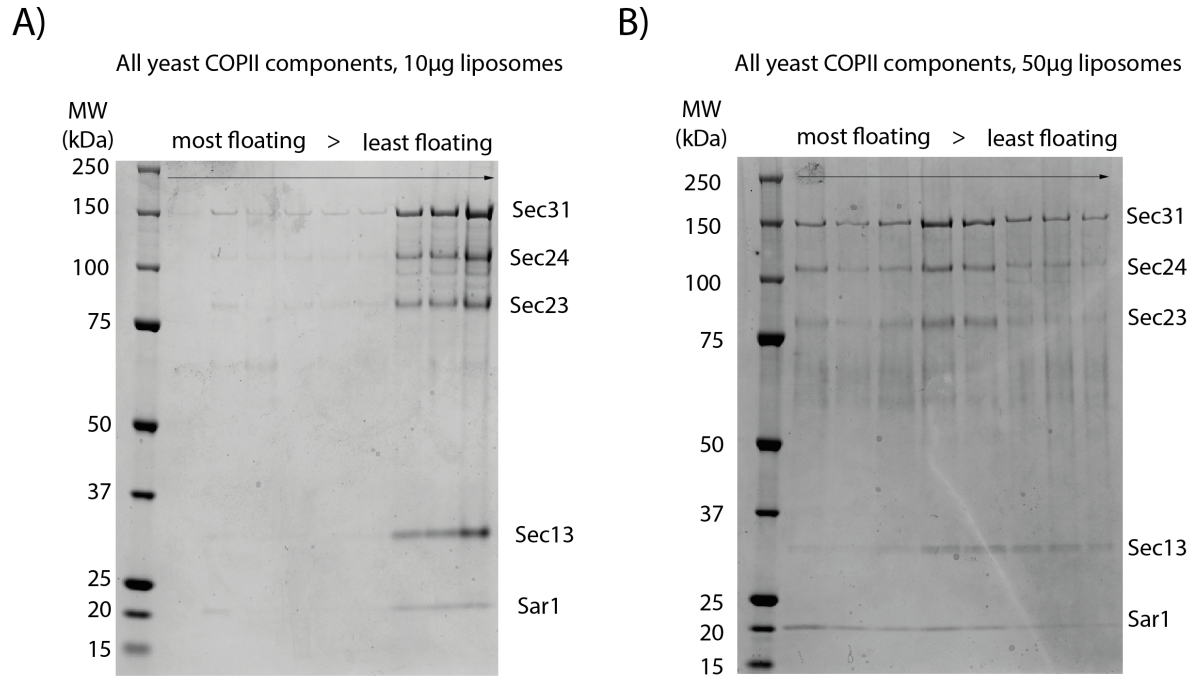

Figure 3.11: Yeast COPII recruitment to membranes in liposome flotation assays as observed by SDS-PAGE in two separately conducted experiments. (A) Gel lanes 2-9: most to least floating fractions following centrifugation. 10µg of liposomes used per 75µl reconstitution

reaction. (B) Gel lanes 1-8: most to least floating fractions following centrifugation. 50µg of liposomes used.

When I performed liposome flotation assays using a 1µM concentration of Sar1A purified by nickel affinity purification, I could not detect membrane recruitment in the presence of GMP-PNP (Fig. 3.12A, Gel lane 1), suggesting that Sar1A purified using by nickel affinity purification is inefficient in membrane binding. The same concentration of Sar1 was capable of membrane remodelling, albeit inefficient, as observed by EM (see *COPII Budding Reactions by Electron Microscopy*, Section IV.2.). This could be explained by the higher sensitivity of EM analysis.

Aiming to produce Sar1A that efficiently binds membranes, I generated N-terminally GST-tagged Sar1A and purified it by glutathione affinity purification (Section III.2.3.). When I added the same concentration (1µM) of Sar1A purified by glutathione affinity to liposomes as used above for Sar1A purified by nickel affinity, I detected the recruitment of the protein to liposomes (Fig. 3.12B, Gel lane 1). Sar1B purified by glutathione affinity purification was also capable of binding membranes (Fig. 3.12D, Gel lane 1). This suggests that the choice of Sar1 construct and the protein purification protocol used can affect membrane binding. To further optimise the recruitment of Sar1 to membranes, I introduced an incubation step with GMP-PNP to allow for more complete nucleotide exchange.

Both paralogues were recruited to membranes with GMP-PNP (Fig. 3.12). However, membrane binding for both paralogues was also observed in the presence of GDP (Fig. 3.12C and E). The finding that human Sar1 is capable of binding membranes when bound to GDP agree with previous observations by Kim et al. with purified hamster Sar1A, which has a 99% sequence identity to human Sar1B (Kim *et al.*, 2005). I further observed that the nucleotide state made a greater difference to Sar1B than to Sar1A membrane binding.

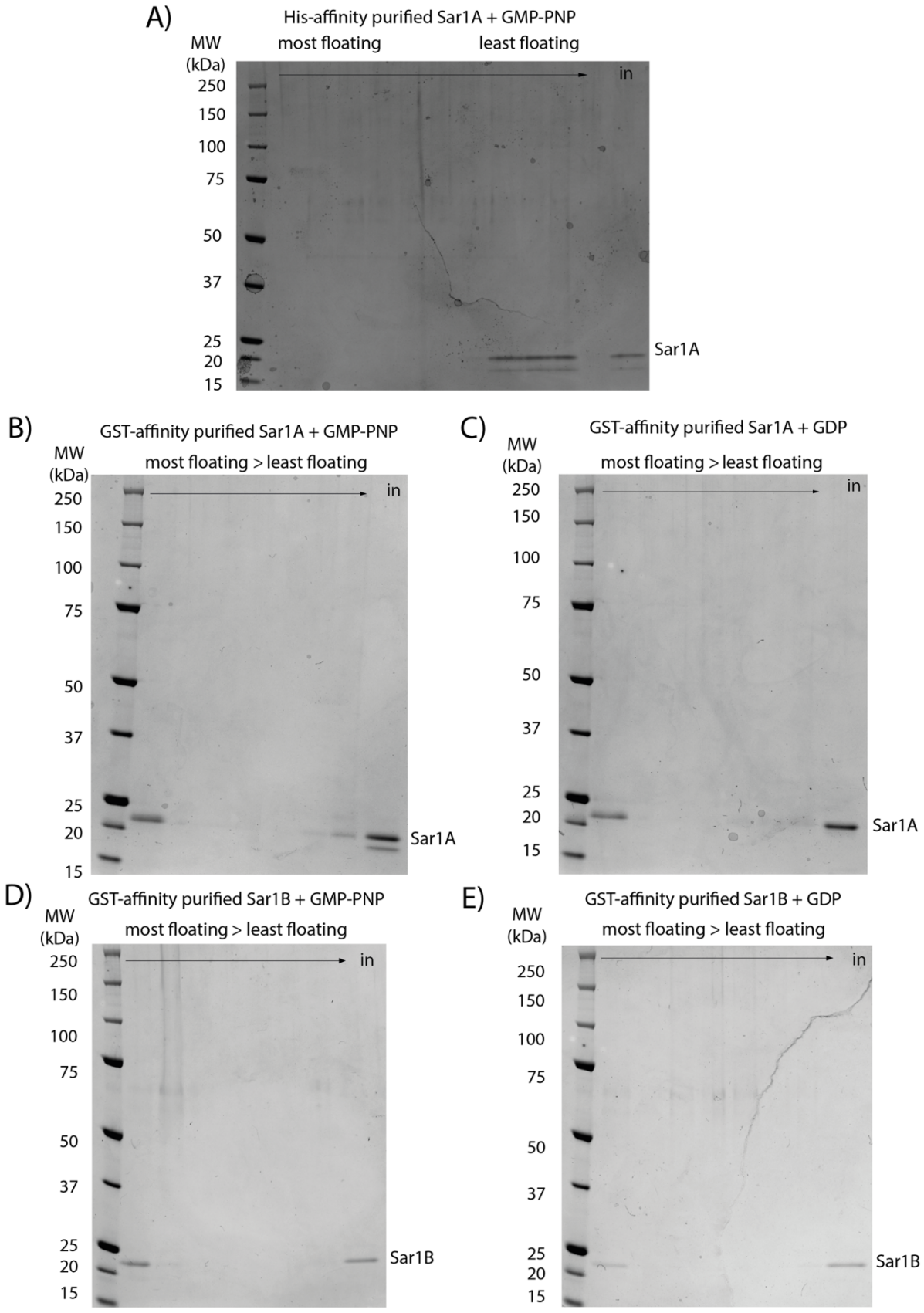

Figure 3.12: Sar1A and Sar1B purified by glutathione affinity purification bind liposomes. The nucleotide state makes a greater difference for Sar1B binding than for Sar1A binding. (A-E)

Gel lanes 1-7: most to least floating fractions following centrifugation. Gel lane 8: protein input. (A) 1µM Sar1A purified by nickel affinity purification (B, C) 1µM Sar1A purified by glutathione affinity purification (D,E) 1µM Sar1B purified by glutathione affinity purification (B,D) 1µM GMP-PNP (C, E) 1µM GDP.

When Sar1A was incubated with GMP-PNP, an additional 17kDa band was visible in the SDS-PAGE input fraction (Fig. 3.12B, Gel lane 8). This band likely represented a Sar1 degradation product. It did not appear when Sar1A was incubated with GDP, suggesting that it only resulted from the GTP-analogue-bound Sar1A state (Fig. 3.12C, Gel lane 8). This band was not observed in the floating fraction incubated with GMP-PNP (Fig. 3.12B, Gel lane 1), suggesting that it is not capable of binding membranes. Furthermore, no additional band was observed for GMP-PNP-bound Sar1B (Fig. 3.12D).

Having established the optimal purification protocol for Sar1 and optimised the conditions for Sar1 membrane recruitment, I set to optimise the recruitment of the inner and outer COPII components to the membrane. First, I tested the recruitment of inner coat components to liposomes in the presence of Sar1B purified by glutathione affinity purification (Fig. 3.13A and B). In the presence of the non-hydrolysable GTP analogue, Sar1B recruited the inner coat components to liposomes (Fig. 3.13A, Gel lane 1). In the presence of GDP, while Sar1B was partially bound to membranes, it did not recruit Sec23A/24C (Fig. 3.13B, Gel lane 1). This suggests that GMP-PNP-bound Sar1B is more efficient at inner coat binding than GDP-bound Sar1B. This observation is in agreement with the results of previous experiments on human COPII membrane binding, where the recruitment of Sar1B and Sec23/24 to liposomes was assessed using liposome flotation assays (Boyadjiev *et al.*, 2006). In these experiments, Sar1B was added to liposomes in the presence of inner coat components and either GDP or the non-hydrolysable GTP analogue GTPφS. Sar1B was recruited to liposomes with either nucleotide. However, it was capable of recruiting the inner coat only in the presence of GTPφS. This suggests that the affinity of Sar1B for Sec23/24 is dependent on its nucleotide state.

After assessing that the inner coat was recruited to membranes by Sar1B in the presence of the GTP analogue, I performed liposome flotation experiments using the full set of COPII proteins: Sar1B, the inner coat components Sec23A/24C, and the outer coat components Sec13/31A. Sar1B recruited the full set of COPII components to liposomes in the presence of

the GTP analogue (Fig. 3.13C). In the presence of GDP, no COPII components could be observed in the floating fraction (Fig. 3.13D). This contrasts previous observations by Kim et al., in which the full set of COPII proteins was recruited to liposomes both in the presence of GMP-PNP and of GDP (Kim *et al.*, 2005). Altogether, purification of Sar1B through N-terminal GST-glutathione affinity produced Sar1 that binds membranes and recruits inner and outer coat components.

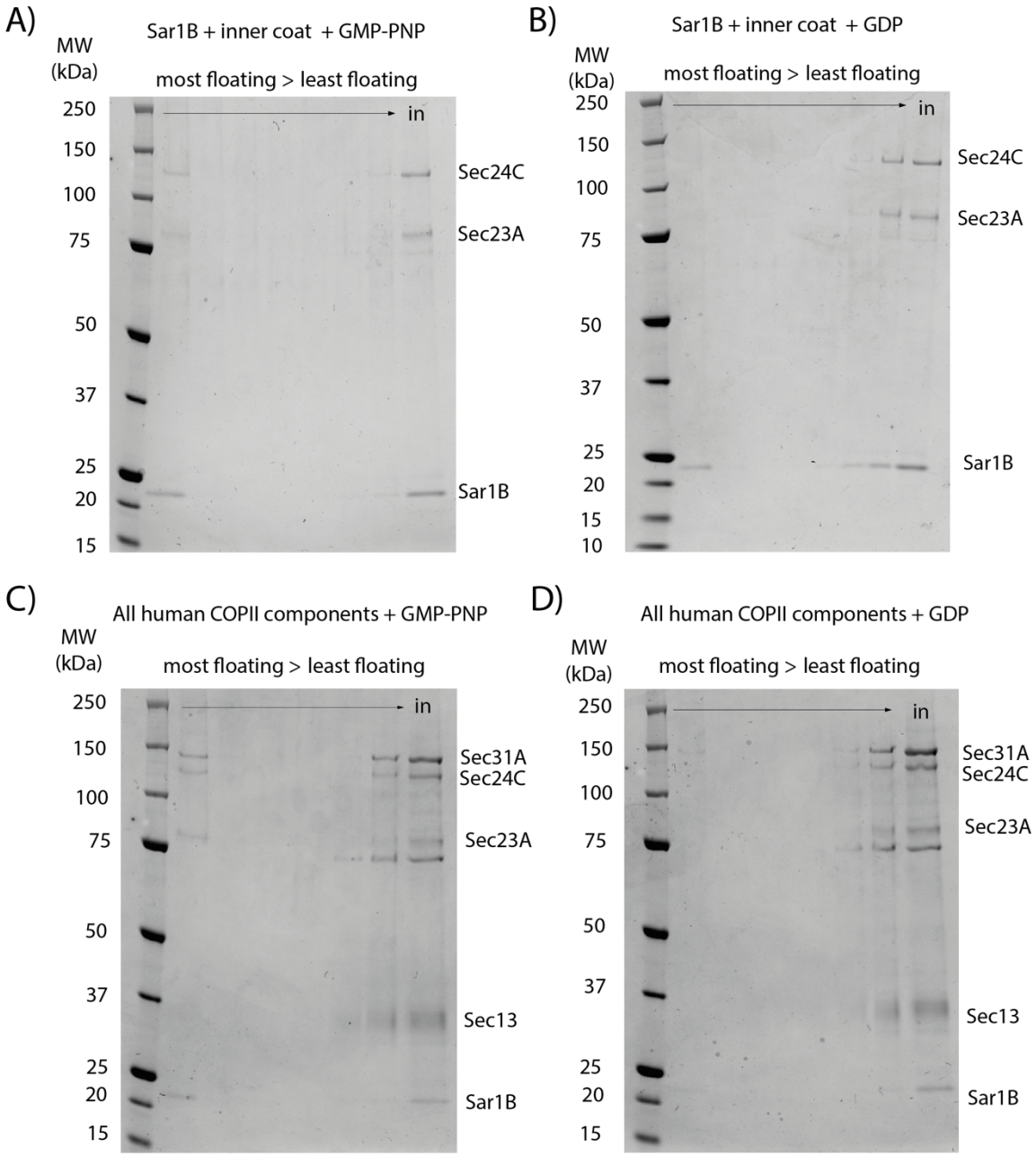

Figure 3.13: Sar1B binding to liposomes in the presence of GMP-PNP recruits the inner and outer COPII components. The COPII coat is not recruited to liposomes in the presence of GDP.

(A,B) Gel lanes 1-6: most to least floating fractions following centrifugation. Gel lane 7: protein input. Reactions contained 1µM Sar1B, 320nM Sec23A/24C, and 320nM Sec13/31A. (C,D) Gel lanes 1-7: most to least floating fractions following centrifugation. Gel lane 8: protein input. Reactions contained 1µM Sar1B, 320nM Sec23A/24C. (A, C) 1µM GMP-PNP (B,D) 1µM GDP.

III.4. GTP hydrolysis activity of Sar1A and Sar1B and COPII

To establish whether the proteins I purified were fully functional, I investigated whether the COPII system had retained its enzymatic activity. Sar1 hydrolyses GTP, which is essential to its function in the cell. The mechanism of GTP hydrolysis by COPII is described in detail in the *Introduction*. Briefly, Sar1 exchanges GDP to GTP as stimulated by its cognate GEF, Sec12 (Nakano, Brada and Schekman, 1988). GTP hydrolysis by Sar1 is stimulated by its GAP, Sec23 (Yoshihisa, Barlowe and Schekman, 1993; Barlowe *et al.*, 1994; Miller *et al.*, 2003). Sec31 further stimulates the GAP activity of Sec23 (Yoshihisa, Barlowe and Schekman, 1993; Antonny *et al.*, 2001).

I performed *in vitro* experiments to investigate whether the Sar1 I purified is a functional GTPase and whether it has retained its functionally relevant interactions with the inner and outer COPII coats. In addition to assessing functionality, the setup of GTP hydrolysis assays is suitable for the investigation of differences in GTP hydrolysis between the two Sar1 paralogues. This can provide insight into their fundamental functional divergence and the implication of Sar1B in paralogue-specific pathologies (see *Introduction*, Section I.5.1.). The GTP hydrolysis activity of the two Sar1 paralogues has previously been studied using tryptophan fluorescence assays (Fromme *et al.*, 2007; Kim *et al.*, 2012; Melville, Studer and Schekman, 2020). In these assays, the nucleotide state of Sar1 is assessed using its tryptophan fluorescence. Due to the conformational differences between GTP- and GDP-bound Sar1, the fluorescence signal of Sar1 is higher in its GTP-bound state than in its GDP-bound state (Antonny *et al.*, 2001; Futai *et al.*, 2004). These studies find no difference between the GTP hydrolysis rate of Sar1A and Sar1B in the presence the other COPII components. Fromme et al. find that the GTP hydrolysis activity of Sar1A and Sar1B is equally stimulated by the addition of inner coat components and further enhanced by the addition of the outer coat components (Fromme *et al.*, 2007). In this study, the intrinsic GTP hydrolysis activity of Sar1 was not assessed. A recent investigation of the differences between the two Sar1 paralogues concluded that the two Sar1 paralogues have similar

intrinsic GTP hydrolysis rates (Melville, Studer and Schekman, 2020). The authors, however, find that Sar1A exchanges GDP for GTP faster than Sar1B.

Initially, I assessed the GTPase activity of nickel affinity-purified Sar1A on its own and in the presence of the purified inner coat components. I used a commercial GTPase activity assay which was previously used for the study of *C. elegans* COPII (Hanna *et al.*, 2016). I added Sar1A at a range of concentrations from 0.2 to 6.4μM, since 6.4μM was the highest Sar1A concentration obtainable in the final reaction, determined by the protein concentration I obtained from purification. The concentration of the inner coat proteins I added, 255nM, was the same as used in the above study of *C. elegans* COPII (Hanna *et al.*, 2016). In this initial experiment, I did not include the outer coat components, as they were not included in the original *C. elegans* study. According to the manufacturer's instructions, the optimal incubation time in these reactions is highly sample-specific, and in this initial experiment I assessed the extent of GTP hydrolysis in the reaction after 30 minutes. I measured the absolute luminescence counts from each reaction, corresponding to the amount of GTP left in the reaction after incubation (see *Materials and Methods*). I observed that in this *in vitro* GTP hydrolysis assay Sar1A hydrolysed GTP in a concentration-dependent manner, as the amount of GTP remaining at higher Sar1A concentrations was lower than that remaining at lower Sar1A concentrations (Fig. 3.14). I further observed that the addition of the purified inner coat components stimulated GTP hydrolysis by Sar1 (Fig. 3.14, compare the orange and blue curves). This suggests that the purified Sec23A/24C is capable of binding Sar1A.

In this experiment, I did not measure the maximal luminescence for each reaction condition in the absence of Sar1-dependent GTP hydrolysis. In future experiments, each reaction condition was also performed in the absence of Sar1 to allow for the normalisation of fluorescence measurements in different reaction conditions.

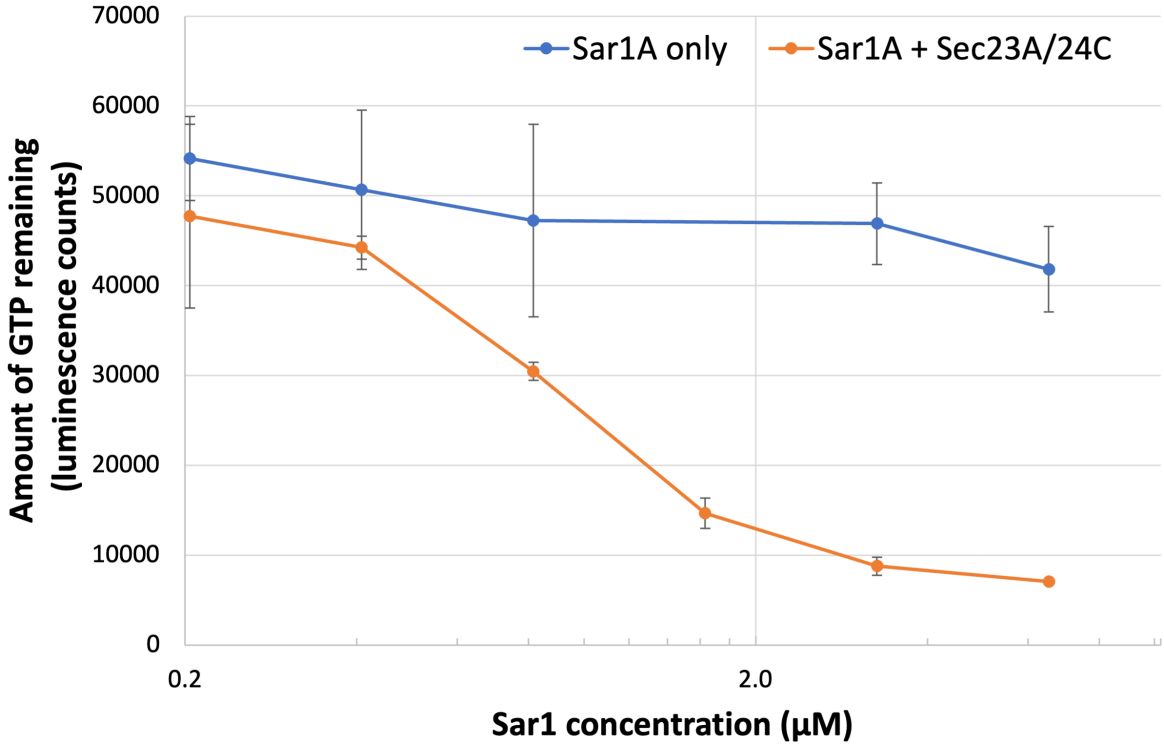

Figure 3.14: Nickel affinity-purified Sar1A hydrolyses GTP in an *in vitro* GTP hydrolysis assay, and its activity is stimulated by the inner coat components. A range of concentrations of Sar1A were incubated with GTP in the presence or absence of inner coat components, and the amount of GTP remaining in the reaction was measured. The error bars represent standard deviation.

After I established that nickel affinity-purified Sar1A was capable of hydrolysing GTP, I set out to assess its membrane binding efficiency. In liposome flotation experiments, I concluded that Sar1A purified by nickel affinity purification was incapable of binding membranes. I changed purification strategy and purified Sar1A and Sar1B using glutathione affinity purification. After I established that glutathione affinity-purified Sar1 paralogues were capable of binding membranes (see Section III.3.), I set out to compare the GTP hydrolysis activities of the two Sar1 paralogues.

First, it was necessary to optimise the concentration range of Sar1 paralogues used in the reaction, such that the highest concentration of Sar1 used fully hydrolyses the GTP present in the reaction in the total reaction time. As a starting point, I measured GTP hydrolysis by Sar1A and Sar1B at a concentration range up to 5µM (Fig. 3.15). The measured values for

the amount of GTP remaining in the reaction following incubation were normalised to the GTP signal obtained in the absence of any GTP hydrolysis by Sar1. This was measured by performing control reactions in the absence of Sar1. I observed that both Sar1A and Sar1B purified by glutathione affinity have an intrinsic GTP hydrolysis activity and hydrolyse GTP in a concentration-dependent manner (Fig. 3.15).

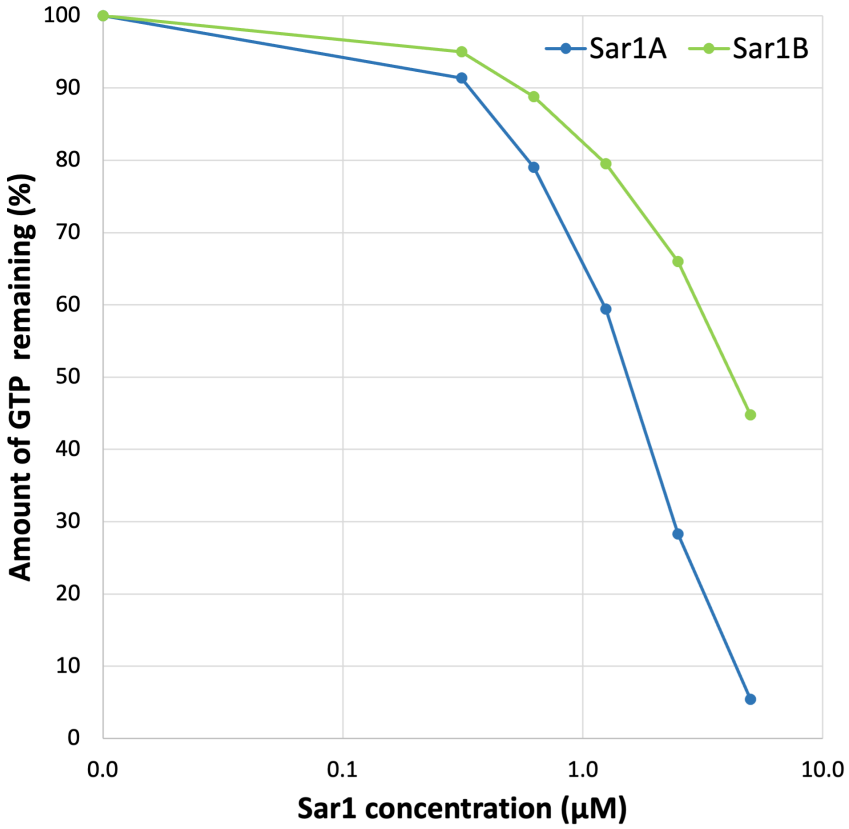

Figure 3.15: Initial GTP hydrolysis experiments using the two Sar1 paralogues. In this experiment, 5µM of Sar1A hydrolyse 95% of the GTP present in the 30 min reaction time. Sar1B at the same concentration hydrolyses 55% of the GTP.

For Sar1A, a concentration range of 0-5µM was well-suited. In this experiment, a 5µM Sar1B concentration was insufficient to hydrolyse the amount of GTP present in the reaction in the 30 min reaction time. Hence, I chose a higher Sar1B concentration range (up to 15µM) and the same Sar1A concentration range (up to 5µM) for the comparison of GTP hydrolysis between the two proteins.

Using these concentration ranges, I compared GTP hydrolysis by the two Sar1 paralogues using proteins purified in consecutive purifications following the same protocol, I discovered a great extent of variability.

The same concentration of Sar1A from different purifications hydrolysed different amounts of GTP in the same reaction time (Fig 3.16A). The same effect, albeit less pronounced, was observed for Sar1B (Fig. 3.16B). When the reaction curves for both paralogues are plotted together, it becomes apparent that a direct comparison between the GTPase activities of the two paralogues is unavailing, as GTP hydrolysis by Sar1 varies greatly between preparation (Fig. 3.16C).

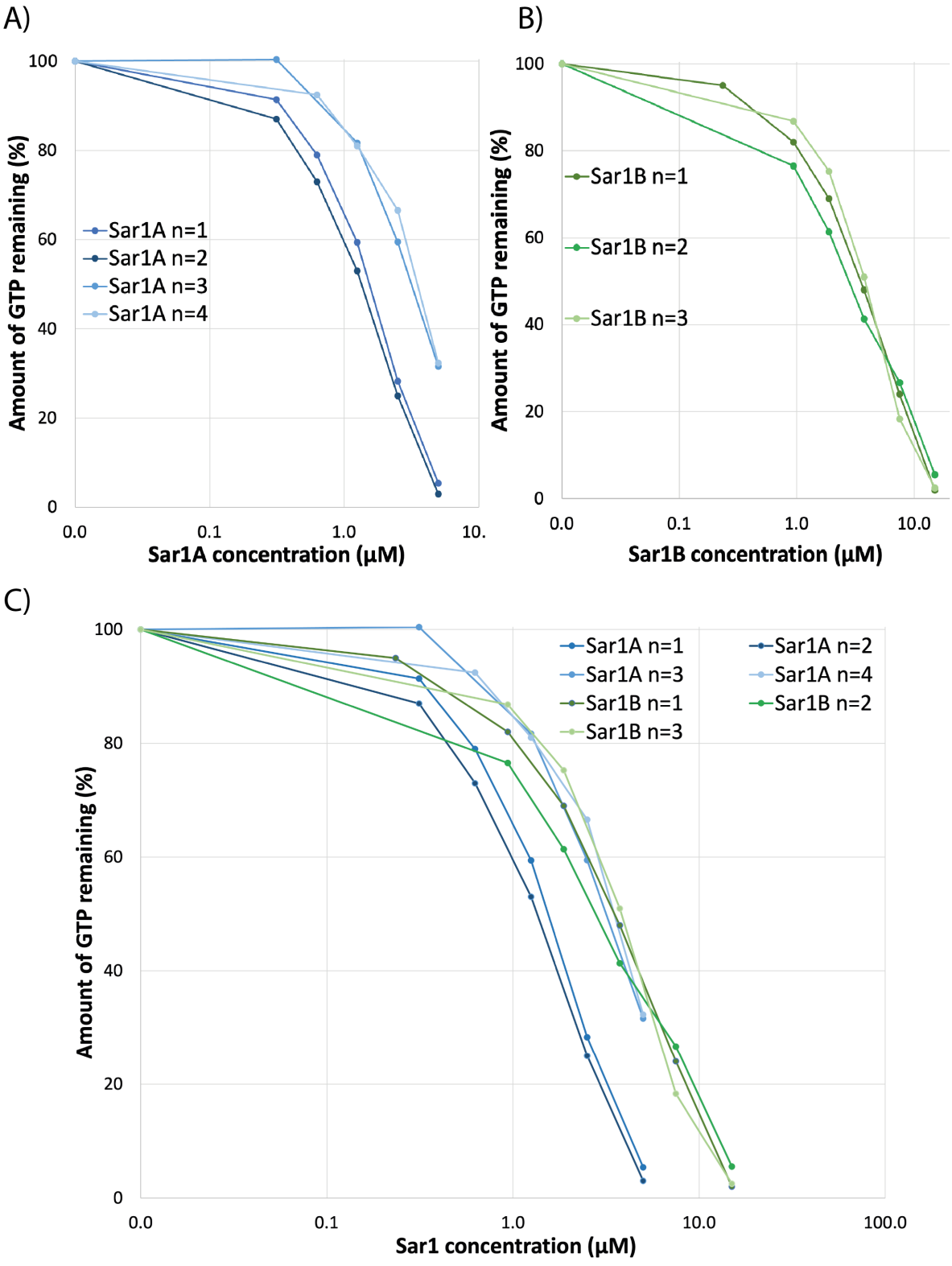

Figure 3.16: Variability in GTP hydrolysis activity between Sar1 proteins purified in separate purifications using the same glutathione affinity purification protocol.

To assess whether the addition of the other COPII components stimulates Sar1 GTP hydrolysis activity, I performed reactions in the presence of the purified inner and outer COPII components using the product of a single Sar1 purification for each paralogue. In membrane binding experiments, I had established that the inner and outer coat components are recruited to membranes at a 320nM concentration (Section III.3.). Hence, I added the same concentration of coat components to GTP hydrolysis reactions.

When reactions were set up with Sar1A in the presence of its GAP Sec23A/24C, more GTP was hydrolysed for the same reaction time when compared to reactions containing only Sar1A. Even higher amounts of GTP were hydrolysed when reactions were performed in the presence of the Sec23A/24C and Sec13/31A, suggesting that inner and outer coat components stimulate the GTP hydrolysis activity of Sar1A (Fig. 3.17).

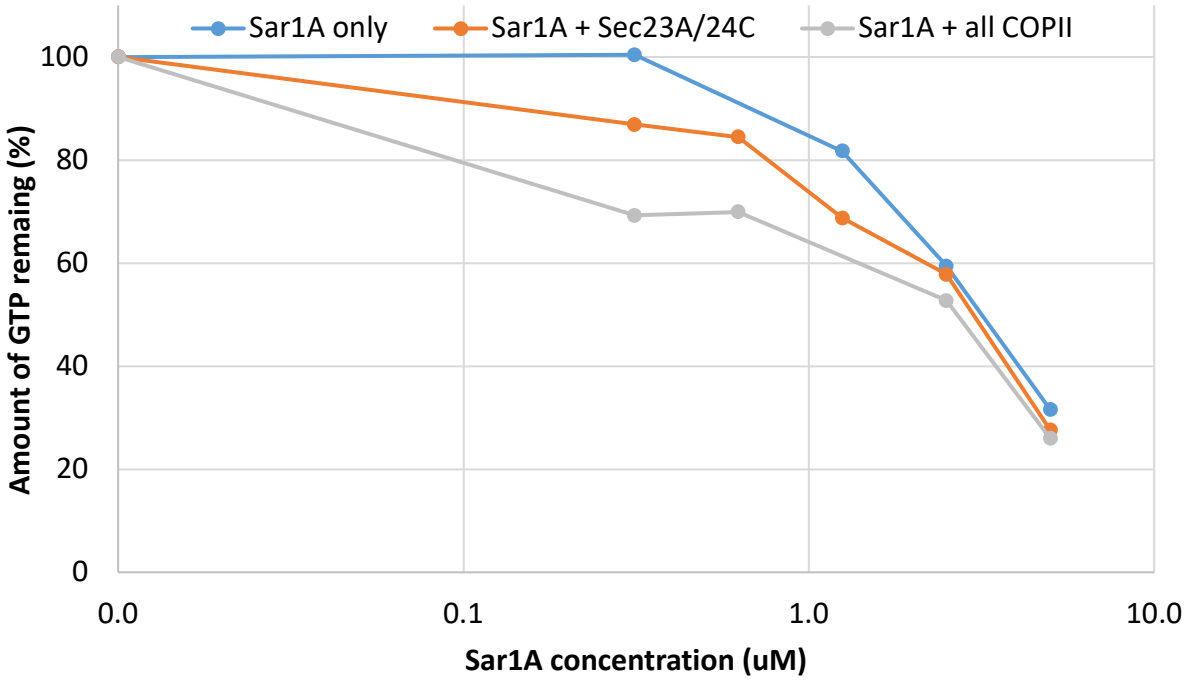

Figure 3.17: GTP hydrolysis by Sar1A in the presence of the inner coat and outer coat COPII components.

When I used the Sar1B paralogue in GTP hydrolysis reactions, addition of the inner coat proteins enhanced Sar1B GTP hydrolysis activity, and the outer coat components stimulated it further (Fig. 3.18).

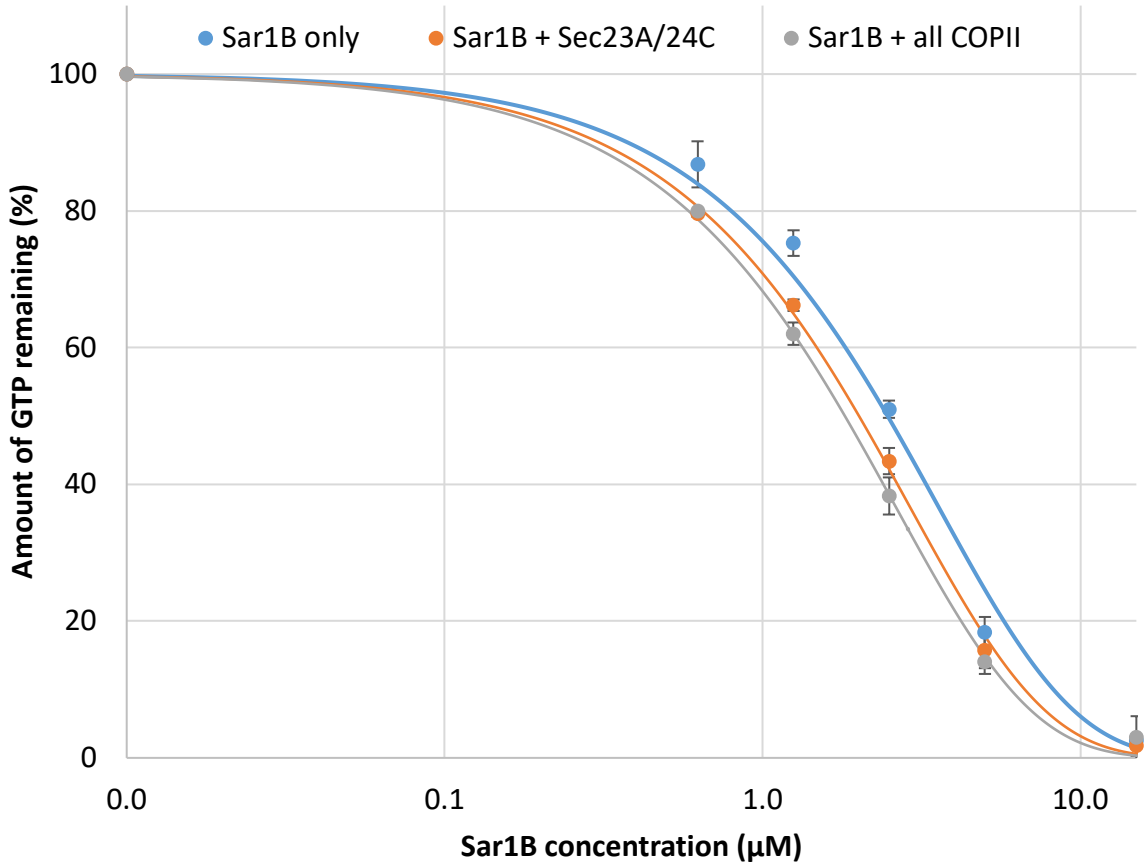

Figure 3.18: GTP hydrolysis by Sar1B is stimulated by the addition of the inner coat components Sec23A/24C and further stimulated by the addition of the outer coat components Sec13/31A. The error bars represent standard deviation.

These results confirm that the human Sar1 paralogues I purified by glutathione affinity purification have an intrinsic GTP hydrolysis activity. The GTP hydrolysis activity of Sar1 was stimulated by the COPII coat components. The finding that GTP hydrolysis activity varies significantly between protein obtained from different purifications calls into question the validity of direct comparisons between the GTP hydrolysis rates of the two paralogues using purified proteins (see *Introduction*, Section I.5.1).

IV. COPII Budding Reactions by Electron Microscopy

To analyse human COPII assembled on membranes, I reconstituted the human COPII secretion system *in vitro* using purified proteins and membrane models. I combined Sec13/31A and Sec23A/24C purified from insect cells and Sar1 purified from *E. coli* with GUVs in the presence of non-hydrolysable GTP analogues and EDTA and analysed the reactions using electron microscopy. Sar1A purified by glutathione affinity purification was capable of deforming GUVs in the absence of COPII components, and upon the addition of COPII components formed tubules protruding from membrane donors. When I added Sar1B purified by glutathione affinity purification to GUVs, I observed concentration-dependent membrane deformation. In reactions performed with Sar1B and the other COPII components, membrane protrusions displayed a beads-on-a-string morphology. When I analysed reconstitution reactions with Sar1B and the other COPII components using cryo-EM, the two layers of the assembled human COPII coat were clearly visible on the membrane.

IV.1. *In vitro* reconstitution of the mammalian COPII secretion system

Studies of the COPII secretion system *in vivo* and *in vitro* provide insight into the mechanisms that allow for cargo export from the ER. I aimed to establish a minimal *in vitro* reconstitution system for the study of mammalian COPII assemblies. While imposing simplification on the study a complex system, *in vitro* reconstitutions can help unravel the foundation mechanisms of COPII assembly in humans. Successfully reconstituting multicomponent molecular systems *in vitro* demonstrates our understanding of the minimal requirements for their formation. The reconstituted reactions are well-suited for structural studies as they include only components of interest at controlled concentrations. This results in minima0l background during imaging and easy identification of components during data processing. Reconstituting the COPII secretion system *in vitro* can also provide a platform for the investigation of COPII regulatory proteins, such as Tango1/cTAGE5, by addition to the reconstitution reaction. Finally, substituting particular COPII components with their paralogues can facilitate an

understanding of their different functions in the context of COPII assembly formation. The establishment of a reconstitution system for yeast has been instrumental in our understanding of COPII binding, COPII-mediated membrane deformation, and large COPII assembly structure (Bacia *et al.*, 2011; Zanetti *et al.*, 2013; Daum *et al.*, 2014; Hutchings *et al.*, 2018). To establish human COPII *in vitro* reconstitution reactions, I combined purified core COPII components with giant unilamellar vesicles as a membrane model in the presence of non-hydrolysable GTP analogue and EDTA.

IV.1.1. Membrane models

IV.1.1.1. Lipid composition

Since Sar1 and Sec23/24 directly interact with the membrane, the lipid composition of the membrane influences their recruitment (Matsuoka *et al.*, 1998). Therefore, when the ER membrane is substituted by membrane models in *in vitro* reconstitution experiments, the lipid composition of those membrane models should be similar that of the ER and maximise binding of COPII components. Furthermore, the remodelling activity of COPII proteins on the membrane depends on the biophysical properties of the membrane, such as its charge and fluidity (Matsuoka *et al.*, 1998; Marsh, 2006). In cells, the COPII machinery itself can affect the membrane lipid composition through its interaction with membrane-remodelling enzymes, such as phospholipases; however, the effects of this interplay require further investigation (Pathre *et al.*, 2003; Melero *et al.*, 2018). In this work, I have used a major-minor and cholesterol lipid mixture. This was based on a major-minor lipid mixture, which was shown to maximise yeast COPII binding and recruitment (*Introduction*, Section I.7.) (Matsuoka *et al.*, 1998). The components of the major-minor mixture were originally established through measurements of the recruitment of purified COPII components to a range of lipids and their combinations (Matsuoka *et al.*, 1998). They are further described in the *Introduction*, Section I.7. The addition of cholesterol reflects the presence of cholesterol in mammalian ER membranes and mirrors the established use of ergosterol for yeast membrane models (Bacia *et al.*, 2011; Zanetti *et al.*, 2013; Daum *et al.*, 2014; Hutchings *et al.*, 2018). Ergosterol does not increase COPII binding, but functions to confer appropriate fluidity and rigidity to the membrane (Matsuoka *et al.*, 1998).

Membrane models do not include protein components that reside in the membrane and can influence COPII recruitment and action, such as Sec12, the GEF for Sar1 (Barlowe and

Schekman, 1993; Weissman, Plutner and Balch, 2001). Following the establishment of a minimal reconstitution system, additional protein components can be studied by addition to the budding reaction.

IV.1.1.2. Giant Unilamellar Vesicles

A range of membrane models are used for *in vitro* experiments with membrane-binding proteins. These vary in their size and their associated curvature. GUVs were chosen based on the large surface area they provide for COPII association and budding. GUVs were also used in studies of large yeast COPII assemblies. As the diameter of GUVs falls in the micrometre range (Fig. 1), using GUVs allowed the visualisation of remodelled membranes as emanating from the surface of GUVs. On the contrary, using smaller membrane models, such as liposomes, with a diameter similar to the size of COPII vesicles (60-80nm) (Barlowe *et al.*, 1994; Zeuschner *et al.*, 2006), would not allow for a distinction between COPII-coated membrane models and active membrane remodeling events (Bacia *et al.*, 2011).

A range of different techniques can be used for GUV formation (Morales-Penningston *et al.*, 2010). I have used electroformation, which involves the coating of opposing electroconductive surfaces with lipids and the generation of a current between the surfaces (Angelova and Dimitrov, 1986). The GUV electroformation chamber is filled with sucrose. Sucrose-filled GUVs are then harvested from the chamber and added to a collection tube filled with glucose solution. When incubated overnight, GUVs settle to the bottom of the collection tube. With this technique, unilamellar vesicles of sizes between 2 and 10µm are generated, as assessed by fluorescence microscopy using Texas Red-labelled PE for visualisation (Fig. 4.1). Those are of sufficient density and size to allow for screening of COPII reactions using EM.

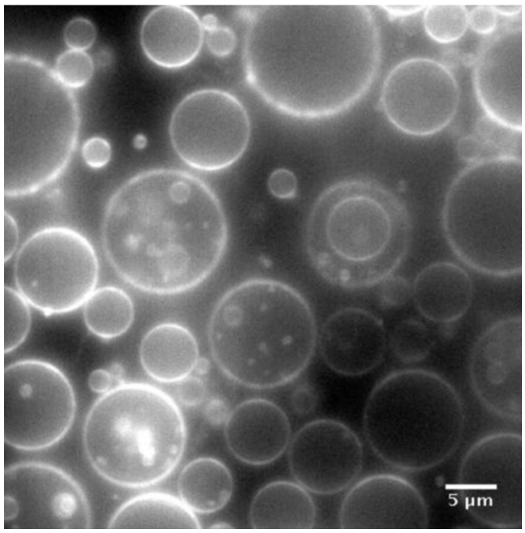

Figure 4.1: GUVs, made from a lipid mixture similar to the lipid composition of the mammalian ER, as visualised by fluorescence microscopy. GUVs produced by electroformation form a mixture of vesicles 2-10µM in size.

IV.1.2. Additional reaction components: Non-hydrolysable GTP analogues and EDTA

Human COPII *in vitro* reconstitution reactions aim to capture COPII components assembled on membranes. As discussed in further detail in Section I.2. of the *Introduction*, Sar1 projects an N-terminal amphipathic helix into the membrane in its active, GTP-bound state and recruits the rest of the COPII machinery (Huang *et al.*, 2001; Bielli *et al.*, 2005). However, COPII assemblies are transient due to their intrinsic propensity for disassembly upon GTP hydrolysis. Disassembly is directly triggered by coat assembly: the inner coat component Sec23 is the GAP of Sar1, and its GAP activity is further stimulated by Sec31 (Zanetti *et al.*, 2012). Upon GTP hydrolysis, Sar1 sheds from the membrane, which ultimately results in coat disassembly (Zanetti *et al.*, 2012). Therefore, to study COPII associated with membranes, we prevent GTP hydrolysis by the addition of non-hydrolysable GTP analogues. Alternatively, a GTP hydrolysis-deficient mutant of Sar1 can be used (Sar1 H79G) which has been established in the literature (Bannykh, Rowe and Balch, 1996; Aridor *et al.*, 2001; Bielli *et al.*, 2005).

Sar1 binding to the non-hydrolysable GTP analogue present in the reaction is essential for Sar1 membrane recruitment and COPII membrane retainment. *In vivo*, the exchange of GDP for GTP by Sar1 is facilitated by its essential GEF Sec12 (Nakano, Brada and Schekman, 1988). No other functions of Sec12 are essential for COPII vesicle formation *in vitro*, as pre-equilibration of Sar1 with GMP-PNP circumvents the requirement for Sec12 in both yeast and mammalian reconstitution reactions (Matsuoka *et al.*, 1998; Bacia *et al.*, 2011; Hariri *et al.*, 2014; Hutchings *et al.*, 2018). For yeast, it has been established that EDTA can substitute for Sec12 in *in vitro* reconstitution reactions (Bacia *et al.*, 2011). The mechanism of the

substitution of the native GEF with EDTA requires further investigation in the case of Sar1 but has been well established for other GTP-binding proteins (Zhang *et al.*, 2000). EDTA is a cation chelating agent, which lowers the concentration of available divalent cations in solution, including Mg^{2+}, hence affecting the turnover of bound Mg^{2+}. The structure of human Sar1A in complex with GDP reveals magnesium coordination of nucleotide binding, similarly to previously released structures of yeast and hamster Sar1 (human Sar1A - PDB ID 2GAO, hamster Sar1 – PDB ID 1F6B, yeast Sar1 – PDB ID 1M20). A structure of hamster Sar1 obtained at a low (1mM) Mg^{2+}concentration reveals that one of its regulatory switches, switch 1, moves to an open conformation in the absence of Mg^{2+} (Rao *et al.*, 2006). For GTPases from the Ras superfamily, which Sar1 belongs to, it has been shown that Mg^{2+} release results in a 50 to 100-fold decrease in nucleotide affinity (Hall and Self, 1986; Klebe *et al.*, 1995). This allows for GDP disassociation. The low nucleotide affinity can then be overcome *in vitro* by using a high non-hydrolysable GTP analogue concentration (in this work 1mM), and the presence of Mg^{2+} in the solution in the budding reaction buffer (in this work HKM, see *Materials and Methods*).

A comparison between the use of Sec12 and EDTA for nucleotide exchange has suggested that both enable the same morphological effect on GUV membranes in the presence of GMP-PNP and yeast COPII components (Bacia *et al.*, 2011). Aiming to minimise the number of protein components to include in *in vitro* reconstitutions, I used 2.5mM EDTA in budding reactions and did not include Sec12.

IV.2. Electron microscopy of budding reactions using Sar1A purified by nickel affinity purification

IV.2.1. Sar1A deforms membranes in the absence of the other COPII components

I first purified Sar1A by nickel affinity purification (*Biochemical Analysis of Human COPII Assembly on Membranes*, Section III.3) and aimed to characterise the optimal concentration of Sar1A to use in budding reactions. As discussed in the *Introduction*, Section I.5.1.1, Sar1A is capable of deforming membranes in the absence of other COPII components. The ability of GTP-locked mammalian Sar1 to generate constrictions on membranes independent of the rest of the COPII machinery has been described and characterised previously (Long *et al.*, 2010; Hariri *et al.*, 2014). I tested the membrane-deforming activity of a range of Sar1A

concentrations by adding Sar1A to GUVs in the absence of other COPII components. Reactions contained GTPφS and EDTA, allowing for stable Sar1A membrane binding. GDP was used instead of GTPφS in negative control reactions. Reactions were assessed by negative stain EM.

To date, we have not established a quantitative measure of budding frequency and rely on visual assessment. To assess budding efficiency, I observed GUVs to assess vesiculation and tubulation emanating from the donors.

I screened a low micromolar range of Sar1A concentrations (0.7μM-3.4μM), informed by the use of similar concentrations for COPII reconstitution reactions with yeast Sar1. At a Sar1A concentration of 0.7μM in GTPφS reactions, GUVs were not deformed. When Sar1A concentration was increased to 1.7μM, few GUVs were deformed, and membranes formed small, connected vesicles ≈30-40nm in diameter (Fig. 4.2). This suggested that Sar1A is sufficient for the generation of curvature on membrane models and that Sar1A membrane deformation is concentration-dependent. However, the efficiency of membrane remodeling by Sar1A was low, as the majority of GUVs were not deformed.

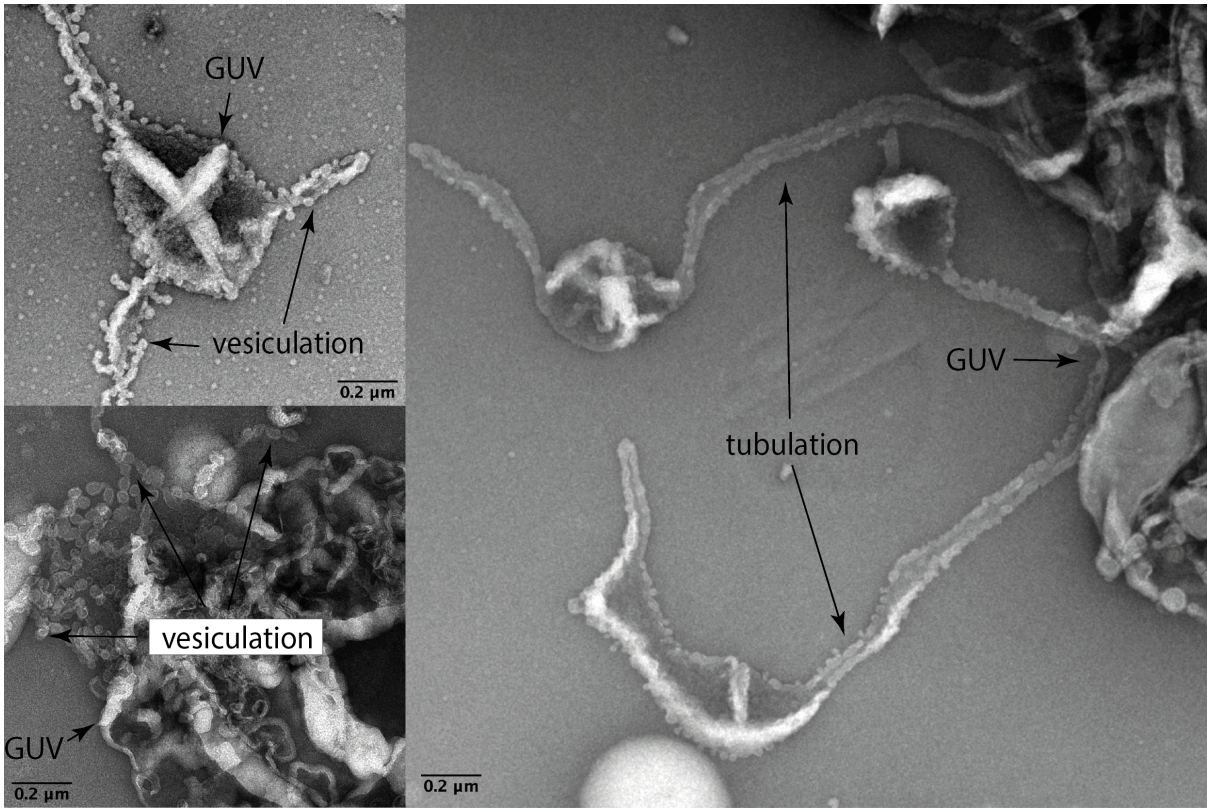

Figure 4.2: Sar1A, purified by nickel affinity purification, generates connected vesiculations and tubulations emanating from GUVs, as observed using negative stain EM. 1.7µM Sar1A was added to GUVs in the presence of 1mM GTPφS and 2.5mM EDTA.

IV.2.2. COPII components deform membranes, but do not form a coat

To reconstitute the COPII coat bound to GUVs, I added COPII components to GUVs in the presence of GTPφS and EDTA. I tested a range of concentrations of nickel affinity purified Sar1A (0.7µM-3.4µM) and analysed budding efficiency and membrane morphology (Fig. 4.3). The concentration of other COPII components was constant. As a starting point, I tested an 80nM Sec23A/24C concentration and a 130nM Sec13/31A concentration. The ratio between inner and outer coat components was as used previously in yeast *in vitro* reconstitution experiments (Zanetti *et al.*, 2013).

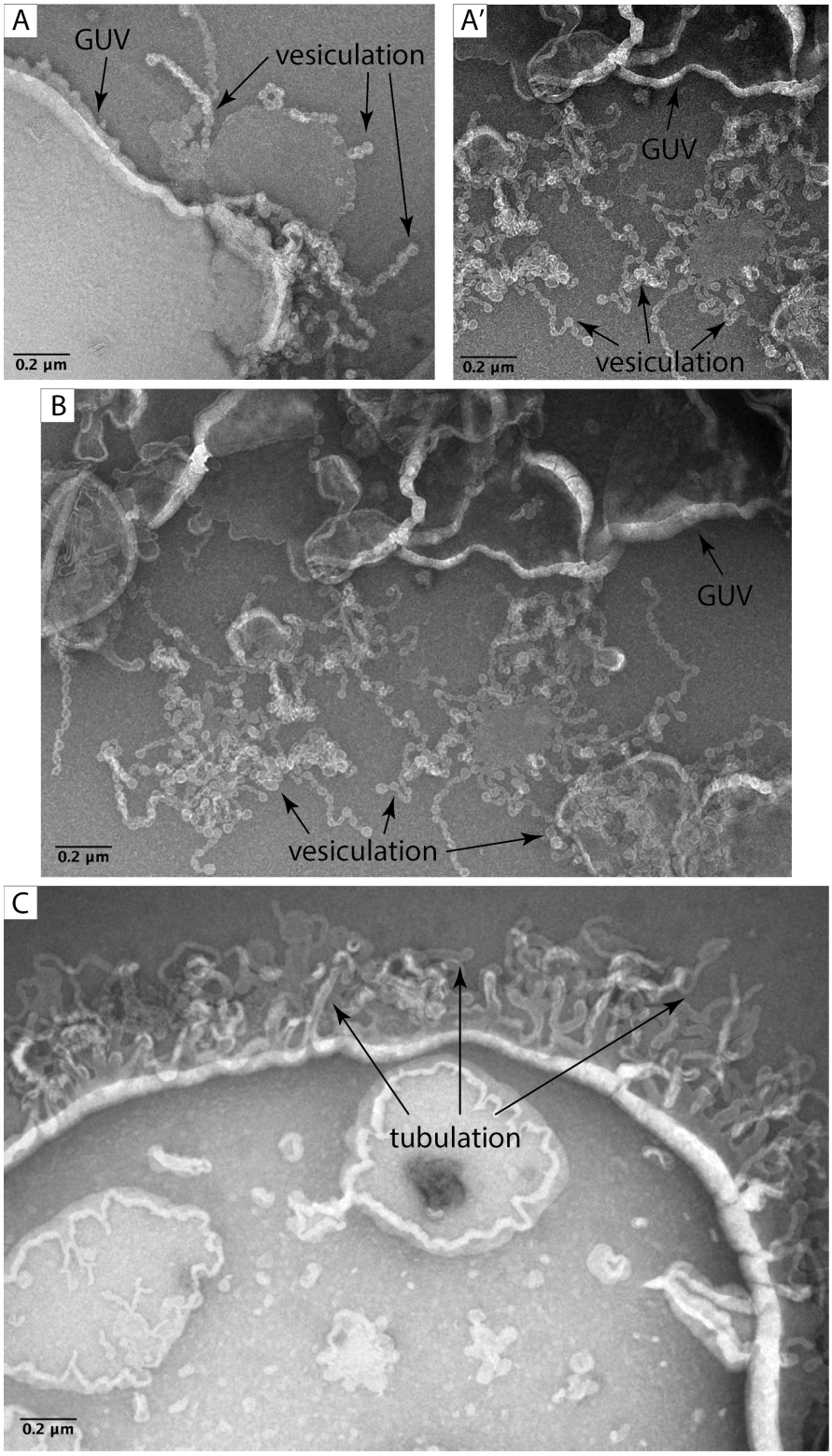

Figure 4.3: The addition of Sar1A, purified by nickel affinity purification, and COPII components to GUVs results in membrane deformation, as observed using negative stain EM. A range of concentrations of Sar1A (0.7µM-3.4µM) and COPII components were added to GUVs. Budding frequency increased with Sar1 concentration, and membrane protrusions

became shorter and more disorderly. (A) 0.7µM Sar1A, 80nM Sec23A/24C, and 130nM Sec13/31A were incubated with GUVs, in the presence of 1mM GTPφS and 2.5mM EDTA. (B) 1.7µM Sar1A, 80nM Sec23A/24C, and 130nM Sec13/31A were incubated with GUVs in the presence of 1mM GTPφS and 2.5mM EDTA. (C) 3.4µM Sar1A, 80nM Sec23A/24C, and 130nM Sec13/31A were incubated with GUVs in the presence of 1mM GTPφS and 2.5mM EDTA.

I observed that the incubation of GUVs with COPII proteins generated membrane curvature and two main morphologies – vesiculations and tubulations, similarly to reactions performed with Sar1 in the absence of other COPII components (Fig. 4.3). I further observed that increasing the concentration of Sar1A increased the incidence of budding events. By visual inspection, GUVs budded more with 1.7µM Sar1A (Fig. 4.3A) than with 0.7µM Sar1A (Fig. 4.3B), and more often when 3.4µM Sar1A was used (Fig. 4.3C). Furthermore, increasing the concentration of Sar1A to 3.4µM visibly decreased the length and increased the 'disorder' of membrane protrusions (Fig. 4.3C).

To assess whether the COPII coat was assembling on membranes, I compared the diameter of vesiculations generated by Sar1A alone and by Sar1A in the presence of the inner and outer coat components. In the literature, Sar1-induced membrane protrusions from membrane models have been reported with a variety of sizes. Upon addition to liposomes and giant unilamellar vesicles, yeast Sar1 forms tubules of a ≈26nm diameter (Lee *et al.*, 2005; Bacia *et al.*, 2011). This is similar to tubules formed by the addition of hamster Sar1 to large unilamellar vesicles (LUVs), which were measured at ≈22nm (Long *et al.*, 2010). On GUVs, the addition of hamster Sar1 produced two kinds of tubes: flexible tubes of a 30-60nm diameter, and rigid tubules wider than 40nm (Long *et al.*, 2010).

In yeast, vesicles and tubes formed by the full COPII coat are larger than those formed by Sar1 alone. Vesicles formed in the presence of all yeast COPII components measure 60-80nm in diameter (Barlowe *et al.*, 1994), while yeast COPII tubes are around 80nm in diameter (Zanetti *et al.*, 2013). I therefore expected that vesiculations formed in the presence of COPII components would have a generally larger diameter than Sar1-only deformations due to the size of the COPII coat. I measured the diameter of the vesicles using ImageJ software. As vesicles were not perfectly circular, the largest vesicle diameter was used. Unexpectedly, I

observed that vesicle diameters were not significantly different: 32nm for Sar1A-only vesicles and 33nm for COPII-formed vesicles, with standard deviations of 6.4nm and 6.9nm, respectively (Fig. 4.4). This suggested that COPII components were not forming a stable coat on the membrane, or that their binding did not change the size of the vesicles as assessed by negative stain.

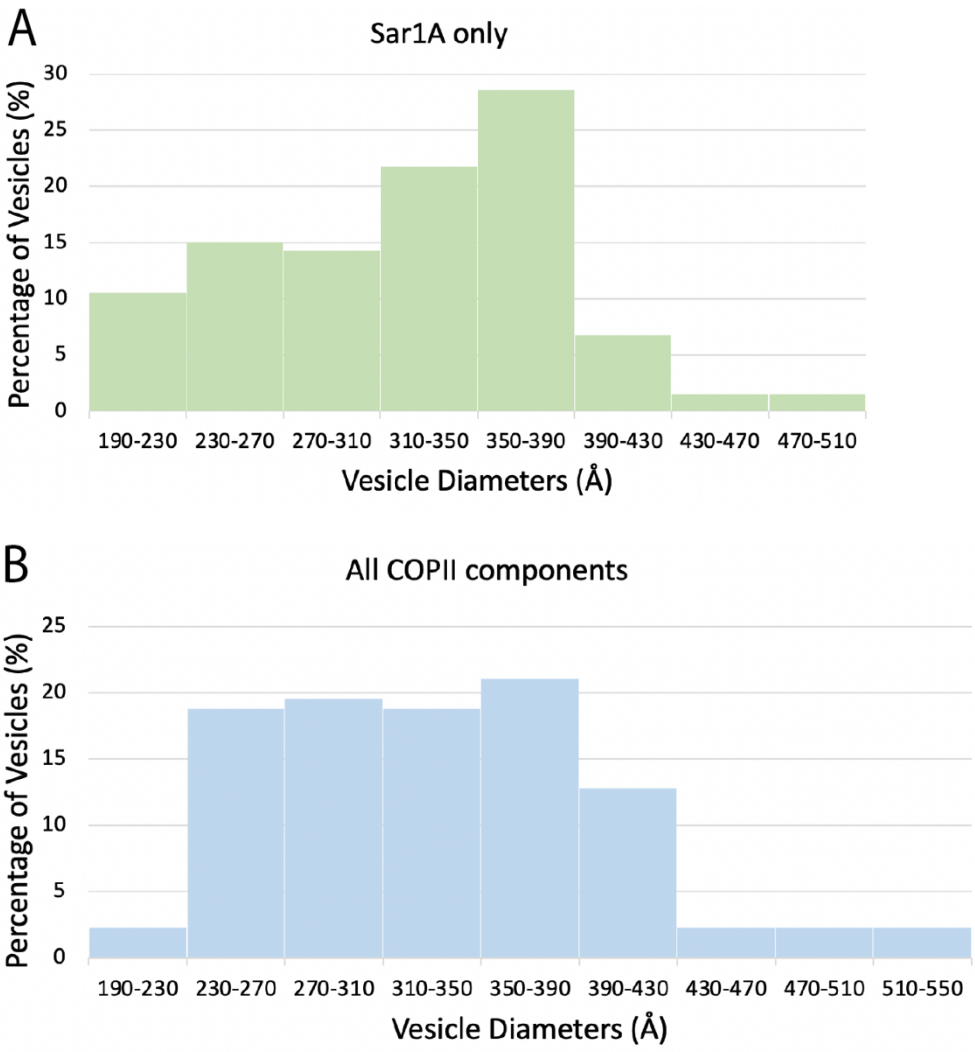

Figure 4.4: Vesiculations formed upon the addition of His-purified Sar1A only (A) and upon the addition of all COPII components (B) are of similar sizes. Reactions consisted of GUVs, 2.5mM EDTA, 1mM GTPφS, 1.7µM Sar1A in the absence (A) or presence (B) of 80nM Sec23A/24C and 130nM Sec13/31A. Diameters of the vesiculations as analysed by negative stain EM were measured using ImageJ software.

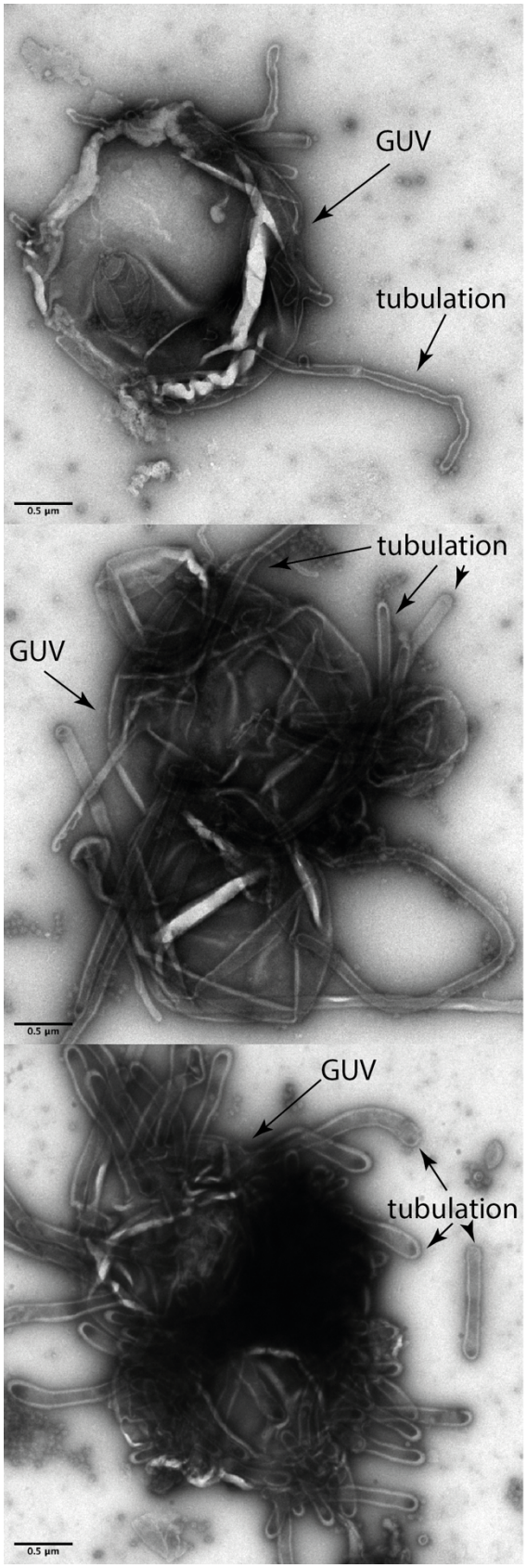

As a positive control for COPII-mediated membrane deformation experiments, I set up *in vitro* reconstitution reactions using yeast COPII proteins and GUVs (Fig. 4.5). This was done using yeast proteins purified by J.Hutchings in-house at the following concentrations: 1µM Sar1, 320nM Sec23/24, and 173nM Sec13/31. Reactions were screened by negative-stain EM.

Tubular protrusions from GUVs were observed in this experiment, suggesting that COPII proteins were deforming GUV membranes (Fig. 4.5).

Figure 4.5: Yeast *in vitro* reconstitutions show tubular protrusions emanating from GUVs.

Hypothesising that higher COPII component concentrations could result in COPII membrane coating, I increased the concentration of COPII components I added in budding reactions. I added Sec23A/24C to a 320nM concentration, and Sec13/31A to a 520nM concentration, as previously used in yeast *in vitro* reconstitutions (Zanetti *et al.*, 2013). I found that the general morphology or size of the vesiculations did not change (compare Fig. 4.6 to Fig. 4.3).

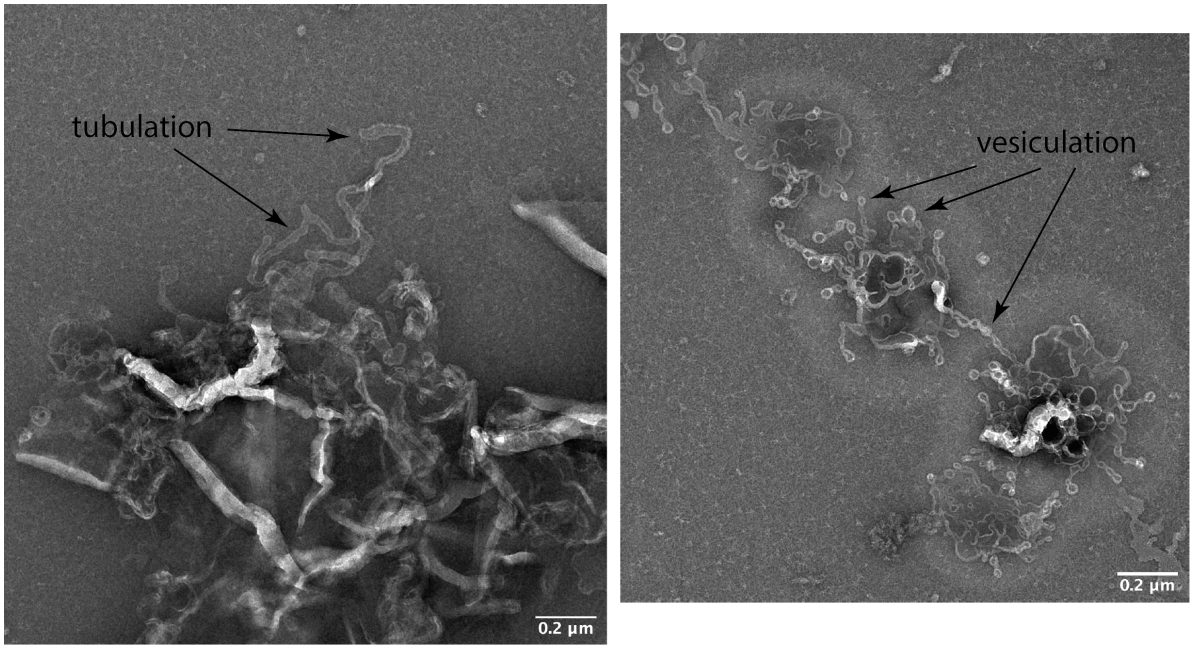

Figure 4.6: Increasing the concentration of COPII components does not alter the general morphology. Vesiculations and tubulations were observed protruding from GUVs. 1µM Sar1A, 320nM Sec23A/24C, 520nM Sec13/31A were added to GUVs in the presence of 1mM GTPγS and 2.5mM EDTA.

Aiming to assess whether COPII components were binding membranes, I tested the recruitment of COPII components to the liposomes using liposome flotation assays (see *Biochemical Analysis of Human COPII Assembly on Membranes*, Section III.3.). Liposomes are an appropriate membrane model for this assay as they are stable enough to allow for the centrifugation that separates the membrane-bound floating fraction from the unbound protein fraction. From these experiments, I concluded that COPII components were not being stably recruited. This prompted an optimisation of COPII binding to membranes, importantly an optimisation of the Sar1 construct and purification strategy, as described in *Biochemical Analysis of Human COPII Assembly on Membranes*, Section III.2.3.

IV.3. Sar1 paralogues purified by glutathione affinity purification deform membranes and recruit the COPII coat

Binding of the Sar1 GTPase to liposomes was optimised as described in *Biochemical Analysis of Human COPII Assembly on Membranes*, Section III.3. I showed that Sar1 paralogues purified by glutathione affinity purification are efficient in binding membranes and recruiting COPII components. Therefore, I used Sar1 paralogues purified by glutathione affinity in subsequent budding reactions.

IV.3.1. Sar1A

To assess membrane deformation by Sar1A in the absence of other COPII components, I added Sar1A purified by glutathione affinity purification to GUVs. When I added 1µM of Sar1A, I did not observe any visible deformation of GUVs (Fig. 4.7A). I then set out to assess whether a higher Sar1A concentration is capable of deforming membrane donors. At the higher protein concentration of 8µM Sar1A, I saw vesicular (4.7B) and tubular (4.7C) protrusions emanating from GUVs. Vesiculations were of a similar size and appearance to those generated by nickel affinity-purified Sar1A (see Section IV.2.). Tubules had a smooth appearance, bearing resemblance to tubules observed previously with hamster Sar1 from large unilamellar vesicles (LUVs) (Long *et al.*, 2010). However, they were wider, measuring 80nm in diameter, as opposed to 30-60nm for those generated by hamster Sar1 on LUVs (Long *et al.*, 2010).

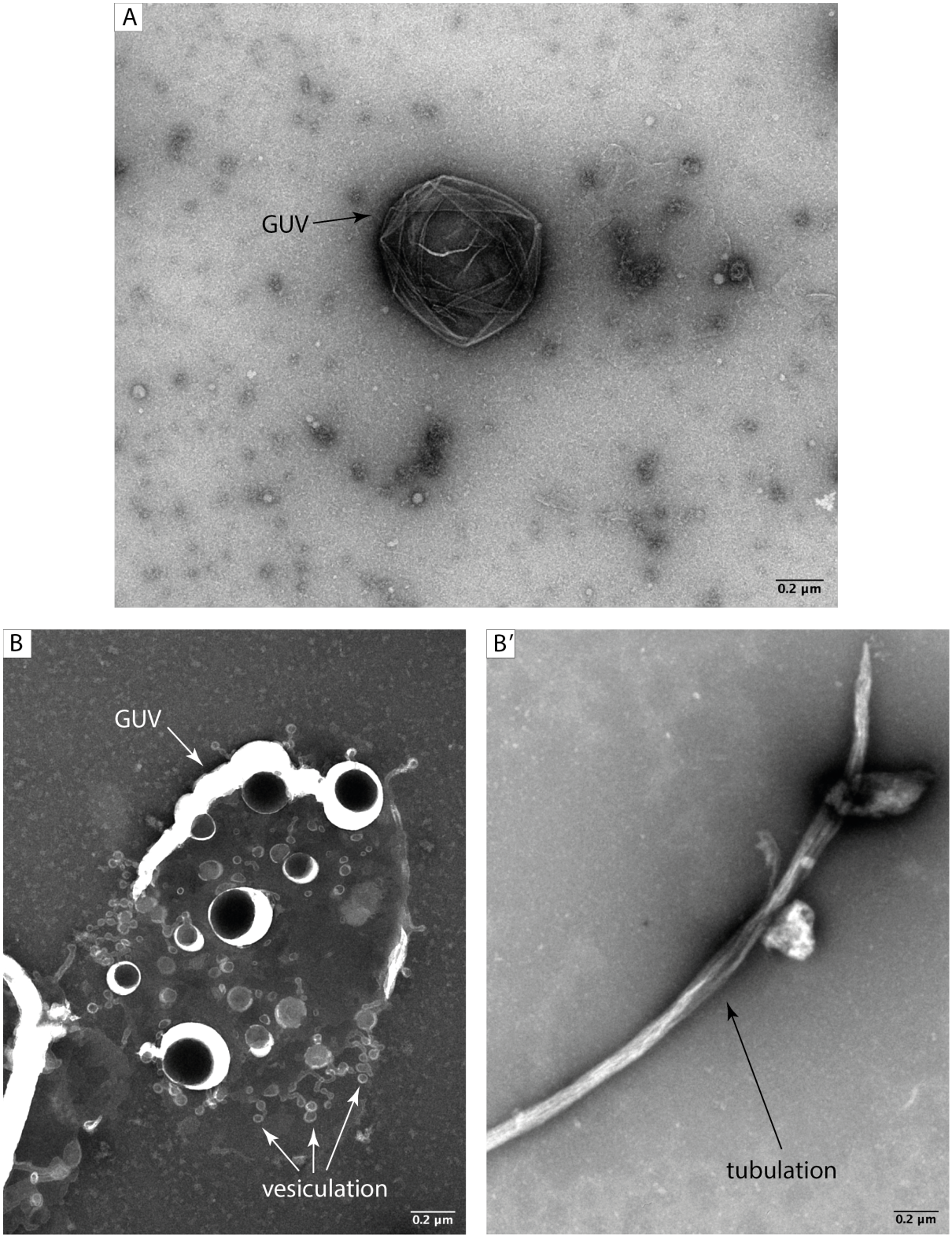

Figure 4.7: Sar1A, purified by glutathione affinity purification, generates vesiculations and tubulations from GUVs, as seen using negative stain EM. (A) 1µM Sar1A was added to GUVs. (B) 8µM Sar1A was added to GUVs. No membrane deformation by Sar1A is observed at 1µM

Sar1A. At an 8µM concentration, Sar1A formed vesiculations and tubulations emanating from membrane donors.

I then set out to assess membrane deformation by Sar1A and the other COPII components. When I added 1µM Sar1A to GUVs in the presence of purified Sec23A/24C and Sec13/31A, I observed tubes of 80-90nm diameter emanating from membrane donors (Fig. 4.8). Tubules were strongly contrasted to the background of the negative stain.

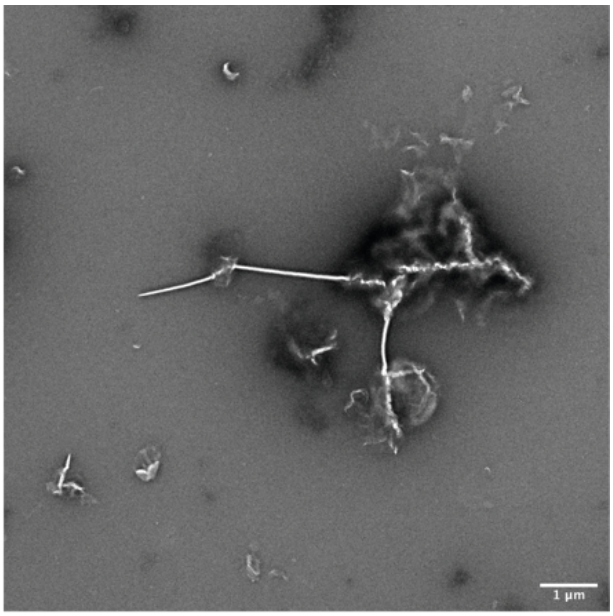

Figure 4.8: Sar1A, purified by glutathione affinity purification, generates tubules emanating from membrane models in the presence of 320nM Sec23A/24C and 320nM Sec13/31A, as assessed using negative stain EM.

Since the diameter of tubules formed by Sar1A in the presence and absence of additional COPII components are comparable, it is possible that COPII components are not recruited to Sar1A-coated membranes. Alternatively, tubules could be collapsing under the negative stain, if they lack rigidity (Asadi *et al.*, 2017). To assess whether Sar1A is efficiently recruiting COPII components to membranes, membrane binding assays can be used, similarly to those that confirmed that Sar1B recruits COPII components to membranes (*Biochemical Analysis of COPII Assembly on Membranes*, Section III.3.).

IV.3.2. Sar1B

IV.3.2.1. Sar1B deforms liposomes and recruits COPII components to assemble a coat

After confirming that Sar1B purified by glutathione affinity purification binds liposomes and recruits COPII components, I visualised this binding using negative stain EM. Upon the addition of Sar1B to liposomes, the majority of liposomes were deformed, and vesicular and tubular protrusions from liposomes were observed (Figure 4.9A). These were similar in

appearance to membrane deformations generated by nickel affinity-purified Sar1 (see Section IV.2). The vesiculations had a diameter of 20-30nm, while tubular protrusions had a diameter of 15-25nm. The diameter of the tubular protrusions is consistent with tubules previously observed by hamster Sar1 on LUVs (Long *et al.*, 2010). When all COPII components were added, coated vesicles of 70-80nm were seen, suggesting that COPII membrane recruitment resulted in COPII coat polymerisation (Figure 4.9B).

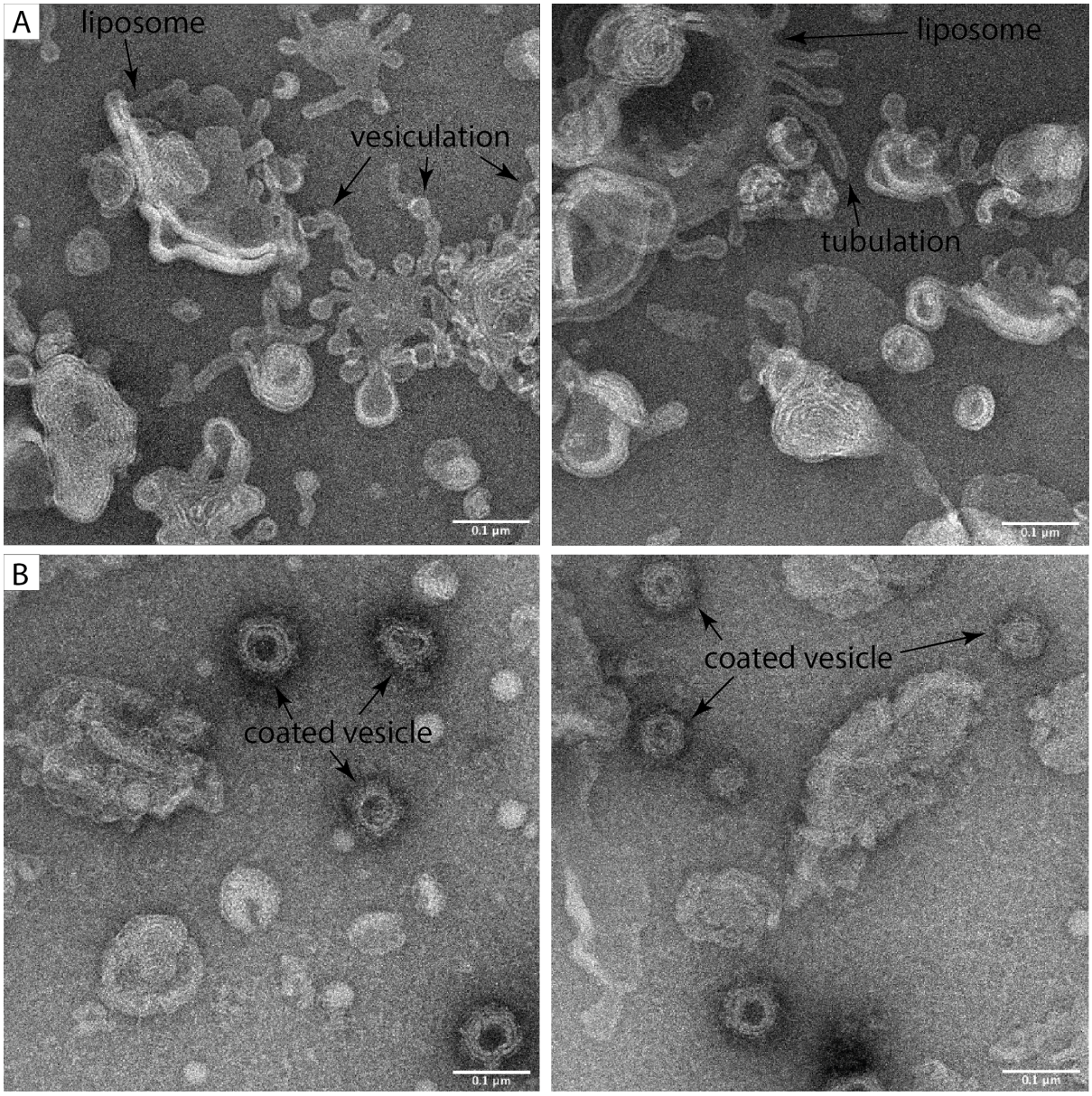

Figure 4.9: Sar1B, purified by glutathione affinity purification, (A) binds and deforms liposomes and (B) recruits the COPII components to coat vesicles, as seen using negative stain EM. (A) 1µM Sar1B was added to liposomes in the presence of 1mM GMP-PNP and 2.5mM

EDTA. (B) 1µM Sar1B, 320nM Sec23A/24C, and 320nM Sec13/31A were added to liposomes with 1mM GMP-PNP and 2.5mM EDTA.

IV.3.2.2. Sar1B deforms GUVs into tubules

I assessed the effect of Sar1B addition to GUVs in budding reactions containing GMP-PNP and EDTA. A range of Sar1B concentrations between 0.25µM and 8µM were tested, and reactions were observed using negative stain EM.

Sar1B deformed vesicles in a concentration-dependent manner (Fig. 4.10). At a 0.25µM Sar1B concentration, no membrane deformation was observed (Fig. 4.10A). At a 1µM concentration, while most GUVs remained unperturbed, long tubules projecting from some GUVs became visible (Fig. 10B). When the concentration was increased to 8µM, the majority of vesicles were deformed and tubes emanating from GUVs were widespread (Fig. 4.10C). The tubular protrusions had a wide range of diameters, ranging from 30 to 75nm. The diameters changed along the length of single tubes, suggesting that they were not defined by a regular protein lattice. These observations indicated that Sar1B efficiently binds membranes of lower curvature, such as GUVs, and not only membranes of higher curvature, such as liposomes, as established in liposome binding experiments.

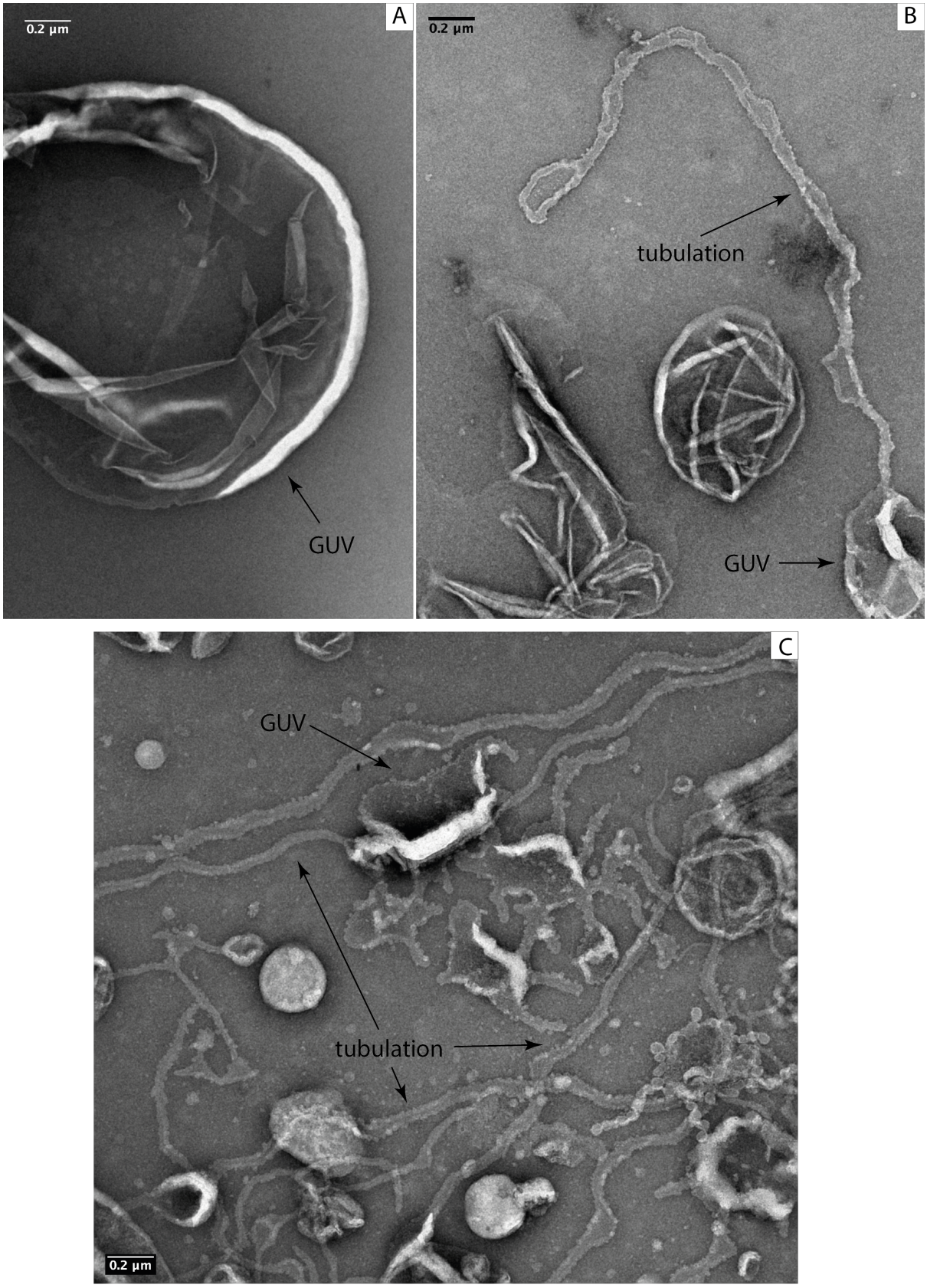

Figure 4.10: Sar1B, purified by glutathione affinity purification, generates tubulations emanating from GUVs, as seen using negative stain EM. Increasing the Sar1B concentrations

results in an increase in tubule formation. (A) 0.25µM Sar1B was added to GUVs in the presence of 1mM GMP-PNP and 2.5mM EDTA. (B) 1µM Sar1B was added. (C) 8µM Sar1B was added.

To observe COPII bound to membranes, a 1µM Sar1B concentration was selected for future budding reactions, identical to the concentration used in liposome flotation assays. This concentration was chosen to allow for efficient membrane binding while avoiding extensive deformation due to Sar1 alone.

IV.3.2.3. COPII deforms GUVs and forms coated vesiculations

To observe COPII membrane binding, 1µM Sar1B, 320nM Sec23A/24C, and 320nM Sec13/31A were added to GUVs. Inner and outer coat concentrations were equal to those used in liposome flotation reactions. Reactions included 1mM GMP-PNP and 2.5mM EDTA and were assessed by negative stain EM.

Membrane deformation was widespread in these reactions (Fig 4.11), compared to reactions using only Sar1B at 1µM (Fig. 4.10). This suggests that inner and outer coat COPII components actively participate in remodelling membranes. Furthermore, a beads-on-a-string morphology was observed, with beads with an average size of 70nm. This differs from the tubular protrusions generated by Sar1B alone, demonstrating that COPII components define membrane curvature when Sar1B is used in budding reactions.

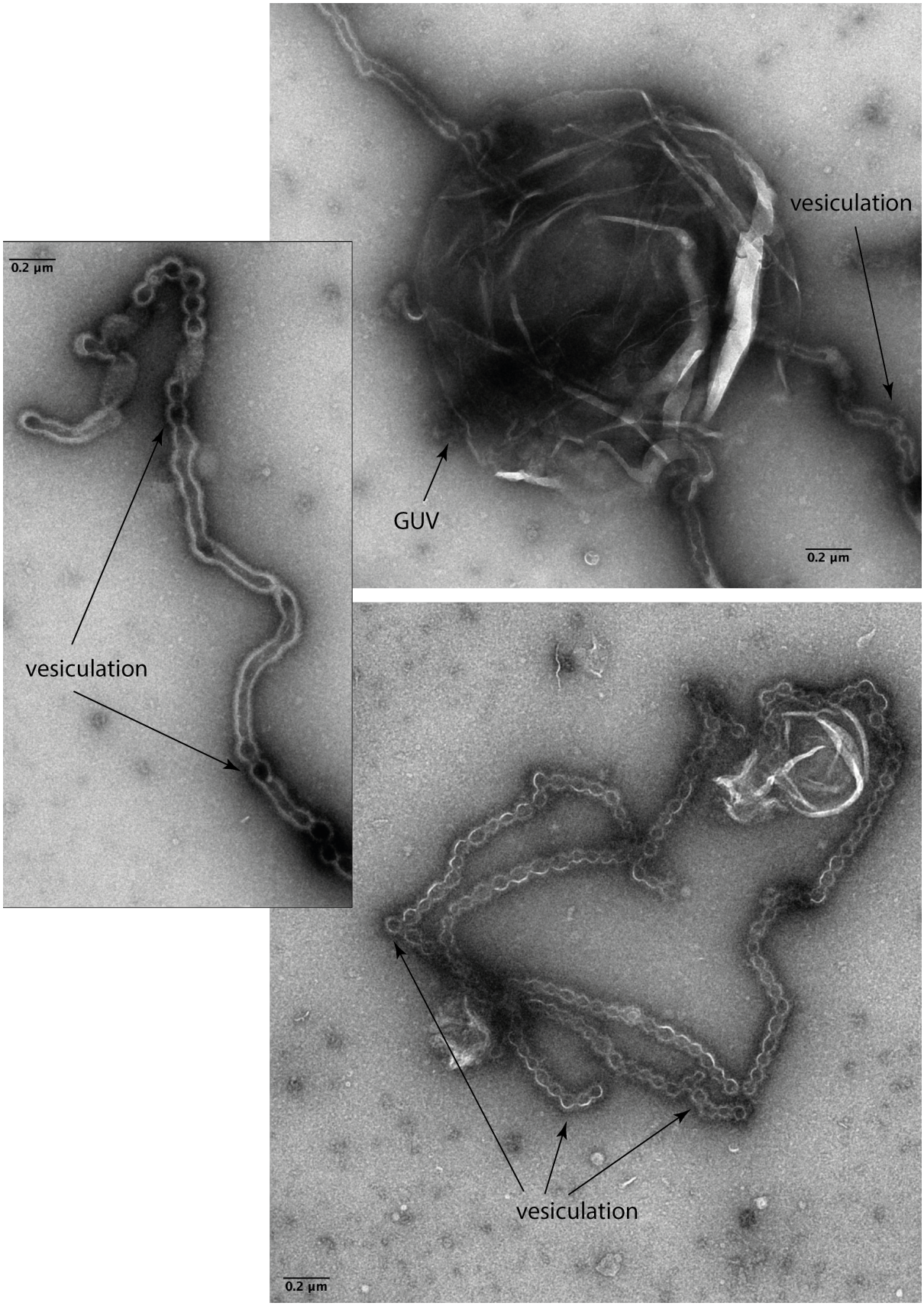

Figure 4.11: Sar1B, purified by glutathione affinity purification, and COPII components form connected vesiculations emanating from GUVs, as seen using negative stain EM. 1µM Sar1B,

320nM Sec23A/24C, and 320nM Sec13/31A were added to GUVs with 1mM GMP-PNP and 2.5mM EDTA.

As I observed that COPII components were recruited to GUVs and were efficiently polymerising, I proceeded to analyse the reactions using cryo-EM. While negative stain EM is well-suited for assessing membrane deformation and optimising reactions, it cannot be used to obtain high-resolution information. In negative stain EM, the sample is surrounded by an envelope of the stain used for sample preparation, and the resolution is limited by the grain size of the stain (Kiselev, Sherman and Tsuprun, 1990; Scarff *et al.*, 2018). Furthermore, the sample is imaged in the non-native environment of the stain. In cryo-EM, the sample is maintained in its native environment prior to freezing, and high-resolution structural information can be obtained. Hence, I prepared vitrified samples of COPII reactions for cryo-EM.

Cryo-EM analysis of COPII reactions revealed pleomorphic membrane deformations resembling strings of vesicles with clearly discernible membrane, inner coat, and outer coat layers (Fig. 4.12). To analyse the position of the human COPII coat layers in respect to each other and the membrane, a small set of particles (n=288) were manually selected from electron micrographs using e2boxer in eman2 (Fig. 4.13A and B) (Tang *et al.*, 2007). These particles were imported into Relion 3.1 and classified into two classes to allow for a separation between true particles and junk particles (Fig. 4.13C) (Scheres, 2012). The first class contained 72% of particles (n=207), and in this class average three layers are clearly visible: the membrane layer, the inner coat, and the outer coat (Fig. 4.13C). To generate a density profile, the grey values along a line perpendicular to the membrane were obtained from the class average (Fig. 4.13D). In the density profile, three clear peaks can be distinguished, corresponding to the outer coat, inner coat, and membrane layers (Fig. 4.13E). The two membrane leaflets produced a single peak in the density profile and cannot be distinguished. The distance between the outer and inner coat layers was ≈35 pixels, equal to 94Å. The distance between the inner coat and the membrane was 70Å (26 pixels). These distances are comparable to those observed for yeast as measured from a low-resolution average of yeast COPII assembled on membranes: for yeast, the distance between the inner and the outer coat

was 91Å, while the distance between the inner coat and the middle of the membrane was 57Å (Hutchings *et al.*, 2020; Zanetti, G., personal communication).

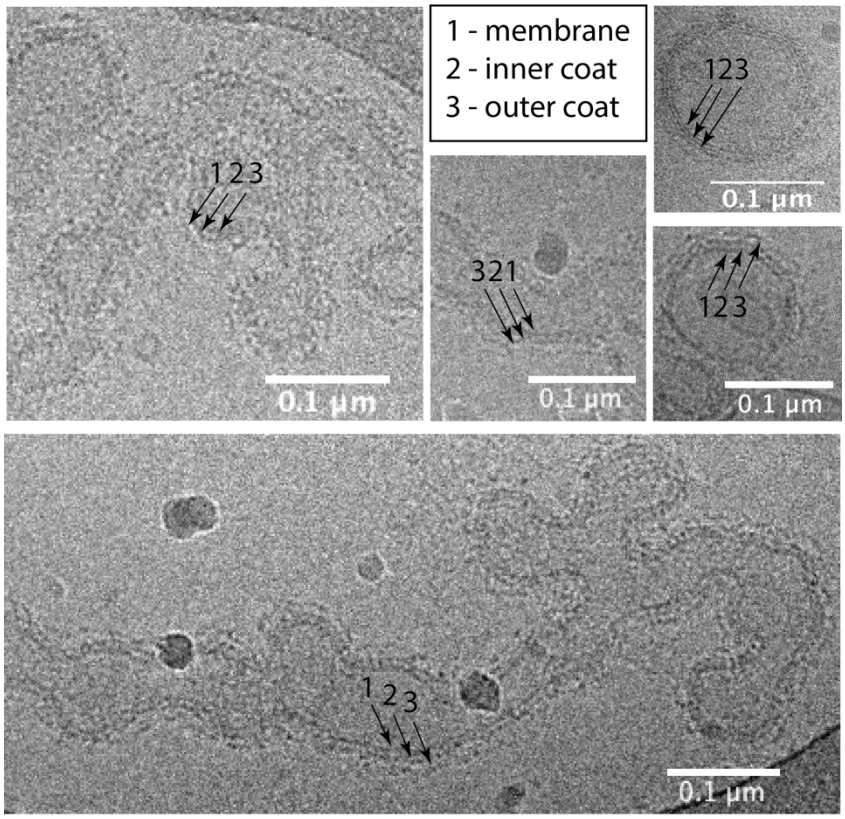

Figure 4.12: COPII components added to GUVs form layers of COPII coat on the membrane, as seen using cryo-EM. Reactions contained 1µM Sar1B, 320nM Sec23A/24C, and 320nM Sec13/31A, which were added to GUVs in the presence of 1mM GMP-PNP and 2.5mM EDTA.

While the observed membrane morphology is irregular and obtaining high-resolution structural information would pose a challenge, the collection of cryo-tomography data of these reactions and analysis using subtomogram averaging could provide low-resolution information about the interfaces that allow for inner and outer coat formation.

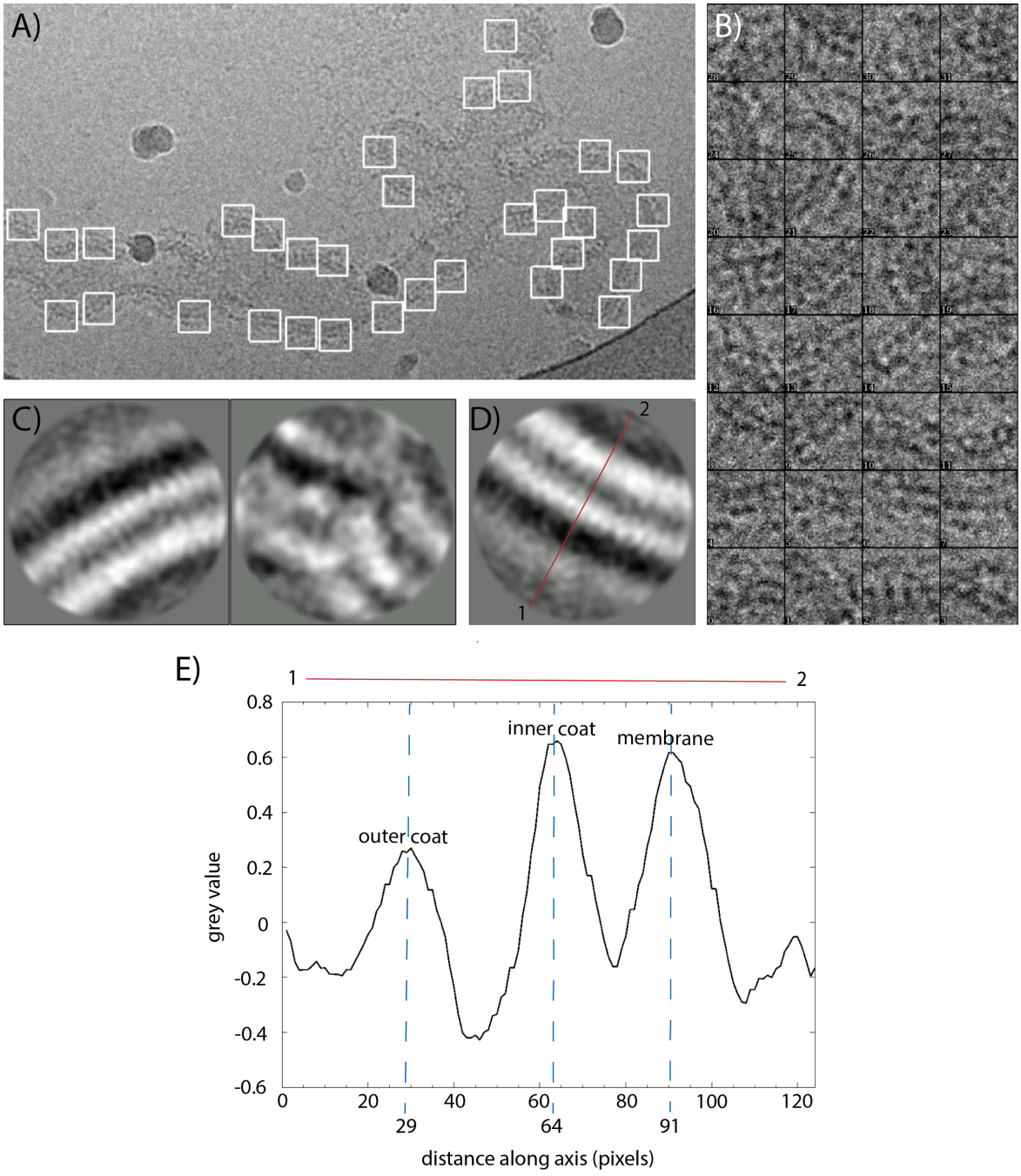

Figure 4.13: Density profile analysis of human COPII assembled on membranes. A small set of particles was selected from electron micrographs (Fig. 4.13A and B) and classified into two classes (Fig. 4.13C). In the average of the first class, (Fig. 4.13C, left-hand side), three layers were clearly visible, corresponding to the membrane, inner, and outer COPII coat. The second class (Fig. 4.12C, right-hand side) was used to separate 'junk' particles.

The intensities of these layers were measured using a line (red) perpendicular to the membrane (Fig. 4.13D). In the density profile, these layers were represented by clear peaks (Fig. 4.12E). Pixel size: 2.678Å.

V. Discussion and Future Directions

The COPII secretion system is an essential and highly conserved vesicular trafficking system, which has evolved significant complexity to meet the transport demands of the cells of higher eukaryotes. This work describes the establishment of an *in vitro* reconstitution platform for the study of human COPII assembled on membranes. Establishing this platform enables us to address outstanding questions about the functioning of this trafficking system in humans: do human COPII components remodel membranes to enable cargo export? What are the minimal requirements for human COPII-dependent membrane remodelling? What is the role of GTP hydrolysis in membrane deformation and vesicle scission? Why are mutations in Sar1B, and not Sar1A, implicated in human disease?

Multiple hypotheses have been proposed about the role of mammalian COPII in the export of cargo. Whether mammalian COPII proteins deform the ER membrane to form carriers has been the subject of debate, crucially because there is a lack of clarity on how COPII carriers can accommodate the demands of the mammalian cell, particularly regarding the export of large cargo (Fromme and Schekman, 2005). As COPII components are nonetheless essential for cargo export, they have alternatively been proposed to organise ER exit sites and concentrate cargo but not deform and coat membranes to enable cargo trafficking (Stephens and Pepperkok, 2001, 2002; Mironov *et al.*, 2003; Siddiqi, 2003; Palmer and Stephens, 2004).

In vivo, regulatory components such as Tango1/cTAGE5 are necessary for the export of large cargo (Saito *et al.*, 2009; Wilson *et al.*, 2011; Ma and Goldberg, 2016; Maeda, Katada and Saito, 2017; Raote *et al.*, 2018). The precise role of these regulatory components in the generation of mammalian COPII carriers has been investigated in biochemical studies. It has been proposed that the ER membrane-resident Tango1 enables the generation of tubular protrusions from the ER by binding the inner COPII coat, outcompeting the outer coat COPII components (Ma and Goldberg, 2016; Raote *et al.*, 2018). This would restrict the outer COPII

coat to ER-distal part of the growing COPII carrier. In this view, Tango1 is essential for the generation of tubular membrane morphologies. In a recent pre-print article, McCaughey et al. use fluorescence and electron microscopy of various Tango1 knock-out cell lines to show that in the absence of Tango1 the ERGIC is disrupted and the number of small COPII vesicles increases. They propose that in mammalian cells which express Tango1-family proteins COPII is inhibited from forming spherical vesicles. They further suggest that Tango1 promotes formation of tubular-vesicular clusters that form the ERGIC, essentially suggesting that in the absence of Tango1 the mammalian secretory pathway defaults to resemble that of yeast (McCaughey *et al.*, 2021).

Three potential roles of COPII in cargo export from the ER are shown in Figure 5:

1. COPII does not sculpt membranes and plays an indirect role in cargo export from the ER, such as organising ER exit sites and concentrating cargo (Fig. 5.1A).
2. COPII sculpts membranes to form small vesicles for the export of small cargo. However, COPII proteins do not participate in the formation of large cargo export carriers (Fig. 5.1B).
3. COPII sculpts membranes to form vesicles and, supported by large cargo adapters, forms large carriers for the export of a wide range of cargo from the ER (Fig. 5.1C).

This study has shown that COPII proteins sculpt membranes to form strings of connected vesicles (‘beads-on-a-string’), suggesting that COPII components are capable of forming vesicles for cargo export. The connectedness between vesicles likely reflects the absence of vesicle scission in the absence of GTP hydrolysis. To further to establish that human COPII proteins can form isolated vesicles for cargo export, a budding reconstitution using native ER membranes and purified proteins in the presence of GTP can be performed. In these conditions, COPII vesicles should bud from the donor membrane and separate during centrifugation.

As for the role of COPII in large cargo export and whether COPII can shape the membrane to accommodate large cargo, this study shows that a range of curvatures can be generated by addition of COPII to membranes. However, beads-on-a-string’ morphologies were most widespread upon addition of Sar1B and the other COPII components to membranes, suggesting that COPII tends to form more spherical vesicles. This work is therefore consistent

with the notion that additional factors, such as Tango1/cTAGE, are required to form elongated membrane protrusions as appropriate for the export of large cargo. The precise role of COPII in the sculpting of these carriers is unclear.

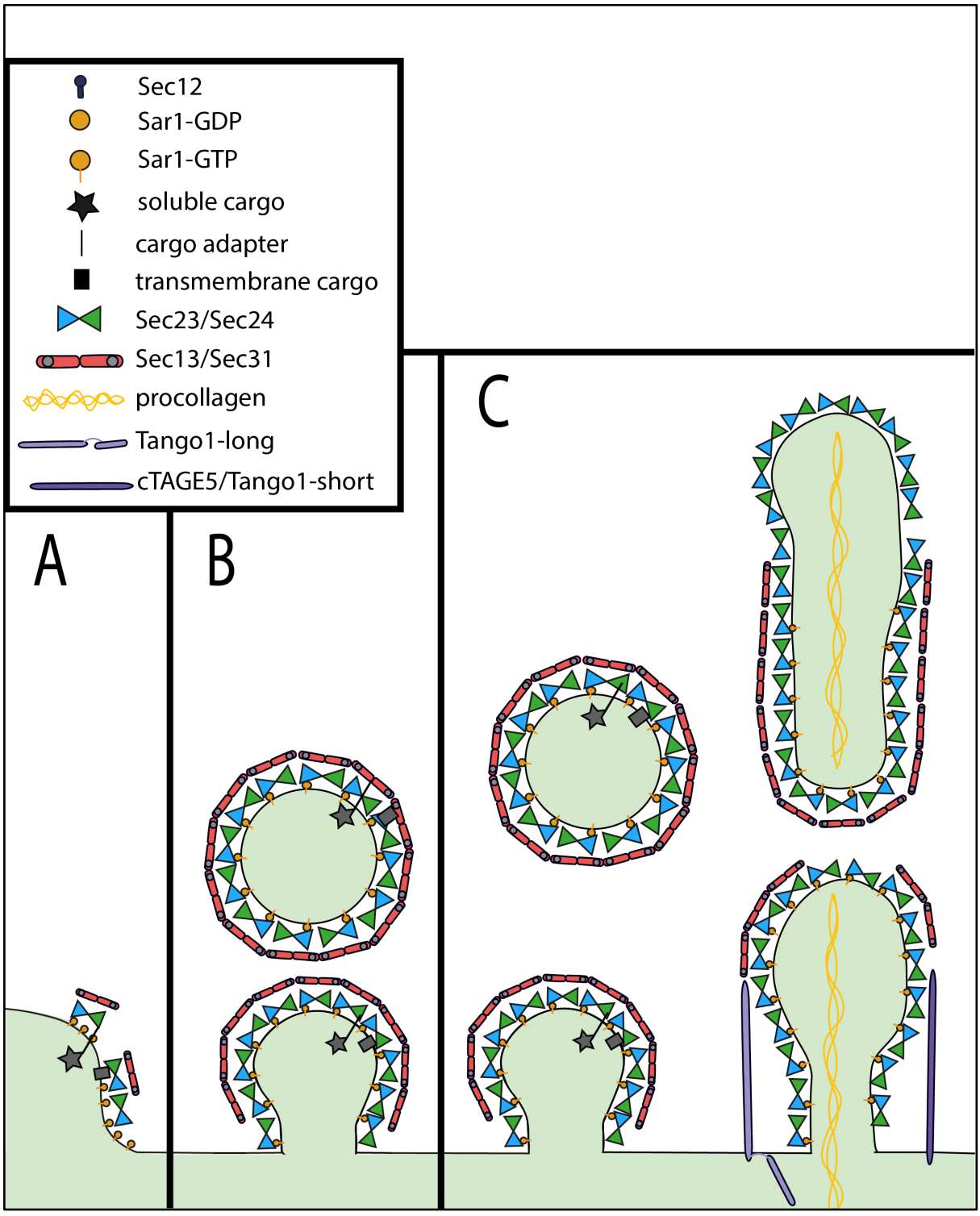

Figure 5.1: Models for the role of COPII in cargo export from the human ER. (A) COPII components function only to organise ER exit sites and concentrate cargo. (B) COPII

components form vesicles for the export of small cargo from the ER, but are not involved in large cargo export. (C) COPII components form small cargo vesicles and participate in the formation of larger carriers.

Using cryo-EM, I clearly observed the layers of the human COPII coat for the first time. Establishing this *in vitro* reconstitution system is therefore the first step towards the structural analysis of human COPII assemblies on membranes. Studying *in vitro* reconstituted human COPII assemblies using cryo-electron tomography and subtomogram averaging can provide insight into the intermolecular contacts that govern human COPII assembly and the mechanism of membrane curvature generation. Using this *in vitro* reconstitution platform, the structural rationale for the presence of different inner and outer COPII coat component paralogues can be studied by substitution with different paralogues in budding reactions.

The key to the establishment of this *in vitro* reconstitution platform was the optimisation of the construct design and purification procedure for human Sar1 to produce protein that was efficient in membrane binding. I produced Sar1 using three alternative Sar1 purification strategies, N-terminal and C-terminal His-nickel affinity and N-terminal His-glutathione affinity. Only glutathione affinity purification produced Sar1 that bound liposomes (Fig. 3.12). Since the amino acid sequences of Sar1 produced by N-terminal His-nickel affinity and N-terminal GST-glutathione affinity were identical, their differences in membrane binding could be caused by differences in conformation or oligomerisation state. Previous studies have identified the ability of mammalian Sar1 to self-oligomerise (Huang *et al.*, 2001; Hariri *et al.*, 2014; Hanna *et al.*, 2016). To enable structural determination of hamster Sar1A by X-ray crystallography, the N-terminus of Sar1A was truncated, and the authors suggested that full-length Sar1A is not suitable for crystal formation as it forms higher-order assemblies (Huang *et al.*, 2001). The oligomeric status of human Sar1B has also been assessed in previous work, and Sar1B was shown to exist in a mixture of monomeric and oligomeric states (Hanna *et al.*, 2016). Hence, it is possible that the Sar1 I purified using nickel affinity purification was forming oligomers in solution and was hence not capable of membrane binding. Two main differences between the two purification protocols can potentially result in different oligomeric states. First, the GST-tag on Sar1 for glutathione affinity purification is larger than the His-tag for nickel affinity purification. It is possible that, prior to the GST-tag cleavage, the size of the tag

inhibits the close association of Sar1 molecules through steric hindrance. Second, during the cleavage step of the GST-tag, GDP was added in the glutathione affinity purification. GDP was and not added at any point during the nickel affinity purification protocol. How the nucleotide state of Sar1 affects its oligomerisation state remains to be experimentally established. However, GTP binding by Sar1 is proposed to induce a conformational change on Sar1 and result in the protrusion of its N-terminal amphipathic helix (Goldberg, 1998; Huang *et al.*, 2001; Bi, Corpina and Goldberg, 2002; Bielli *et al.*, 2005; Rao *et al.*, 2006; Hutchings *et al.*, 2018). It is therefore expected that N-terminal helix of Sar1 is less exposed in a GDP-bound state. As the N-terminal helix of Sar1 has been implicated in Sar1 oligomerisation (Huang *et al.*, 2001), it is possible that GDP binding prevents the formation of higher-order Sar1 oligomers.

While the formation of higher-order oligomers in solution in the absence of membranes could prevent subsequent membrane association, Sar1 oligomerisation on membranes could serve a functional purpose. In the crystal structure of hamster Sar1A, the protein is assembled in dimers (Huang *et al.*, 2001). Dimerisation of Sar1A was also observed in samples of human Sar1A associated with membranes (Hariri *et al.*, 2014). In these samples, Sar1A formed locally ordered arrays of dimers that enabled the generation of membrane curvature in the absence of other COPII components.

I optimised and characterised the human COPII secretion system by focusing on three aspects: measuring the GTP hydrolysis activity of Sar1 and its stimulation by the other coat components, assessing the membrane binding of Sar1 and recruitment of other coat components, and analysing COPII reconstitution reactions by electron microscopy. Importantly, investigating these aspects was central to characterising the differences between the two Sar1 paralogues.

The role of GTP hydrolysis by Sar1 in membrane deformation and fission has been the subject of multiple investigations, and it has been suggested that GTP hydrolysis is needed for membrane remodelling by mammalian Sar1 (Hanna *et al.*, 2016). This work suggests that Sar1 can remodel membranes in the absence of GTP hydrolysis as incubated with non-hydrolysable GTP analogues. Furthermore, membrane deformations emanating from GUVs remained associated with the donor vesicles, suggesting that GTP hydrolysis is necessary for membrane fission, as observed previously for mammalian cells (Bannykh, Rowe and Balch, 1996).

Importantly, by measuring GTP hydrolysis activity, I set out to analyse the differences between Sar1A and Sar1B. Sar1B has been specifically implicated in human diseases caused by large cargo transport deficits (Jones *et al.*, 2003). There are multiple lines of evidence that suggest that large carrier formation is enabled by delayed GTP hydrolysis (Antonny *et al.*, 2001; Saito *et al.*, 2009; Malhotra and Erlmann, 2011). Hence, studies aiming to understand differences between two paralogues have investigated the differences in their GTP hydrolysis rates. Using *in vitro* GTP hydrolysis assays, I confirm that both Sar1A and Sar1B have an intrinsic GTP hydrolysis activity. The GTP hydrolysis rates I measured varied between proteins produced in different purifications, hence comparisons between the GTP hydrolysis rates of the two purified protein paralogues remained uninformative. The inner and outer coat components stimulated GTP hydrolysis activity by Sar1, as expected (Fromme *et al.*, 2007; Melville, Studer and Schekman, 2020), suggesting that the purified proteins are capable of functional binding.

In this work, in addition to assessing Sar1 GTP hydrolysis and comparing GTP hydrolysis activities between Sar1 paralogues, I investigated their membrane binding capability in the presence of GTP analogues and GDP. Membrane recruitment of the two paralogues has not been compared previously.

When I assessed the membrane binding of the two paralogues in liposome flotation experiments, I observed that Sar1A was recruited to liposomes equally with GMP-PNP and GDP, while Sar1B was recruited more efficiently with GMP-PNP than with GDP. These results for Sar1A are in line with a previous study that assessed liposome binding of hamster Sar1A in the presence of GTP analogues and GDP (Kim *et al.*, 2005). For human Sar1B, it has previously been suggested that the N-terminal amphipathic helix that mediates membrane binding is solvent-exposed both with GTP and GDP, but that GTP binding results in more stable membrane association (Hanna *et al.*, 2016). The observation that the nucleotide state of Sar1B affects the efficiency of its recruitment to membranes suggests that Sar1B can be regulated by the local GTP levels at ERES. Regulation of Sar1B membrane binding is necessary in the context of large carrier generation: the formation of large carriers needs to be coupled to the presence of large cargo at particular ER loci.

I compared the membrane morphologies induced by Sar1A and Sar1B, which have not been observed previously. When I assessed membrane deformation by Sar1 paralogues by

negative stain EM in the absence of other coat components, I observed that Sar1A formed vesiculations and smooth wide tubules emanating from GUVs, while Sar1B produced irregular tubules. When COPII components were added to Sar1B reactions with GUVs, membrane morphology was different to that observed with Sar1B alone, suggesting that COPII components dictated the morphology of membrane deformations. These reactions predominantly contained connected membrane vesicles, in contrast with yeast, where the incubation of COPII components with GUVs in the presence of a non-hydrolysable GTP analogue results in ordered tubes emanating from GUVs (Bacia *et al.*, 2011; Zanetti *et al.*, 2013; Hutchings *et al.*, 2018). It remains unclear how the vesicular membrane deformation generated by Sar1B and COPII components can be modulated to accommodate large cargo. *In vivo*, the generation of large COPII carriers requires the large cargo adapters Tango1/cTAGE5 which reside in the ER membrane and potentially compete with the outer coat for inner coat binding (Ma and Goldberg, 2016). Hence, it is possible that the membrane morphologies I observe as dictated by inner and outer COPII coats in the presence of Sar1B are more relevant at ER-distal curved carrier tips, while more ER-proximal morphologies are dictated by Tango1/cTAGE5.

In addition to investigating overall morphology, I observed COPII binding to membranes using cryo-electron microscopy. I observed the human COPII coat assembled on the membrane in two clearly discernible layers, similarly to what has been observed for *in vitro* human COPII assemblies in the absence of membrane (Stagg *et al.*, 2008) and with yeast proteins assembled on membranes (Bacia *et al.*, 2011; Zanetti *et al.*, 2013; Hutchings *et al.*, 2018).

While using a minimal reconstitution system can help address fundamental questions about the human COPII secretion system, this minimalistic approach is also a simplification of a complex system and hence poses limitations. Reconstitutions exclude protein and lipid components that impact COPII function *in vivo*. In fact, while this *in vitro* reconstitution included the five core COPII proteins, proteomic analysis of COPII vesicles derived from human immortalised cells has identified 60 different proteins, which were all components of the early secretory pathway (Adolf *et al.*, 2019). While the role of some additional protein components in the COPIII vesicle formation remains to be investigated, COPII interacting partners such as Sec12 and Sec16 have been well-established as regulators of COPII function (Nakano, Brada and Schekman, 1988; Barlowe *et al.*, 1994; Weissman, Plutner and Balch,

2001; Supek *et al.*, 2002; Bielli *et al.*, 2005; Watson *et al.*, 2006). Including these factors in *in vitro* reconstitution reactions can be a tool for studying the complexity of the regulatory network of COPII assembly. While additional purified cytosolic factors, such as Sec16, can be directly added to budding reactions, the incorporation of transmembrane proteins, such as Sec12 and the large cargo adapters Tango1/cTAGE5, into model membranes remains challenging. Apart from the interaction of specific protein components with the core COPII machinery, the absence of protein components in lipid models has implications for membrane deformability.

In this work, *in vitro* reconstitutions were performed in the absence of cargo. It has been established that the presence of cargo decreases membrane deformability (Čopič *et al.*, 2012; D'Arcangelo *et al.*, 2015; Gomez-Navarro *et al.*, 2020; Stancheva *et al.*, 2020). It has previously been shown that purified mammalian COPII components that bind artificial membranes *in vitro* are incapable of remodelling microsomes (ER-derived membrane vesicles) in the absence of additional cytosolic factors (Kim *et al.*, 2005). Therefore, while I showed that the minimal set of COPII components is sufficient for membrane deformation of GUVs, it remains to be established whether this mix of purified COPII components can deform cargo-loaded membranes, or whether additional factors are needed. Reconstituting COPII budding from microsomes can help gain biologically relevant insight into COPII-mediated deformation of cargo-loaded membranes.

The lipid composition of the membrane models I used to reconstitute the human COPII system was based on a lipid mixture optimised to maximise yeast COPII components (Matsuoka et al., 1998). However, this lipid mixture is not identical to the lipid composition of the ER in mammals, as it excludes lipids that are present in the ER in considerable amounts, such as sphingomyelin and ceramides (Vance, 2015). Furthermore, it includes lipids such as PI4P, which are commonly absent from the ER, which implies that observed membrane deformation effects can be non-physiological (Vance, 2015). The lipid mixture has also not been specifically optimised to maximise human COPII binding. Additionally, recent lipidomic analysis investigated the lipid composition of yeast cell-derived COPII vesicles and established an enrichment of specific lipids compared to the membrane of the ER (Melero et al., 2018). These lysophospholipids were shown to enhance COPII membrane recruitment and increase membrane fluidity. Further human COPII *in vitro* reconstitution

can benefit from reflecting the membrane composition established in human cell lipidomic studies, including specific lipid proportions, in membrane models. Finally, the Sar1 GTPase has been shown to dynamically interact with the local membrane composition. Sar1 enhances the activity of phospholipases, and it has been demonstrated that *in vivo* COPII export is blocked by phospholipase inhibition (Bi, Roth and Ktistakis, 1997; Pathre *et al.*, 2003; Shimoi *et al.*, 2005). Hence, COPII components can moderate ER lipid composition, and this dynamic regulation has functional importance. While such effects are not reflected in *in vitro* reconstitutions, they can impact membrane deformability and COPII binding.

As GTP hydrolysis results in COPII membrane dissociation, to retain COPII components on membranes, I utilised non-hydrolysable GTP analogues. While stable COPII membrane association is essential for structural studies, observing COPII proteins in the act of remodeling membranes in the presence of GTP hydrolysis can help unravel the dynamics of this complex system.

In conclusion, this thesis describes the establishment of an *in vitro* reconstitution platform for the human COPII secretion system. I show that purified core human COPII components bind membranes and are sufficient for the deformation of membrane models. Using cryo-EM, I obtained the first images of human COPII assembled on membranes and show that human COPII components form two discernible coat layers.

References

Adams, E. J. *et al.* (2014) 'Mammalian COPII coat component SEC24C is required for embryonic development in mice', *Journal of Biological Chemistry*, 289(30), pp. 20858–20870. doi: 10.1074/jbc.M114.566687.

Adolf, F. *et al.* (2013) 'Scission of COPI and COPII vesicles is independent of GTP hydrolysis', *Traffic*, 14(8), pp. 922–932. doi: 10.1111/tra.12084.

Adolf, F. *et al.* (2019) 'Proteomic Profiling of Mammalian COPII and COPI Vesicles', *Cell Reports*. doi: 10.1016/j.celrep.2018.12.041.

Alberts, B. *et al.* (2002) 'Transport from the ER through the Golgi Apparatus', in *Molecular Biology of the Cell*. 4th editio. New York: Garland Science. Available at: https://www.ncbi.nlm.nih.gov/books/NBK26941/.

Amodio, G. *et al.* (2017) 'Identification of Cysteine Ubiquitylation Sites on the Sec23A Protein of the COPII Complex Required for Vesicle Formation from the ER', *The Open Biochemistry Journal*, 11(1), pp. 36–46. doi: 10.2174/1874091X01711010036.

Angelova, M. I. and Dimitrov, D. S. (1986) 'Liposome electroformation', *Faraday Discussions of the Chemical Society*, 81, pp. 303–311. doi: 10.1039/DC9868100303.

Antonny, B. *et al.* (2001) 'Dynamics of the COPII coat with GTP and stable analogues', *Nat Cell Biol*, 3, pp. 531–537. doi: 10.1038/35078500.

Antonny, B. *et al.* (2003) 'Self-assembly of minimal COPII cages', *EMBO Reports*. doi: 10.1038/sj.embor.embor812.

Appenzeller-Herzog, C. (2006) 'The ER-Golgi intermediate compartment (ERGIC): in search of its identity and function', *Journal of Cell Science*, 119(11), pp. 2173–2183. doi: 10.1242/jcs.03019.

Aridor, M. *et al.* (1998) 'Cargo selection by the COPII budding machinery during export from the ER', *Journal of Cell Biology*. doi: 10.1083/jcb.141.1.61.

Aridor, M. *et al.* (2001) 'The Sar1 GTPase coordinates biosynthetic cargo selection with endoplasmic reticulum export site assembly', *Journal of Cell Biology*, 152(1), pp. 213–229. doi: 10.1083/jcb.152.1.213.

Asadi, J. *et al.* (2017) 'Enhanced imaging of lipid rich nanoparticles embedded in methylcellulose films for transmission electron microscopy using mixtures of heavy metals', *Micron*. doi: 10.1016/j.micron.2017.03.019.

Bachinger, H. P. *et al.* (1982) 'Structural implications from an electronmicroscopic comparison of procollagen V with procollagen I, pC-collagen I, procollagen IV, and a Drosophila procollagen', *Journal of Biological Chemistry*.

Bacia, K. *et al.* (2011) 'Multibudded tubules formed by COPII on artificial liposomes', *Scientific Reports*. doi: 10.1038/srep00017.

Baines, A. C. *et al.* (2013) 'Disruption of the Sec24d gene results in early embryonic lethality in the mouse', *PLoS One*, 8(4), p. e61114. doi: 10.1371/journal.pone.0061114.

Bannykh, S. I., Rowe, T. and Balch, W. E. (1996) 'The organization of endoplasmic reticulum export complexes', *Journal of Cell Biology*, 135(1), pp. 19–35. doi: 10.1083/jcb.135.1.19.

Bard, F. *et al.* (2006) 'Functional genomics reveals genes involved in protein secretion and Golgi organization', *Nature*, 439(7076), pp. 604–607. doi: 10.1038/nature04377.

Barlowe, C. *et al.* (1994) 'COPII: A membrane coat formed by Sec proteins that drive vesicle budding from the endoplasmic reticulum', *Cell*, 77(6), pp. 895–907. doi: 10.1016/0092-8674(94)90138-4.

Barlowe, C. (1997) 'Coupled ER to golgi transport reconstituted with purified cytosolic proteins', *Journal of Cell Biology*, 139(5), pp. 1097–1108. doi: 10.1083/jcb.139.5.1097.

Barlowe, C. (2003) 'Signals for COPII-dependent export from the ER: What's the ticket out?', *Trends in Cell Biology*, pp. 295–300. doi: 10.1016/S0962-8924(03)00082-5.

Barlowe, C., d'Enfert, C. and Schekman, R. (1993) 'Purification and characterization of SAR1p, a small GTP-binding protein required for transport vesicle formation from the endoplasmic reticulum.', *The Journal of biological chemistry*, 268(2), pp. 873–879.

Barlowe, C. and Schekman, R. (1993) 'SEC12 encodes a guanine-nucleotide-exchange factor essential for transport vesicle budding from the ER', *Nature*, 365(6444), pp. 347–349. doi: 10.1038/365347a0.

Ben-Tekaya, H. (2005) 'Live imaging of bidirectional traffic from the ERGIC', *Journal of Cell Science*, 118(2), pp. 357–367. doi: 10.1242/jcs.01615.

Bhattacharya, N., O'Donnell, J. and Stagg, S. M. (2012) 'The structure of the Sec13/31 COPII cage bound to Sec23', *Journal of Molecular Biology*. doi: 10.1016/j.jmb.2012.04.024.

Bhattacharyya, D. and Glick, B. S. (2007) 'Two Mammalian Sec16 Homologues Have Nonredundant Functions in Endoplasmic Reticulum (ER) Export and Transitional ER Organization', *Molecular Biology of the Cell*, 18(3), pp. 839–849. doi: 10.1091/mbc.E06-08-0707.

Bi, K., Roth, M. G. and Ktistakis, N. T. (1997) 'Phosphatidic acid formation by phospholipase D is required for transport from the endoplasmic reticulum to the Golgi complex', *Current Biology*. doi: 10.1016/S0960-9822(06)00153-9.

Bi, X., Corpina, R. A. and Goldberg, J. (2002) 'Structure of the Sec23/24-Sar1 pre-budding complex of the COPII vesicle coat', *Nature*, 419(6904), pp. 271–277. doi: 10.1038/nature01040.

Bi, X., Mancias, J. D. and Goldberg, J. (2007) 'Insights into COPII Coat Nucleation from the Structure of Sec23•Sar1 Complexed with the Active Fragment of Sec31', *Developmental Cell*, 13(5), pp. 635–645. doi: 10.1016/j.devcel.2007.10.006.

Bielli, A. *et al.* (2005) 'Regulation of Sar1 NH2terminus by GTP binding and hydrolysis promotes membrane deformation to control COPII vesicle fission', *Journal of Cell Biology*, 171(6), pp. 919–924. doi: 10.1083/jcb.200509095.

Bigay, J. and Antonny, B. (2006) 'Real-time assays for the assembly-disassembly cycle of COP coats on liposomes of defined size', *Methods in Enzymology*, 404, pp. 95–107. doi: 10.1016/S0076-6879(05)04010-3.

Bock, J. B. *et al.* (2001) 'A genomic perspective on membrane compartment organization', *Nature*, pp. 839–841. doi: 10.1038/35057024.

Bonifacino, J. S. and Glick, B. S. (2004) 'The Mechanisms of Vesicle Budding and Fusion', *Cell*, pp. 153–166. doi: 10.1016/S0092-8674(03)01079-1.

Bosserhoff, A. K., Moser, M. and Buettner, R. (2004) 'Characterization and expression pattern of the novel MIA homolog TANGO', *Gene Expression Patterns*. doi: 10.1016/j.modgep.2003.12.002.

Botstein, D. and Fink, G. R. (1988) 'Yeast: an experimental organism for modern biology.', *Science (New York, N.Y.)*, 240(4858), pp. 1439–43. doi: 10.1126/science.3287619.

Botstein, D. and Fink, G. R. (2011) 'Yeast: An experimental organism for 21st century biology', *Genetics*, 189(3), pp. 695–704. doi: 10.1534/genetics.111.130765.

Boyadjiev *et al.* (2011) 'Cranio-lenticulo-sutural dysplasia associated with defects in collagen secretion', *Clinical Genetics*, 80(2), pp. 169–176. doi: 10.1111/j.1399-0004.2010.01550.x.

Boyadjiev, S. A. *et al.* (2006) 'Cranio-lenticulo-sutural dysplasia is caused by a SEC23A mutation leading to abnormal endoplasmic-reticulum-to-Golgi trafficking', *Nature Genetics*, 38(10), pp. 1192–1197. doi: 10.1038/ng1876.

Cai, H. *et al.* (2007) 'TRAPPI tethers COPII vesicles by binding the coat subunit Sec23',

Nature, 445(7130), pp. 941–944. doi: 10.1038/nature05527.

Chen, X. W. *et al.* (2013) 'SEC24A deficiency lowers plasma cholesterol through reduced PCSK9 secretion', *eLife*, 2013(2). doi: 10.7554/eLife.00444.

Christiano, A. M. *et al.* (1994) 'Cloning of human type VII collagen. Complete primary sequence of the α1(VII) chain and identification of intragenic polymorphisms', *Journal of Biological Chemistry*. doi: 10.1016/s0021-9258(17)31984-1.

Cohen, M. *et al.* (2003) 'Ubp3 requires a cofactor, Bre5, to specifically de-ubiquitinate the COPII protein, Sec23', *Nature Cell Biology*, 5(7), pp. 661–667. doi: 10.1038/ncb1003.

Cooper GM (2000) 'The Mechanism of Vesicular Transport.', in *The Cell: A Molecular Approach*. 2nd editio. Available at: https://www.ncbi.nlm.nih.gov/books/NBK9886/.

Čopič, A. *et al.* (2012) 'ER cargo properties specify a requirement for COPII coat rigidity mediated by Sec13p', *Science*. doi: 10.1126/science.1215909.

Cui, Y. *et al.* (2019) 'A COPII subunit acts with an autophagy receptor to target endoplasmic reticulum for degradation', *Science*. doi: 10.1126/science.aau9263.

D'Arcangelo, J. G. *et al.* (2015) 'Traffic of p24 proteins and COPII coat composition mutually influence membrane scaffolding', *Current Biology*. doi: 10.1016/j.cub.2015.03.029.

D'Enfert, C. *et al.* (1991) 'Secl2p-dependent Membrane Binding of the Small GTPbinding Protein Sarlp Promotes Formation of Transport Vesicles from the ER', *The Journal of cell biology*, 114(4), pp. 663–670. doi: 10.1083/jcb.114.4.663.

Daum, S. *et al.* (2014) 'Insights from reconstitution reactions of COPII vesicle formation using pure components and low mechanical perturbation', *Biological Chemistry*, 395(7–8), pp. 801–812. doi: 10.1515/hsz-2014-0117.

Dodonova, S. O. *et al.* (2015) 'A structure of the COPI coat and the role of coat proteins in membrane vesicle assembly', *Science*. doi: 10.1126/science.aab1121.

Donaldson, J. G. and Honda, A. (2005) 'Localization and function of Arf family GTPases', *Biochemical Society Transactions*, 33(4), pp. 639–642. doi: 10.1042/BST0330639.

Drulyte, I. *et al.* (2018) 'Approaches to altering particle distributions in cryo-electron microscopy sample preparation', *Acta Crystallographica Section D: Structural Biology*. doi: 10.1107/S2059798318006496.

Dudognon, P. *et al.* (2004) 'Regulation of a COPII component by cytosolic O-glycosylation

during mitosis', *FEBS Letters*, 561(1–3), pp. 44–50. doi: 10.1016/S0014-5793(04)00109-7.

Espenshade, P. *et al.* (1995) 'Yeast SEC16 gene encodes a multidomain vesicle coat protein that interacts with Sec23p', *Journal of Cell Biology*, 131(2), pp. 311–324. doi: 10.1083/jcb.131.2.311.

Fan, J. Y., Roth, J. and Zuber, C. (2003) 'Ultrastructural analysis of transitional endoplasmic reticulum and pre-Golgi intermediates: A highway for cars and trucks', *Histochemistry and Cell Biology*, 120(6), pp. 455–463. doi: 10.1007/s00418-003-0597-1.

Fath, S. *et al.* (2007) 'Structure and Organization of Coat Proteins in the COPII Cage', *Cell*, 129(7), pp. 1325–1336. doi: 10.1016/j.cell.2007.05.036.

Feng, Z., Yang, K. and Pastor-Pareja, J. C. (2021) 'Tales of the ER-Golgi Frontier: Drosophila-Centric Considerations on Tango1 Function', *Frontiers in Cell and Developmental Biology*. doi: 10.3389/fcell.2020.619022.

Forster, R. *et al.* (2006) 'Secretory cargo regulates the turnover of COPII subunits at single ER exit sites', *Current Biology*, 16(2), pp. 173–179. doi: 10.1016/j.cub.2005.11.076.

Fromme, J. C. *et al.* (2007) 'The Genetic Basis of a Craniofacial Disease Provides Insight into COPII Coat Assembly', *Developmental Cell*, 13(5), pp. 623–634. doi: 10.1016/j.devcel.2007.10.005.

Fromme, J. C., Orci, L. and Schekman, R. (2008) 'Coordination of COPII vesicle trafficking by Sec23', *Trends in Cell Biology*, pp. 330–336. doi: 10.1016/j.tcb.2008.04.006.

Fromme, J. C. and Schekman, R. (2005) 'COPII-coated vesicles: Flexible enough for large cargo?', *Current Opinion in Cell Biology*, pp. 345–352. doi: 10.1016/j.ceb.2005.06.004.

Futai, E. *et al.* (2004) 'GTP/GDP exchange by Sec12p enables COPII vesicle bud formation on synthetic liposomes', *EMBO Journal*. doi: 10.1038/sj.emboj.7600430.

Gan, W. *et al.* (2017) 'ULK1 phosphorylates Sec23A and mediates autophagy-induced inhibition of ER-to-Golgi traffic', *BMC Cell Biology*, 18(1). doi: 10.1186/s12860-017-0138-8.

Garbes, L. *et al.* (2015) 'Mutations in SEC24D, encoding a component of the COPII machinery, cause a syndromic form of osteogenesis imperfecta', *American Journal of Human Genetics*, 96(3), pp. 432–439. doi: 10.1016/j.ajhg.2015.01.002.

Ge, L., Zhang, M. and Schekman, R. (2014) 'Phosphatidylinositol 3-kinase and COPII generate LC3 lipidation vesicles from the ER-Golgi intermediate compartment', *eLife*. doi: 10.7554/eLife.04135.

Gimeno, R. E., Espenshade, P. and Kaiser, C. a (1996) 'COPII Coat Subunit Interactions: Sec24p and Sec23p Bind to Adjacent Regions of Secl6p', *Mol Biol Cell*, 7(November), pp. 1815–1823. doi: 10.1091/mbc.7.11.1815.

Glick, D., Barth, S. and Macleod, K. F. (2010) 'Autophagy: Cellular and molecular mechanisms', *Journal of Pathology*. doi: 10.1002/path.2697.

Goldberg, J. (1998) 'Structural basis for activation of ARF GTPase: Mechanisms of guanine nucleotide exchange and GTP-myristoyl switching', *Cell*, 95(2), pp. 237–248. doi: 10.1016/S0092-8674(00)81754-7.

Gomez-Navarro, N. *et al.* (2020) 'Cargo crowding contributes to sorting stringency in COPII vesicles', *Journal of Cell Biology*. doi: 10.1083/JCB.201806038.

Gorur, A. *et al.* (2017) 'COPII-coated membranes function as transport carriers of intracellular procollagen I', *Journal of Cell Biology*, 216(6), pp. 1745–1759. doi: 10.1083/jcb.201702135.

Hall, A. and Self, A. J. (1986) 'The effect of Mg2+ on the guanine nucleotide exchange rate of p21N-ras.', *The Journal of biological chemistry*, 261(24), pp. 10963–5. Available at: http://www.ncbi.nlm.nih.gov/pubmed/3525557.

Hanna, M. G. *et al.* (2016) 'Sar1 GTPase activity is regulated by membrane curvature', *Journal of Biological Chemistry*, 291(3). doi: 10.1074/jbc.M115.672287.

Hanna, M. G. *et al.* (2017) 'TFG facilitates outer coat disassembly on COPII transport carriers to promote tethering and fusion with ER–Golgi intermediate compartments', *Proceedings of the National Academy of Sciences of the United States of America*. doi: 10.1073/pnas.1709120114.

Hariri, H. *et al.* (2014) 'Insights into the mechanisms of membrane curvature and vesicle scission by the small GTPase Sar1 in the early secretory pathway', *Journal of Molecular Biology*, 426(22), pp. 3811–3826. doi: 10.1016/j.jmb.2014.08.023.

Hauri, H. P. and Schweizer, A. (1992) 'The endoplasmic reticulum-Golgi intermediate compartment', *Current Opinion in Cell Biology*. doi: 10.1016/0955-0674(92)90078-Q.

Hsia, K. C. *et al.* (2007) 'Architecture of a Coat for the Nuclear Pore Membrane', *Cell*, 131(7), pp. 1313–1326. doi: 10.1016/j.cell.2007.11.038.

Huang, M. *et al.* (2001) 'Crystal structure of Sar1-GDP at 1.7 Å resolution and the role of the NH2 terminus in ER export', *Journal of Cell Biology*, 155(6), pp. 937–948. doi: 10.1083/jcb.200106039.

Hussain, M. M. (2000) ‘A proposed model for the assembly of chylomicrons.’, *Atherosclerosis*.

Hutchings, J. *et al.* (2018) ‘Subtomogram averaging of COPII assemblies reveals how coat organization dictates membrane shape’, *Nature Communications*. doi: 10.1038/s41467-018-06577-4.

Hutchings, J. *et al.* (2020) ‘Structure of the complete, membrane-assembled COPII coat reveals a complex interaction network.’, *bioRxiv*. doi: 10.1101/2020.06.18.159608.

Huttner, W. B. and Zimmerberg, J. (2001) ‘Implications of lipid microdomains for membrane curvature, budding and fission: Commentary’, *Current Opinion in Cell Biology*. doi: 10.1016/S0955-0674(00)00239-8.

Ishii, M. *et al.* (2016) ‘COPI is essential for Golgi cisternal maturation and dynamics’, *Journal of Cell Science*. doi: 10.1242/jcs.193367.

Jin, L. *et al.* (2012) ‘Ubiquitin-dependent regulation of COPII coat size and function’, *Nature*, 482(7386), pp. 495–500. doi: 10.1038/nature10822.

Jing, J., Wang, B. and Liu, P. (2019) ‘The functional role of sec23 in vesicle transportation, autophagy and cancer’, *International Journal of Biological Sciences*. doi: 10.7150/ijbs.37008.

Jones, B. *et al.* (2003) ‘Mutations in a Sar1 GTPase of COPII vesicles are associated with lipid absorption disorders’, *Nature Genetics*, 34(1), pp. 29–31. doi: 10.1038/ng1145.

Junqueira, L. and Carneiro, J. (2005) ‘Basic Histology: Text & Atlas’, *Statrefcom*.

Kawaguchi, K. *et al.* (2018) ‘Ubiquitin-specific protease 8 deubiquitinates Sec31A and decreases large COPII carriers and collagen IV secretion’, *Biochemical and Biophysical Research Communications*. doi: 10.1016/j.bbrc.2018.03.202.

Kesimer, M. and Sheehan, J. K. (2012) ‘Mass spectrometric analysis of mucin core proteins’, *Methods in Molecular Biology*. doi: 10.1007/978-1-61779-513-8_4.

Khoriaty, R. *et al.* (2017) ‘SEC23B is required for pancreatic acinar cell function in adult mice’, *Molecular Biology of the Cell*, 28(15). doi: 10.1091/mbc.E17-01-0001.

Kim *et al.* (2005) ‘Uncoupled packaging of amyloid precursor protein and presenilin 1 into coat protein complex II vesicles’, *Journal of Biological Chemistry*, 280(9), pp. 7758–7768. doi: 10.1074/jbc.M411091200.

Kim, S. D. *et al.* (2012) ‘SEC23-SEC31 the interface plays critical role for export of

procollagen from the endoplasmic reticulum', *Journal of Biological Chemistry*, 287(13), pp. 10134–10144. doi: 10.1074/jbc.M111.283382.

Kinuta, M. *et al.* (2002) 'Phosphatidylinositol 4,5-bisphosphate stimulates vesicle formation from liposomes by brain cytosol', *Proceedings of the National Academy of Sciences of the United States of America*. doi: 10.1073/pnas.261715599.

Kiselev, N. A., Sherman, M. B. and Tsuprun, V. L. (1990) 'Negative staining of proteins', *Electron Microscopy Reviews*. doi: 10.1016/0892-0354(90)90013-I.

Klebe, C. *et al.* (1995) 'Interaction of the Nuclear GTP-Binding Protein Ran with Its Regulatory Proteins RCC1 and RanGAP1', *Biochemistry*, 34(2), pp. 639–647. doi: 10.1021/bi00002a031.

Klumperman, J. *et al.* (1998) 'The recycling pathway of protein ERGIC-53 and dynamics of the ER-Golgi intermediate compartment', *Journal of Cell Science*.

Kovtun, O. *et al.* (2018) 'Structure of the membrane-assembled retromer coat determined by cryo-electron tomography', *Nature*. doi: 10.1038/s41586-018-0526-z.

Kuge, O. *et al.* (1994) 'Sar1 promotes vesicle budding from the endoplasmic reticulum but not Golgi compartments', *Journal of Cell Biology*, 125(1), pp. 51–65. doi: 10.1083/jcb.125.1.51.

Lang, M. R. *et al.* (2006) 'Secretory COPII coat component Sec23a is essential for craniofacial chondrocyte maturation', *Nature Genetics*, 38(10), pp. 1198–1203. doi: 10.1038/ng1880.

Langhans, M. *et al.* (2012) 'ERES (ER exit sites) and the "Secretory Unit Concept"', *Journal of Microscopy*, 247(1), pp. 48–59. doi: 10.1111/j.1365-2818.2011.03597.x.

Lee, C. and Goldberg, J. (2010) 'Structure of Coatomer Cage Proteins and the Relationship among COPI, COPII, and Clathrin Vesicle Coats', *Cell*, 142(1), pp. 123–132. doi: 10.1016/j.cell.2010.05.030.

Lee, M. C. S. *et al.* (2004) 'BI-DIRECTIONAL PROTEIN TRANSPORT BETWEEN THE ER AND GOLGI', *Annual Review of Cell and Developmental Biology*, 20(1), pp. 87–123. doi: 10.1146/annurev.cellbio.20.010403.105307.

Lee, M. C. S. *et al.* (2005) 'Sar1p N-terminal helix initiates membrane curvature and completes the fission of a COPII vesicle', *Cell*. doi: 10.1016/j.cell.2005.07.025.

Lekszas, C. *et al.* (2020) 'Biallelic TANGO1 mutations cause a novel syndromal disease due to hampered cellular collagen secretion', *eLife*. doi: 10.7554/eLife.51319.

Levic, D. S. *et al.* (2015) 'Animal model of Sar1b deficiency presents lipid absorption deficits similar to Anderson disease', *Journal of Molecular Medicine*, 93(2), pp. 165–176. doi: 10.1007/s00109-014-1247-x.

Li, Z., Huang, W. and Wang, W. (2020) 'Multifaceted roles of COPII subunits in autophagy', *Biochimica et Biophysica Acta - Molecular Cell Research*. doi: 10.1016/j.bbamcr.2019.118627.

Lippincott-Schwartz, J. (1993) 'Bidirectional membrane traffic between the endoplasmic reticulum and Golgi apparatus', *Trends Cell Biol*, 3(3), pp. 81–88.

Liu, M. *et al.* (2017) 'Tango1 spatially organizes ER exit sites to control ER export', *Journal of Cell Biology*. doi: 10.1083/jcb.201611088.

Long, K. R. *et al.* (2010) 'Sar1 assembly regulates membrane constriction and ER export', *Journal of Cell Biology*, 190(1), pp. 115–128. doi: 10.1083/jcb.201004132.

Lord, C. *et al.* (2011) 'Sequential interactions with Sec23 control the direction of vesicle traffic', *Nature*, 473(7346), pp. 181–186. doi: 10.1038/nature09969.

Ma, W. and Goldberg, J. (2016) 'TANGO1/cTAGE5 receptor as a polyvalent template for assembly of large COPII coats', *Proceedings of the National Academy of Sciences*, 113(36), pp. 10061–10066. doi: 10.1073/pnas.1605916113.

Maeda, M., Katada, T. and Saito, K. (2017) 'TANGO1 recruits Sec 16 to coordinately organize ER exit sites for efficient secretion', *Journal of Cell Biology*. doi: 10.1083/jcb.201703084.

Maeda, M., Saito, K. and Katada, T. (2016) 'Distinct isoform-specific complexes of TANGO1 cooperatively facilitate collagen secretion from the endoplasmic reticulum', *Molecular Biology of the Cell*. doi: 10.1091/mbc.E16-03-0196.

Malhotra, V. and Erlmann, P. (2011) 'Protein export at the ER: Loading big collagens into COPII carriers', *EMBO Journal*. doi: 10.1038/emboj.2011.255.

Mancias, J. D. and Goldberg, J. (2007) 'The Transport Signal on Sec22 for Packaging into COPII-Coated Vesicles Is a Conformational Epitope', *Molecular Cell*. doi: 10.1016/j.molcel.2007.03.017.

Mancias, J. D. and Goldberg, J. (2008) 'Structural basis of cargo membrane protein discrimination by the human COPII coat machinery', *EMBO Journal*, 27(21), pp. 2918–2928. doi: 10.1038/emboj.2008.208.

Markova, E. A. and Zanetti, G. (2019) 'Visualizing membrane trafficking through the electron microscope : cryo-tomography of coat complexes research papers', *Acta Crystallographica*

Section D. International Union of Crystallography, 75, pp. 467–474. doi: 10.1107/S2059798319005011.

Marsh, D. (2006) 'Elastic curvature constants of lipid monolayers and bilayers', *Chemistry and Physics of Lipids*, 144(2), pp. 146–159. doi: 10.1016/j.chemphyslip.2006.08.004.

Mastronarde, D. N. (2003) 'SerialEM: A Program for Automated Tilt Series Acquisition on Tecnai Microscopes Using Prediction of Specimen Position', *Microscopy and Microanalysis*. doi: 10.1017/s1431927603445911.

Matsuoka, K. *et al.* (1998) 'COPII-coated vesicle formation reconstituted with purified coat proteins and chemically defined liposomes', *Cell*. doi: 10.1016/S0092-8674(00)81577-9.

Matsuoka, K. *et al.* (2001) 'Surface structure of the COPII-coated vesicle', *Proceedings of the National Academy of Sciences*, 98(24), pp. 13705–13709. doi: 10.1073/pnas.241522198.

Matsuoka, K. and Schekman, R. (2000) 'The use of liposomes to study COPII- and COPI-coated vesicle formation and membrane protein sorting', *Methods*, 20(4), pp. 417–428. doi: 10.1006/meth.2000.0955.

McCaughey, A. J. *et al.* (2021) 'MIA3 / TANGO1 enables efficient secretion by constraining COPII vesicle budding', *bioRxiv*, c.

McCaughey, J. and Stephens, D. J. (2018) 'COPII-dependent ER export in animal cells: adaptation and control for diverse cargo', *Histochemistry and Cell Biology*. doi: 10.1007/s00418-018-1689-2.

McGourty, C. A. *et al.* (2016) 'Regulation of the CUL3 Ubiquitin Ligase by a Calcium-Dependent Co-adaptor', *Cell*. doi: 10.1016/j.cell.2016.09.026.

McMahon, C. *et al.* (2012) 'The structure of Sec12 implicates potassium ion coordination in Sar1 activation', *Journal of Biological Chemistry*, 287(52), pp. 43599–43606. doi: 10.1074/jbc.M112.420141.

McMahon, H. T. and Gallop, J. L. (2005) 'Membrane curvature and mechanisms of dynamic cell membrane remodelling', *Nature*. doi: 10.1038/nature04396.

Melero, A. *et al.* (2018) 'Lysophospholipids Facilitate COPII Vesicle Formation', *Current Biology*. doi: 10.1016/j.cub.2018.04.076.

Mellman, I. and Simons, K. (1992) 'The Golgi complex: In vitro veritas?', *Cell*, pp. 829–840. doi: 10.1016/0092-8674(92)90027-A.

Melville, D. B., Studer, S. and Schekman, R. (2020) 'Small sequence variations between two mammalian paralogs of the small GTPase SAR1 underlie functional differences in coat protein complex II assembly', *Journal of Biological Chemistry*. doi: 10.1074/jbc.RA120.012964.

Miller, E. *et al.* (2002) 'Cargo selection into COPII vesicles is driven by the Sec24p subunit', *EMBO Journal*, 21(22), pp. 6105–6113. doi: 10.1093/emboj/cdf605.

Miller, E. A. *et al.* (2003) 'Multiple cargo binding sites on the COPII subunit Sec24p ensure capture of diverse membrane proteins into transport vesicles', *Cell*, 114(4), pp. 497–509. doi: 10.1016/S0092-8674(03)00609-3.

Mironov, A. *et al.* (2003) 'ER-to-Golgi carriers arise through direct en bloc protrusion and multistage maturation of specialized ER exit domains', *Developmental Cell*, 5(4), pp. 583–594. doi: 10.1016/S1534-5807(03)00294-6.

Montegna, E. A. *et al.* (2012) 'Sec12 binds to Sec16 at transitional ER sites', *PLoS ONE*, 7(2). doi: 10.1371/journal.pone.0031156.

Morales-Penningston, N. F. *et al.* (2010) 'GUV preparation and imaging: Minimizing artifacts', *Biochimica et Biophysica Acta - Biomembranes*. doi: 10.1016/j.bbamem.2010.03.011.

Nakano, A., Brada, D. and Schekman, R. (1988) 'A membrane glycoprotein, Sec12p, required for protein transport from the endoplasmic reticulum to the Golgi apparatus in yeast.', *Journal of Cell Biology*, 107(3), pp. 851–863. doi: 10.1083/jcb.107.3.851.

Nakano, A. and Muramatsu, M. (1989) 'A novel GTP-binding protein, sar1p, is involved in transport from the endoplasmic reticulum to the Golgi apparatus', *Journal of Cell Biology*, 109(6 I), pp. 2677–2691. doi: 10.1083/jcb.109.6.2677.

Noble, A. J. *et al.* (2013) 'A pseudoatomic model of the COPII cage obtained from cryo-electron microscopy and mass spectrometry', *Nature Structural and Molecular Biology*. doi: 10.1038/nsmb.2467.

Ohisa, S. *et al.* (2010) 'Sec24d encoding a component of COPII is essential for vertebra formation, revealed by the analysis of the medaka mutant, vbi', *Developmental Biology*. doi: 10.1016/j.ydbio.2010.03.016.

Oka, T. and Nakano, A. (1994) 'Inhibition of GTP hydrolysis by Sar1p causes accumulation of vesicles that are a functional intermediate of the ER-to-Golgi transport in yeast', *Journal of Cell Biology*, 124(4), pp. 425–434. doi: 10.1083/jcb.124.4.425.

Okamoto, M. *et al.* (2012) 'High-curvature domains of the ER are important for the

organization of ER exit sites in Saccharomyces cerevisiae', *Journal of Cell Science*. doi: 10.1242/jcs.100065.

Olsen, J. V *et al.* (2010) 'Quantitative Phosphoproteomics Reveals Widespread Full Phosphorylation Site Occupancy During Mitosis -- Olsen et al. 3 (104): ra3 -- Science Signaling (Supplemental)', *Science signaling*.

Orci, L., Glick, B. S. and Rothman, J. E. (1986) 'A new type of coated vesicular carrier that appears not to contain clathrin: Its possible role in protein transport within the Golgi stack', *Cell*. doi: 10.1016/0092-8674(86)90734-8.

Pagano, A. *et al.* (1999) 'Sec24 proteins and sorting at the endoplasmic reticulum', *Journal of Biological Chemistry*, 274(12), pp. 7833–7840. doi: 10.1074/jbc.274.12.7833.

Palmer, K. J. and Stephens, D. J. (2004) 'Biogenesis of ER-to-Golgi transport carriers: Complex roles of COPII in ER export', *Trends in Cell Biology*. doi: 10.1016/j.tcb.2003.12.001.

Pastor-Pareja, J. C. and Xu, T. (2011) 'Shaping Cells and Organs in Drosophila by Opposing Roles of Fat Body-Secreted Collagen IV and Perlecan', *Developmental Cell*, 21(2), pp. 245–256. doi: 10.1016/j.devcel.2011.06.026.

Pathre, P. *et al.* (2003) 'Activation of phospholipase D by the small GTPase Sar1p is required to support COPII assembly and ER export', *EMBO Journal*, 22(16), pp. 4059–4069. doi: 10.1093/emboj/cdg390.

Petley-Ragan, L. M. *et al.* (2016) 'Accumulation of Laminin monomers in Drosophila Glia leads to Glial endoplasmic reticulum stress and disrupted larval locomotion', *Journal of Neuroscience*. doi: 10.1523/JNEUROSCI.1797-15.2016.

Presley, J. F. *et al.* (1997) 'ER-to-Golgi transport visualized in living cells', *Nature*, 389(6646), pp. 81–85. doi: 10.1038/38001.

Rao, Y. *et al.* (2006) 'An open conformation of switch I revealed by Sar1-GDP crystal structure at low Mg2+', *Biochemical and Biophysical Research Communications*, 348(3), pp. 908–915. doi: 10.1016/j.bbrc.2006.07.148.

Raote, I. *et al.* (2017) 'TANGO1 assembles into rings around COP II coats at ER exit sites', *Journal of Cell Biology*, 216(4), pp. 901–909. doi: 10.1083/jcb.201608080.

Raote, I. *et al.* (2018) 'TANGO1 builds a machine for collagen export by recruiting and spatially organizing COPII, tethers and membranes', *eLife*. doi: 10.7554/eLife.32723.

Reynolds, H. M. *et al.* (2019) 'Tango1 coordinates the formation of endoplasmic reticulum/ Golgi docking sites to mediate secretory granule formation', *Journal of Biological Chemistry*.

doi: 10.1074/jbc.RA119.011063.

Rezaei, N., Lyons, A. and Forde, N. R. (2018) 'Environmentally Controlled Curvature of Single Collagen Proteins', *Biophysical Journal*. doi: 10.1016/j.bpj.2018.09.003.

Roberts, B., Clucas, C. and Johnstone, I. L. (2003) 'Loss of SEC-23 in Caenorhabditis elegans causes defects in oogenesis, morphogenesis, and extracellular matrix secretion.', *Molecular biology of the cell*, 14(11), pp. 4414–26. doi: 10.1091/mbc.E03-03-0162.

Robinson, M. S. (1994) 'The role of clathrin, adaptors and dynamin in endocytosis', *Current Opinion in Cell Biology*, 6(4), pp. 538–544. doi: 10.1016/0955-0674(94)90074-4.

Rossanese, O. W. *et al.* (1999) 'Golgi structure correlates with transitional endoplasmic reticulum organization in Pichia pastoris and Saccharomyces cerevisiae', *Journal of Cell Biology*, 145(1), pp. 69–81. doi: 10.1083/jcb.145.1.69.

Rowe, T. *et al.* (1996) 'COPII vesicles derived from mammalian endoplasmic reticulum microsomes recruit COPI', *Journal of Cell Biology*. doi: 10.1083/jcb.135.4.895.

Russell, C. and Stagg, S. M. (2010) 'New insights into the structural mechanisms of the COPII coat', *Traffic*, 11(3), pp. 303–310. doi: 10.1111/j.1600-0854.2009.01026.x.

Russell, R. C. *et al.* (2013) 'ULK1 induces autophagy by phosphorylating Beclin-1 and activating VPS34 lipid kinase', *Nature Cell Biology*. doi: 10.1038/ncb2757.

Saito, K. *et al.* (2009) 'TANGO1 Facilitates Cargo Loading at Endoplasmic Reticulum Exit Sites', *Cell*, 136(5), pp. 891–902. doi: 10.1016/j.cell.2008.12.025.

Saito, K. *et al.* (2011) 'cTAGE5 mediates collagen secretion through interaction with TANGO1 at endoplasmic reticulum exit sites', *Molecular Biology of the Cell*, 22(13), pp. 2301–2308. doi: 10.1091/mbc.E11-02-0143.

Saito, K. *et al.* (2014) 'Concentration of Sec12 at ER exit sites via interaction with cTAGE5 is required for collagen export', *Journal of Cell Biology*. doi: 10.1083/jcb.201312062.

Saito, K. and Maeda, M. (2019) 'Not just a cargo receptor for large cargoes; an emerging role of TANGO1 as an organizer of ER exit sites', *Journal of biochemistry*. doi: 10.1093/jb/mvz036.

Sané, A. *et al.* (2019) 'SAR1B GTPase is necessary to protect intestinal cells from disorders of lipid homeostasis, oxidative stress, and inflammation', *Journal of Lipid Research*. doi: 10.1194/jlr.RA119000119.

Sano, R. and Reed, J. C. (2013) 'ER stress-induced cell death mechanisms', *Biochimica et Biophysica Acta - Molecular Cell Research*. doi: 10.1016/j.bbamcr.2013.06.028.

Santos, A. J. M. *et al.* (2015) 'TANGO1 recruits ERGIC membranes to the endoplasmic reticulum for procollagen export', *eLife*, 4(NOVEMBER2015). doi: 10.7554/eLife.10982.001.

Santos, A. J. M. *et al.* (2016) 'TANGO1 and Mia2/cTAGE5 (TALI) cooperate to export bulky pre-chylomicrons/VLDLs from the endoplasmic reticulum', *Journal of Cell Biology*, 213(3), pp. 343–354. doi: 10.1083/jcb.201603072.

Sarmah, S. *et al.* (2010) 'Sec24D-dependent transport of extracellular matrix proteins is required for zebrafish skeletal morphogenesis', *PLoS ONE*. doi: 10.1371/journal.pone.0010367.

Sato, K. and Nakano, A. (2005) 'Dissection of COPII subunit-cargo assembly and disassembly kinetics during Sar1p-GTP hydrolysis', *Nature Structural and Molecular Biology*, 12(2), pp. 167–174. doi: 10.1038/nsmb893.

Scarff, C. A. *et al.* (2018) 'Variations on negative stain electron microscopy methods: Tools for tackling challenging systems', *Journal of Visualized Experiments*. doi: 10.3791/57199.

Scheres, S. H. W. (2012) 'RELION: Implementation of a Bayesian approach to cryo-EM structure determination', *Journal of Structural Biology*. doi: 10.1016/j.jsb.2012.09.006.

Schindler, A. J. and Schekman, R. (2009) 'In vitro reconstitution of ER-stress induced ATF6 transport in COPII vesicles', *Proceedings of the National Academy of Sciences*, 106(42), pp. 17775–17780. doi: 10.1073/pnas.0910342106.

Schneider, C. A., Rasband, W. S. and Eliceiri, K. W. (2012) 'NIH Image to ImageJ: 25 years of image analysis', *Nature Methods*. doi: 10.1038/nmeth.2089.

Schwarz, K. *et al.* (2009) 'Mutations affecting the secretory COPII coat component SEC23B cause congenital dyserythropoietic anemia type II', *Nature Genetics*, 41(8), pp. 936–940. doi: 10.1038/ng.405.

Schweizer, A. *et al.* (1988) 'Identification, by a monoclonal antibody, of a 53-kD protein associated with a tubulo-vesicular compartment at the cis-side of the Golgi apparatus', *Journal of Cell Biology*. doi: 10.1083/jcb.107.5.1643.

Seaman, M. N. J. *et al.* (1997) 'Endosome to Golgi retrieval of the vacuolar protein sorting receptor, Vps10p, requires the function of the VPS29, VPS30, and VPS35 gene products', *Journal of Cell Biology*. doi: 10.1083/jcb.137.1.79.

Sheetz, M. P. and Singer, S. J. (1974) 'Biological membranes as bilayer couples. A molecular

mechanism of drug erythrocyte interactions', *Proceedings of the National Academy of Sciences of the United States of America*. doi: 10.1073/pnas.71.11.4457.

Shima, T., Kirisako, H. and Nakatogawa, H. (2019) 'COPII vesicles contribute to autophagosomal membranes', *Journal of Cell Biology*. doi: 10.1083/jcb.201809032.

Shimoi, W. *et al.* (2005) 'p125 is localized in endoplasmic reticulum exit sites and involved in their organization', *Journal of Biological Chemistry*. doi: 10.1074/jbc.M409673200.

Shoulders, C. C., Stephens, D. J. and Jones, B. (2004) 'The intracellular transport of chylomicrons requires the small GTPase, Sar1b', *Current Opinion in Lipidology*. doi: 10.1097/00041433-200404000-00012.

Siddiqi, S. A. (2003) 'COPII proteins are required for Golgi fusion but not for endoplasmic reticulum budding of the pre-chylomicron transport vesicle', *Journal of Cell Science*, 116(2), pp. 415–427. doi: 10.1242/jcs.00215.

Sievers, F. *et al.* (2011) 'Fast, scalable generation of high-quality protein multiple sequence alignments using Clustal Omega', *Molecular Systems Biology*. doi: 10.1038/msb.2011.75.

Sitia, R. and Meldolesi, J. (1992) 'Endoplasmic reticulum: a dynamic patchwork of specialized subregions.', *Molecular biology of the cell*, 3(10), pp. 1067–72. doi: 10.1091/mbc.3.10.1067.

Stagg, S. M. *et al.* (2006) 'Structure of the Sec13/31 COPII coat cage', *Nature*, 439(7073), pp. 234–238. doi: 10.1038/nature04339.

Stagg, S. M. *et al.* (2008) 'Structural Basis for Cargo Regulation of COPII Coat Assembly', *Cell*, 134(3), pp. 474–484. doi: 10.1016/j.cell.2008.06.024.

Stancheva, V. G. *et al.* (2020) 'Combinatorial multivalent interactions drive cooperative assembly of the COPII coat', *Journal of Cell Biology*. doi: 10.1083/jcb.202007135.

Stankewich, M. C. (2006) 'Human Sec31B: a family of new mammalian orthologues of yeast Sec31p that associate with the COPII coat', *Journal of Cell Science*, 119(5), pp. 958–969. doi: 10.1242/jcs.02751.

Stephens, D. J. (2003) 'De novo formation, fusion and fission of mammalian COPII-coated endoplasmic reticulum exit sites', *EMBO Reports*, 4(2), pp. 210–217. doi: 10.1038/sj.embor.embor736.

Stephens, D. J. and Pepperkok, R. (2001) 'Illuminating the secretory pathway: When do we need vesicles?', *Journal of Cell Science*.

Stephens, D. J. and Pepperkok, R. (2002) 'Imaging of procollagen transport reveals COPI-dependent cargo sorting during ER-to-Golgi transport in mammalian cells.', *Journal of cell science*, 115, pp. 1149–1160. doi: 10.1016/j.aqpro.2013.07.003.

Supek, F. *et al.* (2002) 'Sec16p potentiates the action of COPII proteins to bud transport vesicles', *Journal of Cell Biology*. doi: 10.1083/jcb.200207053.

Szul, T. and Sztul, E. (2011) 'COPII and COPI Traffic at the ER-Golgi Interface', *Physiology*, 26(5), pp. 348–364. doi: 10.1152/physiol.00017.2011.

Tanabe, T. *et al.* (2016) 'Dual function of cTAGE5 in collagen export from the endoplasmic reticulum', *Molecular Biology of the Cell*. doi: 10.1091/mbc.E16-03-0180.

Tang, G. *et al.* (2007) 'EMAN2: An extensible image processing suite for electron microscopy', *Journal of Structural Biology*. doi: 10.1016/j.jsb.2006.05.009.

Temkin, P. *et al.* (2011) 'SNX27 mediates retromer tubule entry and endosome-to-plasma membrane trafficking of signalling receptors', *Nature Cell Biology*. doi: 10.1038/ncb2252.

Townley, A. K. *et al.* (2008) 'Efficient coupling of Sec23-Sec24 to Sec13-Sec31 drives COPII-dependent collagen secretion and is essential for normal craniofacial development', *Journal of Cell Science*, 121(18), pp. 3025–3034. doi: 10.1242/jcs.031070.

Vance, J. E. (2015) 'Phospholipid Synthesis and Transport in Mammalian Cells', *Traffic*. doi: 10.1111/tra.12230.

Venditti, R. *et al.* (2012) 'Sedlin controls the ER export of procollagen by regulating the Sar1 cycle', *Science*, 337(6102), pp. 1668–1672. doi: 10.1126/science.1224947.

Voynow, J. A. and Fischer, B. M. (2006) 'Mucins', in *Encyclopedia of Respiratory Medicine, Four-Volume Set*. doi: 10.1016/B0-12-370879-6/00248-9.

Waldron, T. T. and Murphy, K. P. (2003) 'Stabilization of proteins by ligand binding: Application to drug screening and determination of unfolding energetics', *Biochemistry*. doi: 10.1021/bi034212v.

Wang, B. *et al.* (2018) 'The COPII cargo adapter SEC24C is essential for neuronal homeostasis', *Journal of Clinical Investigation*. doi: 10.1172/JCI98194.

Watson, P. *et al.* (2006) 'Sec16 defines endoplasmic reticulum exit sites and is required for secretory cargo export in mammalian cells', *Traffic*, 7(12), pp. 1678–1687. doi: 10.1111/j.1600-0854.2006.00493.x.

Watson, P. and Stephens, D. J. (2005) 'ER-to-Golgi transport: Form and formation of vesicular and tubular carriers', *Biochimica et Biophysica Acta - Molecular Cell Research*, pp. 304–315. doi: 10.1016/j.bbamcr.2005.03.003.

Weissman, J. T., Plutner, H. and Balch, W. E. (2001) 'The mammalian guanine nucleotide exchange factor mSec12 is essential for activation of the Sar1 GTPase directing endoplasmic reticulum export', *Traffic*, 2(7), pp. 465–475. doi: 10.1034/j.1600-0854.2001.20704.x.

Wendeler, M. W., Paccaud, J. P. and Hauri, H. P. (2007) 'Role of Sec24 isoforms in selective export of membrane proteins from the endoplasmic reticulum', *EMBO Reports*, 8(3), pp. 258–264. doi: 10.1038/sj.embor.7400893.

Whittle, J. R. R. and Schwartz, T. U. (2010) 'Structure of the Sec13-Sec16 edge element, a template for assembly of the COPII vesicle coat', *Journal of Cell Biology*, 190(3), pp. 347–361. doi: 10.1083/jcb.201003092.

Wilson, D. G. *et al.* (2011) 'Global defects in collagen secretion in a Mia3/TANGO1 knockout mouse', *Journal of Cell Biology*, 193(5), pp. 935–951. doi: 10.1083/jcb.201007162.

Xu, D. and Hay, J. C. (2004) 'Reconstitution of COPII vesicle fusion to generate a pre-Golgi intermediate compartment', *Journal of Cell Biology*, 167(6), pp. 997–1003. doi: 10.1083/jcb.200408135.

Yang *et al.* (2013) 'Mutations in the COPII vesicle component gene SEC24B are associated with human neural tube defects', *Human Mutation*. doi: 10.1002/humu.22338.

Yang, E. *et al.* (2013) 'Maternal hyperglycemia activates an ASK1-FoxO3a-Caspase 8 pathway that leads to embryonic neural tube defects', *Science Signaling*, 6(290). doi: 10.1126/scisignal.2004020.

Yeliseev, A., Zoubak, L. and Gawrisch, K. (2007) 'Use of dual affinity tags for expression and purification of functional peripheral cannabinoid receptor', *Protein Expression and Purification*. doi: 10.1016/j.pep.2006.12.003.

Yoshihisa, T., Barlowe, C. and Schekman, R. (1993) 'Requirement for a GTPase-activating protein in vesicle budding from the endoplasmic reticulum', *Science*, 259(5100), pp. 1466–1468. doi: 10.1126/science.8451644.

Yuan, L. *et al.* (2018) 'TANGO1 and SEC12 are copackaged with procollagen I to facilitate the generation of large COPII carriers', *Proceedings of the National Academy of Sciences of the United States of America*. doi: 10.1073/pnas.1814810115.

Zanetti, G. *et al.* (2012) 'COPII and the regulation of protein sorting in mammals', *Nature Cell Biology*, pp. 20–28. doi: 10.1038/ncb2390.

Zanetti, G. *et al.* (2013) 'The structure of the COPII transport-vesicle coat assembled on membranes', *eLife*. doi: 10.7554/eLife.00951.

Zeuschner, D. *et al.* (2006) 'Immuno-electron tomography of ER exit sites reveals the existence of free COPII-coated transport carriers', *Nature Cell Biology*, 8(4), pp. 377–383. doi: 10.1038/ncb1371.

Zhang, B. *et al.* (2000) 'The role of Mg2+ cofactor in the guanine nucleotide exchange and GTP hydrolysis reactions of Rho family GTP-binding proteins', *Journal of Biological Chemistry*, 275(33), pp. 25299–25307. doi: 10.1074/jbc.M001027200.

Zhou, C. *et al.* (2017) 'Regulation of mATG9 trafficking by Src- and ULK1-mediated phosphorylation in basal and starvation-induced autophagy', *Cell Research*. doi: 10.1038/cr.2016.146.

Zhou, H. *et al.* (2013) 'Toward a comprehensive characterization of a human cancer cell phosphoproteome', *Journal of Proteome Research*. doi: 10.1021/pr300630k.

Zhu, M. *et al.* (2015) 'Neural tube opening and abnormal extraembryonic membrane development in SEC23A deficient mice', *Scientific Reports*, 5. doi: 10.1038/srep15471.

Zimmerberg, J. and McLaughlin, S. (2004) 'Membrane curvature: How BAR domains bend bilayers', *Current Biology*. doi: 10.1016/j.cub.2004.02.060.

Zinser, E. and Daum, G. (1995) 'Isolation and biochemical characterization of organelles from the yeast, Saccharomyces cerevisiae', *Yeast*. doi: 10.1002/yea.320110602.